The Development of a Gamma-(γ)-Aminobutyric Acid (GABA) Biosensor and Characterisation of an L-Glutamate Biosensor for Neurochemical Analysis

Kobi P. Bermingham B. Sc. (Hons)

This report is submitted in fulfillment of the Requirements for the M.Sc. Degree in Chemistry

Maynooth University Department of Chemistry

Maynooth University

Date: October 2022

Supervisors: Prof. John P. Lowry

Head of Department: Prof. Denise Rooney

I would like to dedicate this work to my mother, Stephanie M^{c}Givern, and my sisters; Nicole, Jodie and, Chantelle. I didn't always realised it or in fact, deserve it, but you were always there. Thank you.

"If you can meet with Triumph and Disaster

And treat those two impostures just the same"

Rudyard Kipling

"Whatever your excuse is, Death's heard it and responses with the gentle questioning

'What were you waiting for? When did your hesitation become a full stop?'"

Shane Koyczan

"Nothing etched in stone until, it is"

"It got darker and snowier until finally the road delivered us to the one place that all my youthful trips west never could, home"

John Green

"Slowly at first. And then… all at once"

Pablo Escobar

Certificate of Originality

I, Kobi P. Bermingham, certify that the work done in this thesis is my original work and that it has not been submitted at Maynooth University or any other institution at any time. I also certify that it has not been copied from a published book, photograph, magazine, or by another person.

Signed …….

Kobi P. Bermingham

Date:

Acknowledgements

This experience has brought highs and lows and every variation between along the way. I learned so much of what it means to be a chemist and truly analyse not only an experiment and results but also a situation. To adapt and improve. Propping me up will always be my family and friends. I am who I am because of you. My family have helped me along more than I understood at the time. My friends, Niclas, Dom and My, without you I wouldn't have made it this far.

To my supervisor Prof. John P. Lowry, I couldn't begin to thank you enough. You gave me an opportunity I hadn't thought I would ever have. Unfortunately it didn't end how either of us intended but I will forever be grateful. You're expertise at times was truly impressive and inspiring. And beyond that, your compassion and understanding are a true highlight to your character. If I become half the man you are, I will consider that a life will spent.

To those I was lucky enough to share a lab with, you made this experience one of the most enjoyable in my life. Michelle D., my mentor and someone I respect more than I could even begin to put into words. You introduced me to the department and I'll never be able to think of my time in Maynooth without you being an immediate thought. Your patience and educating nature was always obvious. The absolute expert in biosensors. Thank you for everything. Gama and Sean, you both took the time to explain whatever I needed without hesitation. Michelle S., the glue that held the lab together. Often helping me without me even having to ask. Jason, I think I'll miss that sharp but hilarious tongue. And Caytlin, we started together and after some time it became clear that we'll always be in touch to some degree. You were always an emotional confidant and we became truly close friends. I'll always look back fondly on the first two years. God knows I put you lot through enough with my endless supply of questions. I still giggle when I think back to our agreed rule that I couldn't ask any questions until 10:30. Our lab and afternoon coffees. There were definitely times when each of you helped me and I'll carry these memories always.

To the Chemistry Department staff, you were all welcoming for the get-go. I have yet to find a single staff member who wasn't accommodating when I showed up unannounced at your door. You not only helped me but also my family. I couldn't have asked for more out of a work environment and the people I got to share hallways with.

I would be remiss if I didn't acknowledge the resources available at Maynooth University. Sandra and Deidre helped me through a lot and they truly deserve some credit for this milestone.

I would also like to acknowledge and thank the funding body Science Foundation of Ireland (SFI) under the grant number 15/IA/3176 for making this opportunity possible.

For a long time, it wasn't guaranteed I would finish this thesis. A special acknowledgement needs to be made to those who refused to let this opportunity pass me. In particular Dom, My and Jason. All of whom took extra time to convince me to just sit down and write, work harder now for a better future. Thank you.

Abbreviations

5-hydroxyindolacetic acid	5-HIAA
5-hydroxytryptomine	5-HT
Adenosine triphosphate	ATP
Alpha-keto glutarate	AKG
Analogue-to-digital	ADC
Artificial cerebrospinal fluid	aCSF
Ascorbic acid	AA
Bioresource unit	BRU
Blood brain barrier	BBB
Bilayer lipid membrane	BLM
Bovine serum albumin	BSA
Carbon paste electrode	CPE
Central nervous system	CNS
Cerebrospinal fluid	CSF
Constant potential amperometry	CPA
Cyclic voltammetry	CV
Dehydroascorbic acid	DHAA
Dichloroacetate	DCA
Differential pulse amperometry	DPA
Digital-to-analogue	DAC
Dihydroxyphenylacetic acid	DOPAC

Dopamine	DA
Electroencephalography	EEG
Extracellular fluid	ECF
Fast scan cyclic voltammetry	FSCV
Flavin adenine dinucleotide	FAD
Functional magnetic resonance imaging	fMRI
Gama-(γ)-aminobutyric acid	GAB/GABA
Glassy carbon electrode	GCE
Glutaraldehyde	GA
L-Glutamate	Glu
Glutamate Oxidase	GluOx
Highest occupied molecular orbital	HOMO
Homovanillic acid	HVA
Horse radish peroxidase	HRP
Hydrogen peroxide	H_2O_2
Limit of detection	LOD
Linear region slope	LRS
Long term in-vivo electrochemistry	LIVE
Lowest unoccupied molecular orbital	LUMO
Methyl methacrylate	MMA
Nicotinamide adenine dinucleotide phosphate	NADPH
Nitrogen gas	N_2
ortho-Phenylenediamine	*o*PD

One-way analysis of variance	ANOVA
Oxygen	O_2
Phosphate buffer saline	PBS
Platinum/iridium	Pt/Ir
Poly-*ortho*-phenylenediamine	P*o*PD
Polyethyleneimine	PEI
Polyurethane	PU
Potassium chloride	KCl
Potassium phosphate dibasic	K_2HPO_4
Potassium phosphate monobasic	KH_2PO_4
Regional cerebral blood flow	rCBF
Saturated calomel electrode	SCE
Styrene	Sty
Sodium chloride	NaCl
Uric acid	UA

Abstract

The research presented in this thesis started off as a PhD project with the aim to develop and characterise an *in vitro* biosensor appropriate for *in vivo* detection and monitoring of gamma-(γ)-aminobutyric acid (GABA). The ambition was simultaneous monitoring of GABA and L-glutamate. It was also hoped that simultaneous D-serine monitoring would be performed using a newly developed and validated sensor for this co-agonist of the glutamatergic N-methyl D-aspartate (NMDA) receptor. The development of a GABase-based biosensor was found to be too large an undertaking and consequently, the research plan converted to refinement of an L-glutamate biosensor. Some development work (pH and temperature studies) was also performed on the D-serine biosensor.

Gamma-(γ)-aminobutyric acid is the major inhibitory neurotransmitter but has yet to receive wide examination in the scientific community. In contrast, L-glutamate, the major excitatory, neurotransmitter has not only experienced vast amounts of research but is also present in the public eye unlike GABA. As neurotransmitters are chemicals producing electrical stimulation in the brain, electrochemical techniques offer a unique insight into their operation and reactions.

The development of a first generation GABA biosensor used an underlying L-glutamate biosensor as GABA is the precursor to L-glutamate. An appropriate enzyme unit activity for the GABase solution was the first barrier to be overcome. After this, the position of the GABase in the composite design was investigated. This experimentation didn't garner any results that suggested a response would be produced. The active surface was examined to ensure that the production of hydrogen peroxide would be detected. An alternate reaction scheme was also investigated which didn't produce any response either. This suggested the enzyme solution was, at least in part, at fault. Further exploration and refinement of the enzyme solution could potentially alleviate the issues encountered during this development work.

The characterisation of the L-glutamate biosensor then became the priority. The optimal composite design was found to be:

$$Pt/Ir_C - PoPD - (Sty - GluOx(100\ U/mL) - BSA{:}GA(1.0{:}0.1\ \%) - PEI(1\%))_{15}$$

After the optimal design was found and had appropriate sensitivity (90.4 ± 2.0 nA·cm^{-2}·μM^{-1}) comparable to previously reported sensors, the *in vitro* characterisation was performed. This consisted of ensuring the biosensor would remain operational after implantation in the extracellular fluid *i.e.* under the chemical and physical parameters present in the brain. The shelf-life was found to be several weeks (28 days) and there was no recorded loss in sensitivity after repeated calibrations, or exposure to *ex vivo* rodent brain tissue. The sensor performed as desired under all physiologically relevant pH and temperature ranges. The interference was mitigated with the use of poly-*ortho*-phenylenediamine (P*o*PD) (interferent species were typically < 5% of the basal glutamate (10 μM) glutamate response) and reliable detection of L-glutamate was still observed. Preliminary *in vivo* characterisation performed in freely moving animals suggested the suitability of this sensor design for *in vivo* use. Expected signal changes were observed and a stable baseline over 16 days. Future work will include further *in vivo* characterisation and validation of this biosensor. Tentatively, the dual monitoring of L-glutamate and D-serine would be examined because of their co-agonist role at the NMDA receptor.

Table of Contents

CHAPTER ONE

Introduction

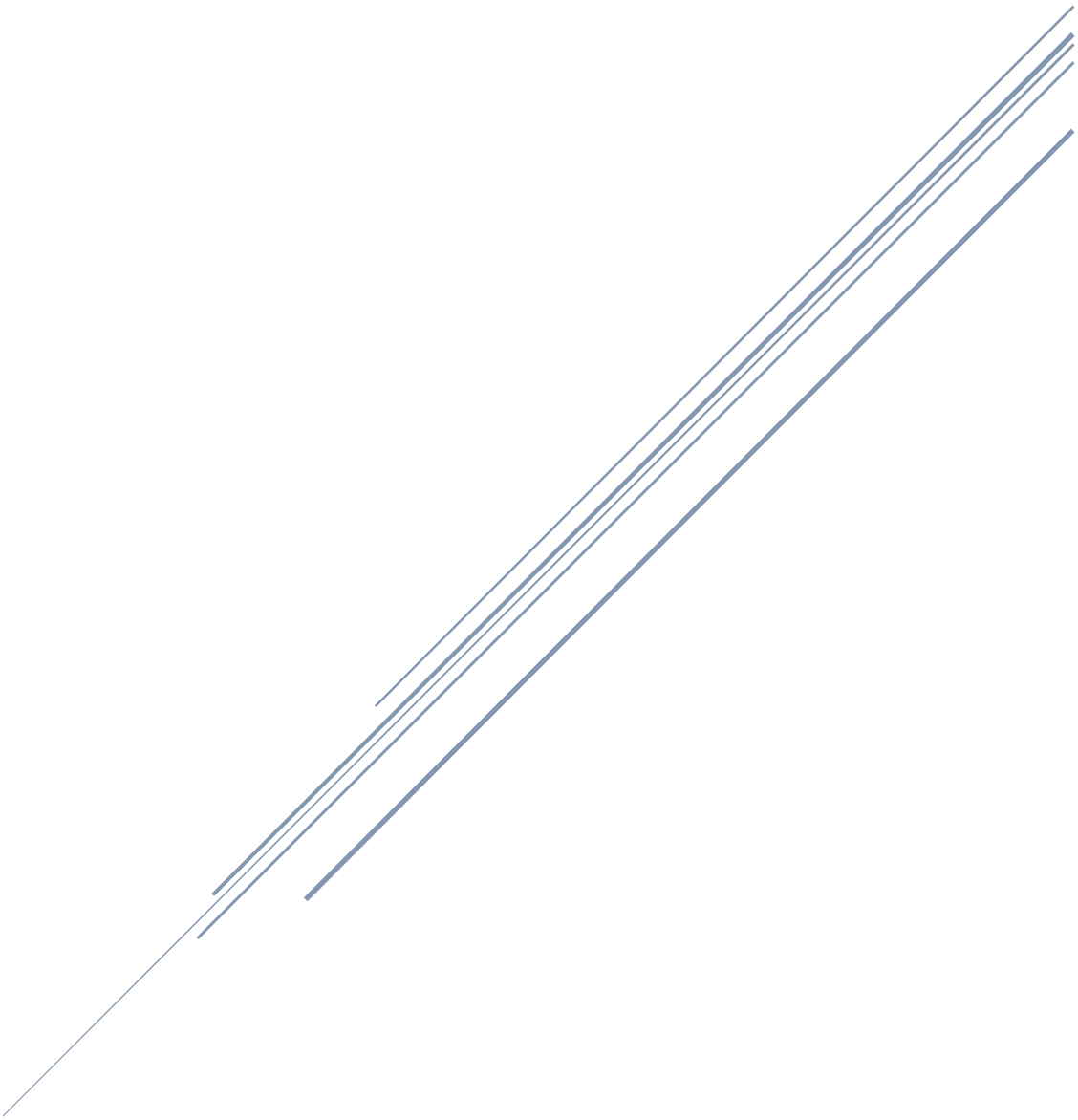

Chapter 1 – Introduction

1.1 Introduction

The brain is, with little to no argument, our most complex organ. It sits as the head of the central nervous system (CNS) tasked with enabling nerve cells (neurons) to communicate with each other [1]. This communication occurs in the synaptic cleft, a region between these neighbour neurons. The presynaptic neuron will release neurotransmitters into the cleft in order to communicate with the postsynaptic neuron (Scheme 1.1). These neurotransmitters carry, boost and modulate signals between the neurons. Numerous in classifications, the scope of this body of work only delves into excitatory and inhibitory neurotransmitters (Section 1.3). This use of a combination of electrical and chemical impulses has allowed electrochemistry to take a strong foothold in the frontiers of understanding the normal operation and malfunction of this vital organ. Recent decades of research have greatly enhanced our collective knowledge but major questions still remain unanswered.

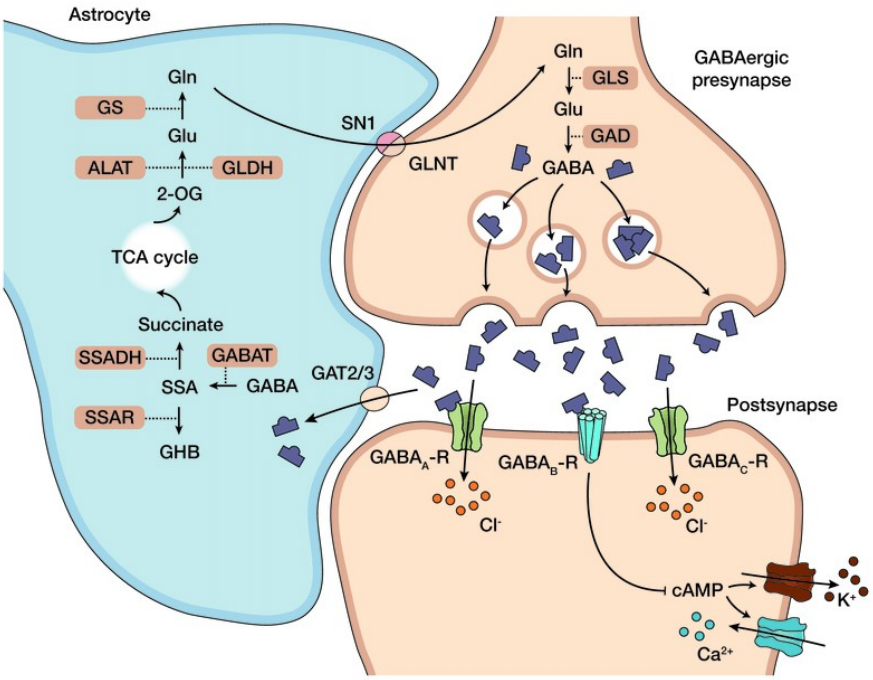

Scheme 1.1: Schematic depicting GABAergic synaptic cleft where the neurotransmitter is released via chemical transmission of a nerve impulse. [2]

This project started off with a challenging aim, to develop and characterise an *in vitro* biosensor for the detection and monitoring of gamma-(γ)-aminobutyric acid (GABA) (see Figure 1.1) appropriate for *in vivo* application. This was to be followed up by the simultaneous *in vivo* monitoring of GABA and L-glutamate (Glu) (see Figure 1.2). GABA being the major inhibitory neurotransmitter and Glu being the major excitatory neurotransmitter. While apparently straightforward in aim, the logistics and implementation were not due to neither GABA nor Glu being electroactive, and the availability of appropriate biological recognition elements for GABA. This meant that indirect means of detection needed to be used. This is where first generation biosensor technology came into play *i.e.* using an enzymatic system that produces hydrogen peroxide (H_2O_2), which is electroactive and thus can be detected or monitored electrochemically (discussed further in Section 3.1). Biosensors improve spatial and temporal resolution which is needed to garner vital information on the sub-second neurotransmitter profile. GABA and Glu have been implicated in various neurodegenerative diseases and conditions (discussed further in Section 4.1 & Section 5.1, respectively).

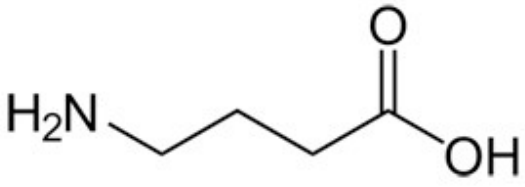

Figure 1.1: Structure of GABA

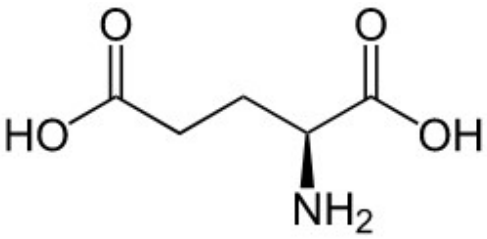

Figure 1.2: Structure of Glu

Constant potential amperometry (CPA) and cyclic voltammetry (CV), electrochemical techniques, were performed throughout this project (discussed in detail in 2.3). Electrochemistry

offers a unique insight into neurochemistry due to the interlinking of chemistry and electricity, the dialects of the brain. Excitatory neurotransmitters (chemistry) are used to stimulate an electric potential (electricity) that travels down the post-synaptic neuron while inhibitory neurotransmitters diminish this electric potential.

Despite the prolific sensor development for many biologically important analytes, very little work has been published on GABA monitoring. This may be due to the lack of awareness in the public's discourse (discussed further in Section 4.1). The development of a GABA biosensor, enabling continuous and uninterrupted monitoring of GABA may provide much needed understanding on the progression or development of the associated diseases and conditions or indeed, provide pharmacological assistance in treating such. The further development of a Glu biosensor may enhance the knowledge of the same.

1.2 Methodology

The primary aim of this research was to develop a biosensor capable of detecting and monitoring GABA, which even with the extensive work into neurochemical biosensors has remained greatly under studied. A vast number of methodologies exist in the realm of neurochemical monitoring aiming to enhance the understanding of the great complexity that is neurochemical processes. Previously employed techniques that have contributed to answering some of the questions regarding the fundamental understanding of our most complex organ have come from: microdialysis, spectroscopy, histology, fMRI and, electrochemistry to name but a few.

Briefly, CV and CPA, techniques involve the use of two to three electrodes, a working electrode *i.e.* an indicator electrode, a reference electrode and an auxiliary electrode. The working electrode is modified with a biological recognition component. In this body of work enzymes were used; specifically glutamate oxidase to generate hydrogen peroxide (H_2O_2). This is important as the oxidation potential of H_2O_2 is well established and will be used to generate the observed current (see Section 2.6).

The extracellular fluid (ECF) is a very tightly regulated environment and from which, we get the physical and chemical parameters a biosensor needs to operate within to be viable for neurochemical analysis (discussed in Section 2.1). The physical parameters to operate in are

physiologically relevant temperature and pH. The chemical parameters include appropriate limit of detection, adequate interferent rejection and, stabile oxygen dependence (see section 5.1).

1.3 Gamma-(γ)-aminobutyric Acid & L-Glutamate *In Vivo*

Neurotransmitters are endogenous chemicals and function as messengers enabling communication between neurons throughout the body (see Scheme 1.1) [3]. They are vital in every aspect of mammalian life from development, normal brain function, muscle movement, organ functions, down to neurological disorders. The communication occurs in the synaptic cleft *i.e.* the space between the presynaptic and postsynaptic neuron. Neurotransmitters cross this synaptic cleft to reply, amplify and modulate the signals between these neighbouring neurons.

This communication between neighbouring neurons can be inhibitory, excitatory or, modulatory in nature. The nature of the communication is determined by the receptors the transmitters act upon at the surface of the post-synaptic neuron. Inhibitory neurotransmitters, such as GABA, decrease the probability that the post-synaptic neuron will produce an action potential. An action potential is when the membrane potential rapidly rises and falls [4]. This depolarisation causes the neighbouring neuron to depolarise (see Scheme 1.2A), whereas excitatory neurotransmitters, such as glutamate, increase this probability. Both of these effects are due to the transmitters influence on trans-membrane ion flow (see Scheme 1.2). This depolarisation causes the neighbouring neuron to depolarise (see Scheme 1.2A). Synapses with excitatory effects are referred to as Type 1 and inhibitory effects as Type 2 [5].

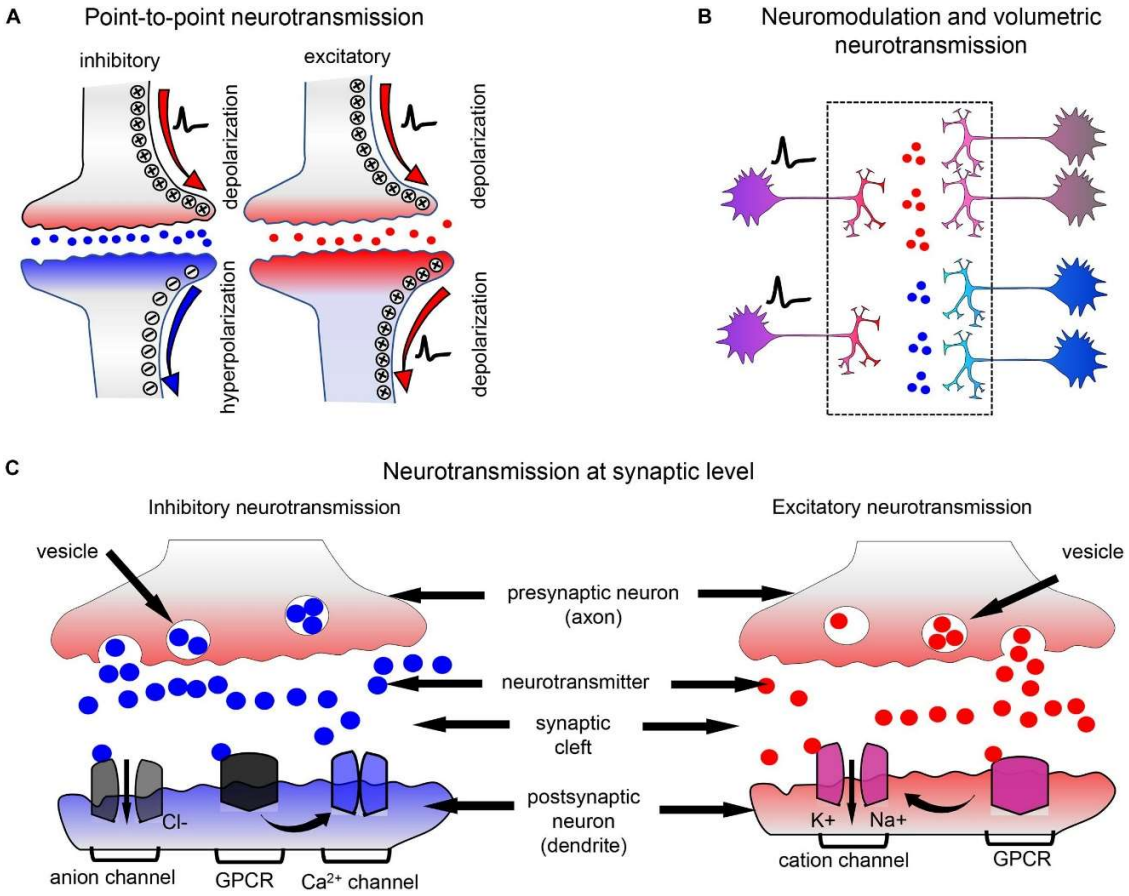

Scheme 1.2: Schematic showing the principles of neurotransmission and neuromodulation. (**A**) Depicts the reaction of inhibitory and excitatory neurotransmitters on the action potential. (**B**) Depicts neuromodulars released by a single neuron act on groups of neurons. (**C**) Neurotransmission at a synaptic level. Inhibitory neurotransmitters activate the anion channels and excitatory neurotransmitters active the cation channels. [6]

GABA is the major inhibitory neurotransmitter, acting on approximately one third of synapses [7, 8] but surprisingly hasn't received anywhere near the same interest from the scientific community, with very little research having been performed to elucidate its exact mechanisms with [9-15] comprising a majority of it. It is known to have a significant effect on sleep, mood and act as the excitatory neurotransmitter in immature mammalian brain development [16-19]. Dysregulation has been linked to epilepsy, Huntington's, depression, anxiety and schizophrenia [20-24] to name but a few. Unfortunately, the lack of a suitable biological recognition unit has

hindered the development of a biosensor for neurochemical monitoring of GABA in the past. This body of work aims to aid in this discussion through the development of a first generation biosensor with the use of the enzyme GABase (see section 4.1 for further discussion).

Glutamate is the major excitatory neurotransmitter, acting on 60 – 70 % of synapses [25] and as such, a lot of research has been performed to elucidate its exact mechanisms [26-31]. It has been shown to play a significant role in development, plasticity, learning and memory, and sensory and motor systems [32]. Dysregulation of glutamate has been linked to epilepsy, stroke and both neurodegenerative and psychiatric diseases [33-36] to only mention a few. While various biosensors capable of monitoring glutamate exist, the majority of these have been applied in anaesthetised animals. As such, worked also focused on further refining a biosensor design developed by Prof. Lowry's research group for monitoring glutamate in freely-moving animals. Progressing this, the design was characterised to ensure operation in the harsh extracellular fluid *i.e.* under the physical and chemical constraints present (see Section 5.1 for further discussion) in the brain.

In summary, Chapter 2 gives a detailed account of the theory relevant to the studies undertaken in this body of work. Chapter 3 provides an in-depth description of the experimental techniques, equipment and parameters utilised throughout. The aim to develop an *in vitro* biosensor capable of monitoring GABA is discussed in Chapter 4. Chapter 5 serves to lay out the refinement and characterisation of an *in vitro* biosensor optimised for neurochemical glutamate monitoring and preliminary *in vivo* characterisation of this biosensor. The overall conclusions for this body of work are presented in Chapter 6.

1.4 References

1. Campbell, N.A., J.B. Reece, and L. Urry, *Biology*. Biology. 2005: Pearson, Benjamin Cummings.
2. Didiasova, M., et al., *Succinic Semialdehyde Dehydrogenase Deficiency: An Update.* Cells, 2020. **9**: p. 477.
3. Rizo, J., *Mechanism of neurotransmitter release coming into focus.* Protein Sci, 2018. **27**(8): p. 1364-1391.
4. Hodgkin, A.L. and A.F. Huxley, *A quantitative description of membrane current and its application to conduction and excitation in nerve.* J Physiol, 1952. **117**(4): p. 500-44.
5. Peters, A. and S.L. Palay, *The morphology of synapses.* Journal of Neurocytology, 1996. **25**(1): p. 687-700.
6. Leopold, A.V., D.M. Shcherbakova, and V.V. Verkhusha, *Fluorescent Biosensors for Neurotransmission and Neuromodulation: Engineering and Applications.* Frontiers in Cellular Neuroscience, 2019. **13**: p. 474.
7. Hampel, L. and T. Lau, *Neurobiological Principles: Neurotransmitters*, in *NeuroPsychopharmacotherapy*, P. Riederer, et al., Editors. 2020, Springer International Publishing: Cham. p. 1-21.
8. de Leon, A.S. and P. Tadi, *Biochemistry, Gamma Aminobutyric Acid*. 2021: StatPearls Publishing, Treasure Island (FL).
9. Niwa, O., et al., *Small-Volume On-Line Sensor for Continuous Measurement of γ-Aminobutyric Acid.* Analytical Chemistry, 1998. **70**(1): p. 89-93.
10. Jinnarak, A. and S. Teerasong, *A novel colorimetric method for detection of gamma-aminobutyric acid based on silver nanoparticles.* Sensors and Actuators B: Chemical, 2016. **229**: p. 315-320.
11. Zhou, A. and J. Muthuswamy, *Acoustic biosensor for monitoring antibody immobilization and neurotransmitter GABA in real-time.* Sensors and Actuators B: Chemical, 2004. **101**(1): p. 8-19.
12. Sekioka, N., et al., *Improved detection limit for an electrochemical γ-aminobutyric acid sensor based on stable NADPH detection using an electron cyclotron resonance sputtered carbon film electrode.* Sensors and Actuators B: Chemical, 2008. **129**(1): p. 442-449.

13. Smith, S. and T. Sharp, *Measurement of GABA in rat brain microdialysates using o-phthaldialdehyde—sulphite derivatization and high-performance liquid chromatography with electrochemical detection.* Journal of Chromatography B: Biomedical Sciences and Applications, 1994. **652**(2): p. 228-233.
14. Ferraro, L., et al., *Striatal NTS1, dopamine D2 and NMDA receptor regulation of pallidal GABA and glutamate release - a dual-probe microdialysis study in the intranigral 6-hydroxydopamine unilaterally lesioned rat.* The European journal of neuroscience, 2011. **35**: p. 207-20.
15. Mazzei, F., et al., *Peroxidase based amperometric biosensors for the determination of γ-aminobutyric acid.* Analytica Chimica Acta, 1996. **328**(1): p. 41-46.
16. Gottesmann, C., *GABA mechanisms and sleep.* Neuroscience, 2002. **111**(2): p. 231-9.
17. Petty, F., *GABA and mood disorders: a brief review and hypothesis.* J Affect Disord, 1995. **34**(4): p. 275-81.
18. Rivera, C., et al., *The K+/Cl− co-transporter KCC2 renders GABA hyperpolarizing during neuronal maturation.* Nature, 1999. **397**(6716): p. 251-255.
19. Cherubini, E., J.L. Gaiarsa, and Y. Ben-Ari, *GABA: an excitatory transmitter in early postnatal life.* Trends in Neurosciences, 1991. **14**(12): p. 515-519.
20. Fritschy, J.M., et al., *GABAergic neurons and GABA(A)-receptors in temporal lobe epilepsy.* Neurochem Int, 1999. **34**(5): p. 435-45.
21. Rosas-Arellano, A., et al., *Huntington's disease leads to decrease of GABA-A tonic subunits in the D2 neostriatal pathway and their relocalization into the synaptic cleft.* Neurobiol Dis, 2018. **110**: p. 142-153.
22. Möhler, H., *The GABA system in anxiety and depression and its therapeutic potential.* Neuropharmacology, 2012. **62**(1): p. 42-53.
23. Petroff, O.A., *GABA and glutamate in the human brain.* Neuroscientist, 2002. **8**(6): p. 562-73.
24. O'Connor, W.T. and S.D. O'Shea, *Clozapine and GABA transmission in schizophrenia disease models: establishing principles to guide treatments.* Pharmacol Ther, 2015. **150**: p. 47-80.
25. Victor Nadler, J., *Plasticity of glutamate synaptic mechanisms.* Epilepsia, 2010. **51**(s5): p. 17-17.

26. R. Ryan, M., J. P. Lowry, and R. D. O'Neill, *Biosensor for Neurotransmitter L-Glutamic Acid Designed for Efficient Use of L-Glutamate Oxidase and Effective Rejection of Interference.* Analyst, 1997. **122**(11): p. 1419-1424.
27. Miele, M. and M. Fillenz, *In vivo determination of extracellular brain ascorbate.* Journal of Neuroscience Methods, 1996. **70**(1): p. 15-19.
28. Galvan, A., Y. Smith, and T. Wichmann, *Continuous monitoring of intracerebral glutamate levels in awake monkeys using microdialysis and enzyme fluorometric detection.* Journal of Neuroscience Methods, 2003. **126**(2): p. 175-185.
29. Dawson, L.A., J.M. Stow, and A.M. Palmer, *Improved method for the measurement of glutamate and aspartate using capillary electrophoresis with laser induced fluorescence detection and its application to brain microdialysis.* Journal of Chromatography B: Biomedical Sciences and Applications, 1997. **694**(2): p. 455-460.
30. Kiba, N., et al., *Chemiluminometric sensor for simultaneous determination of L-glutamate and L-lysine with immobilized oxidases in a flow injection system.* Analytical Chemistry, 2002. **74**(6): p. 1269-1274.
31. Doong, R.-a. and H.-m. Shih, *Glutamate optical biosensor based on the immobilization of glutamate dehydrogenase in titanium dioxide sol–gel matrix.* Biosensors and Bioelectronics, 2006. **22**(2): p. 185-191.
32. Meldrum, B.S., *Glutamate as a neurotransmitter in the brain: review of physiology and pathology.* J Nutr, 2000. **130**(4S Suppl): p. 1007s-15s.
33. Bradford, H.F., *Glutamate, GABA and epilepsy.* Progress in Neurobiology, 1995. **47**(6): p. 477-511.
34. Coyle, J.T., *Glutamate and schizophrenia: beyond the dopamine hypothesis.* Cell Mol Neurobiol, 2006. **26**(4-6): p. 365-84.
35. Fern, R. and C. Matute, *Glutamate receptors and white matter stroke.* Neuroscience Letters, 2019. **694**: p. 86-92.
36. Lau, A. and M. Tymianski, *Glutamate receptors, neurotoxicity and neurodegeneration.* Pflügers Archiv - European Journal of Physiology, 2010. **460**(2): p. 525-542.

CHAPTER TWO

Theory

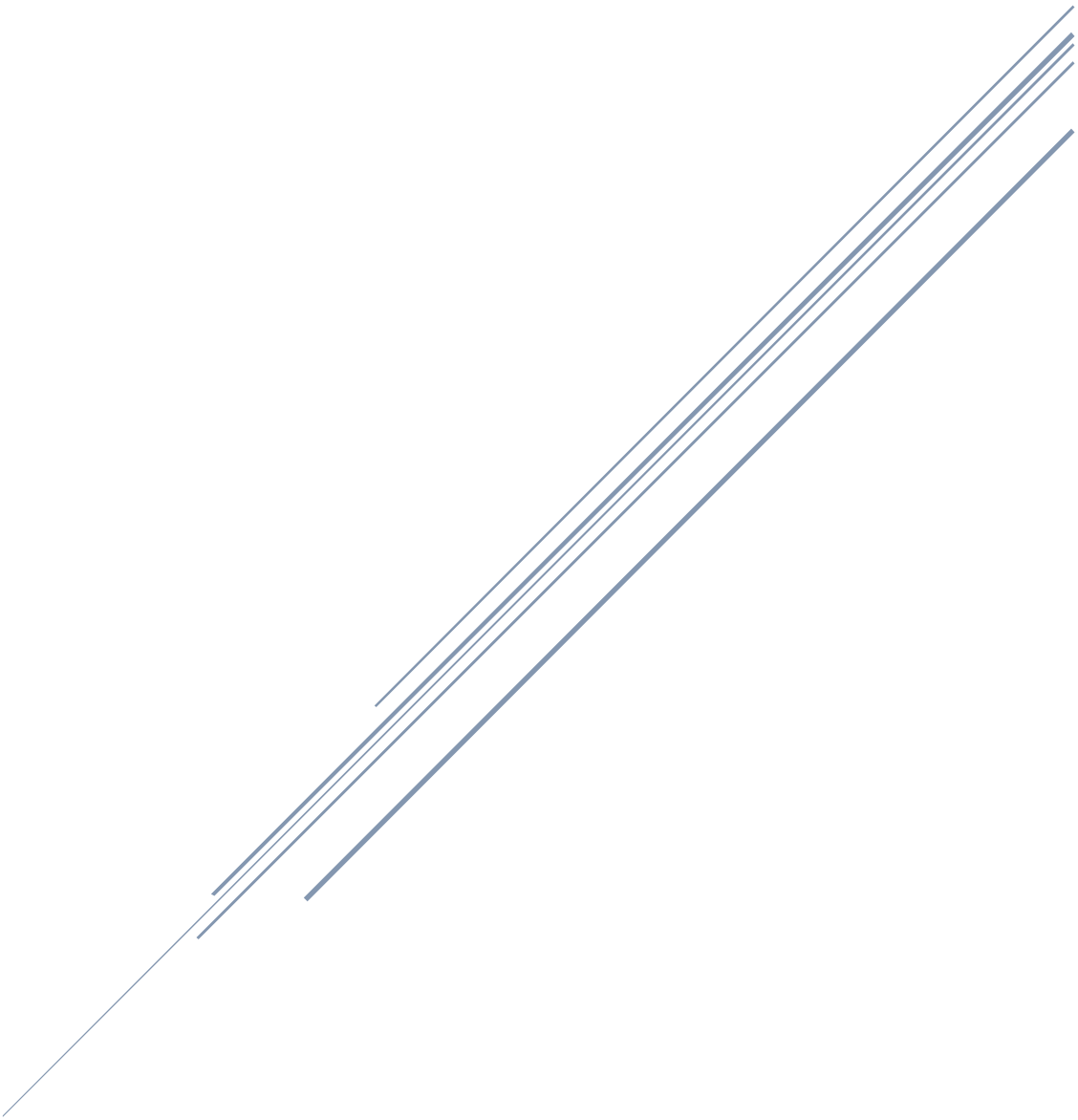

2.1 Biosensors

A biosensor can be defined as a device in which biological recognition units are utilised in conjunction with a transducer to detect the presence of analytes [1] (see Scheme 2.1). The original biosensor was developed by Clark and Lyons in 1962 [2]. The initial design focused on detecting glucose. However, the use of biosensors for biomedical applications spread like wildfire soon after, owing to: the ability to modify the biological recognition unit, the uninterrupted analysis of data and the spatial and temporal resolution achieved to elucidate many biological functions and mechanisms. Biosensors for neurochemical monitoring probes are typically in the micro-meter (μm) diameter range, as this results in minimal tissue damage. Relying on electric current also imparts very high temporal resolution [3]. Therefore, the reliability and cheaply available architecture have enabled biosensors to become integral to many areas of modern life and have been designed for a large degree of medical applications: to detect protein cancer biomarkers [4], implantable pacemaker devices [5], monitor blood levels of compounds like glucose [6], neurochemical monitoring [7] and non-invasive measuring [8].

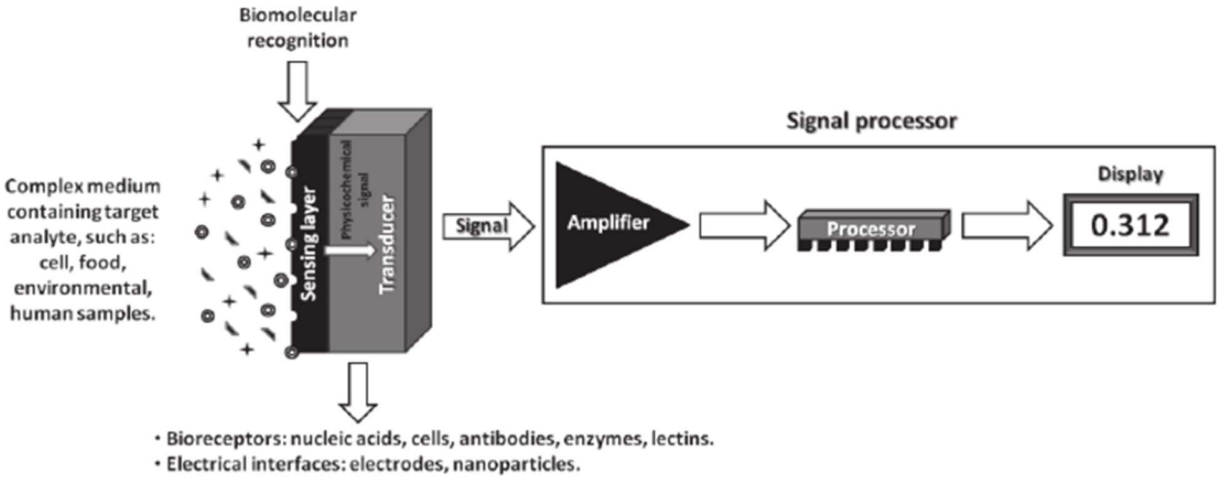

Scheme 2.1: Schematic of general biosensors, where the analyte is bound to the biological recognition unit, measured by the transducer and processed by the detector [9].

Biosensors with enzyme-modified electrodes can be divided into three large groups or families; first, second and third generation. Biosensors are classified into these families based on the overarching sequence of interactions between the analyte and electrode surface (see Scheme 2.2).

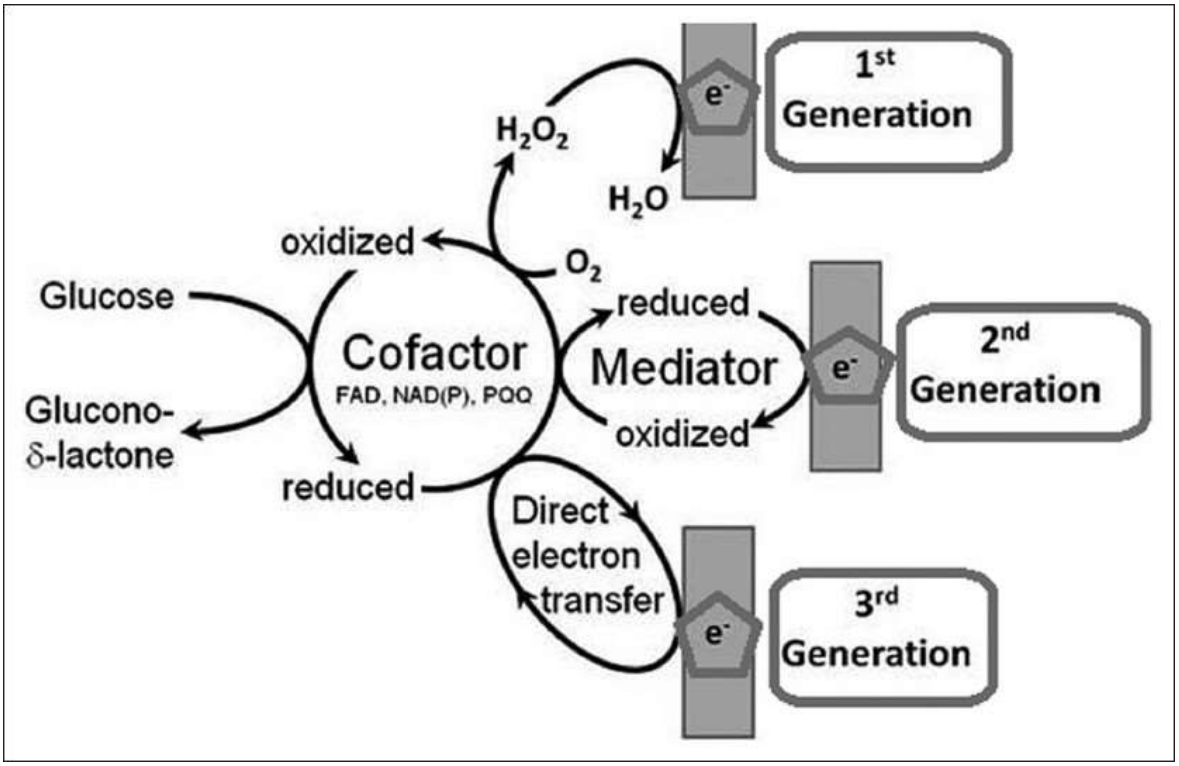

Scheme 2.2: Schematic representation of three generations of glucose biosensor [10].

The first generation of biosensors are concerned with monitoring either the consumption of oxygen [11] or production of hydrogen peroxide (see Scheme 2.2) [12]. First generation biosensors are the most commonly used due to their relative simplicity. For this architecture, the most conventional enzymes immobilised on the electrode surface possess a redox group in order to allow a redox state change to occur during the course of the biochemical reaction. These types of enzymes are classified as oxidases and the nicotinamide adenine dinucleotide (NAD^+) dependent dehydrogenases. These enzymes (like glucose oxidase) will oxidise their substrate thus being converted to an inactive reduced state along with a reduction of the flavin adenine dinucleotide (FAD) redox centre to $FADH_2$. Continuing, the restoration of FAD from $FADH_2$ using dissolved molecular oxygen, typically returning these enzymes to their active state, produces hydrogen peroxide. To end the sequence, hydrogen peroxide is oxidised by an applied potential, which in turn causes an electrical signal [13]. The biochemical reaction can be overseen via the reduction of oxygen (co-substrate) or the oxidation of hydrogen peroxide (product). Designs which monitor the reducing oxygen at the electrode may be the easiest to craft but they are impaired by limited diffusion resulting in slow responses, low accuracy and poor reproducibility. The partial

pressure of molecular oxygen is also difficult to regulate, causing varying amounts to be present in the biosensor's immediate environment [14]. While the design monitoring the oxidation of hydrogen peroxide eliminates these setbacks, the high oxidation potential (≈ +700 mV) will also oxidise other electroactive species with lower oxidation potentials. However, this has been lessened with the use of selectively permeable membranes like cellulose acetate and Nafion® in recent times [14].

Second generation biosensors utilise mediators; a molecule capable of shuttling electrons from the redox centre of the enzyme to the active surface of the electrode, in place of dissolved oxygen for hydrogen peroxide production [14] (See Scheme 2.2). Several factors are needed for a compound to perform as a good mediator. They need to be nontoxic, maintain stability in both redox states, readily react with the reduced state enzyme, be relatively insoluble in aqueous environments and provide good electrochemical properties, such as a low detection potential [15]. Mediators are used because direct electron transfer would typically have kinetically slow electron transfer resolution due to the FAD redox centre being deeply submerged within a protein layer [15]. In this architecture, the oxidised state of the mediator restores the FAD, where dissolved molecular oxygen would have in the previous design, and in turn, is itself reduced. Finishing this process, the mediator in its reduced state is returned to its oxidised state on the surface of the electrode resulting in the measurable electric signal. In some cases, the mediator is found in the electrolyte solution to ease mass transport between the enzyme's active site and the electrode surface. Second generation biosensors removed several of the limitations of the first generation, such as the problems related to the partial pressure of molecular oxygen and the limited diffusion rates. Additionally, as the mediator is returned at relatively low potentials [16], the interference experienced from the high oxidation potential of hydrogen peroxide is no longer an issue. As with most improvements, second generation biosensors also come with their own set of drawbacks. The mediators over time can seep from the electrode surface, making it particularly difficult to design a second generation biosensor suitable for extended *in vivo* monitoring.

Third generation biosensors encompass two architectures; directly coupled enzyme electrodes, which involve equipping an electrode with an enzyme by means of co-immobilising the enzyme and mediator on the electrode surface or, in the neighbouring matrix, like an electroconductive polymer [14] (See Scheme 2.2). These designs have been achieved through

methods such as layer-by-layer deposition of polyelectrolytes, producing hydrogels and confining the enzyme and mediator at the electrode surface via electropolymerisation [17]. Mediators immobilised in this way allow quick transfer of electrons between the enzyme active site and the electrode because of their behaviour as a non-diffusion redox relay station further resulting in a higher current density [13]. A few designs have enabled connection of the enzyme and electrode surface, expanding the performance of the electron transfer. The enzyme being in the immediate vicinity of the mediator has greatly reduced the distance needed to be travelled by the electron(s), giving a much faster response time. Improving on the second generation biosensor's seeping of the mediator, the immobilised mediator in the third generation biosensor has to some extent eliminated this issue. However, there are very few successful third generation systems due to the systems only working for a small groups of enzymes [18].

Evidently, each generation of biosensor was intended to improve on its predecessor in terms of efficiency and selectivity. This has led to advancements in response time, minimising interference and increased intensity of analyte signal. Unfortunately, these improvements have had little effect on overcoming the characteristic shortcomings of the transducers, such as: redox species required to increase current production, no real-time detection *i.e.* inherent latency and, sensitivity to sample matrix effects [19-22]. Recent application of nanomaterials, in particular gold nanoparticles and carbon nanotubes, have been seen to develop biosensors with increased selectivity and signal-to-noise ratios, as well as lower detection limits [13].

2.2 Methods of Immobilisation

As mentioned previously, there is a requirement for the enzyme to be immobilised on the transducer. Immobilisation is the technique employed to fasten the biological recognition unit to the solid support of the electrode, in a matrix, or retained by a membrane [23]. Immobilisation can improve the performance of a biosensor in the following ways: the stability, sensitivity, response time, as well as operational and storage stability, providing greater reproducibility [24]. A large number of techniques have been developed in order to immobilise with each technique influencing the enzyme and its properties [25]. The five main methods of immobilisation are:

Adsorption:

Substances such as alumina, charcoal and silica gel are capable of adsorbing enzymes on the electrode surface. This technique occurs in two forms. The first form, physical adsorption or physisorption, customarily involves the formation of weak van der Waals bonds or more infrequently hydrogen bonds or electrostatic forces. The second form, chemical adsorption or chemisorption, is much stronger than physisorption due to the formation of covalent bonds. This immobilisation can prevent denaturation or deactivation of the enzyme, allowing the catalytic properties of the enzyme to remain intact [26]. A major drawback of such immobilisation is derived from the fact that the enzyme is only adsorbed on the surface with an innate reversible nature of the binding equilibrium, giving it susceptibility to seeping due to minor physical changes in the sample, i.e. pH or temperature or even the substrate itself.

Microencapsulation:

This technique for immobilisation involves "trapping" an inert biomaterial on the transducer [27]. This technique has many advantages such as its close connection of the biomaterial and transducer, it being adaptable and very reliable, and allows the option of using electroconductive molecules to bond the biological recognition unit. As the enzyme is maintained in its natural environment, this affords many enhancements over other methods of immobilisation; it retains a high degree of specificity along with a protection against physical changes such as temperature, pH and substrate concentration. This natural environment will also limit contamination and biodegradation. The difficulties which arise due to the biomaterial on the electrode are the presence of low and high molecular weight substances that may hinder the detection of the analyte and an associated possible diminishing of response time [27]. Each different membrane used to microencapsulate the enzyme will confer specific properties. For example, cellulose acetate excludes proteins and interfering species [28] and Nafion® produces a structure with hydrophilic channels in a hydrophobic matrix as well as repelling anionic interferents [29].

Entrapment:

This is the most utilised technique in modern times. Entrapment is a process in which the biological recognition unit is "trapped" in a conducting polymeric gel matrix grown on the electrode [30]. One of the benefits of growing these polymers, such as poly-*ortho*-phenylenediamine (*PoPD*) (see Figure 2.1) is their ability to be controlled by cycling or stepping the electrode potential. Moreover, this method is simplistic and often results in high enzyme activity. It also enables multiple enzymes

to be immobilised in the matrix in the same layer or via the growth of layers with different enzymes on top of one another. Entrapment as a method provides great stability, permitting ideal conditions for *in vivo* measurements. For example, the thin, insulating, self-sealed *PoPD* permselective membrane is derived from deposition of *ortho*-phenylenediamine, affording an interference-rejection layer from other species [3]. The layers of *PoPD* have been estimated to be as thin as 10-30 nm [31].

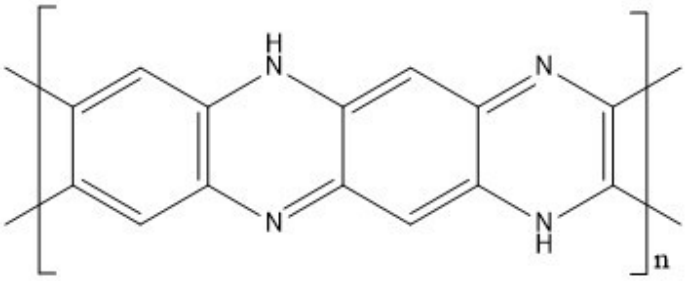

Figure 2.1: Structure of PPD.

There are many other examples of organic polymers capable of immobilisation in this fashion, such as: polyethylenimine (PEI) [32] (see Figure 2.2), polystyrene (Sty) [33] (see Figure 2.3) and poly methyl methacrylate (MMA) [34] (see Figure 2.4). While giving many advantages, entrapment in these matrices produce large diffusional barriers retarding reaction and elongating response time. Pore size distribution tends to be very broad and this has been associated with continuous loss in enzyme activity through the pores.

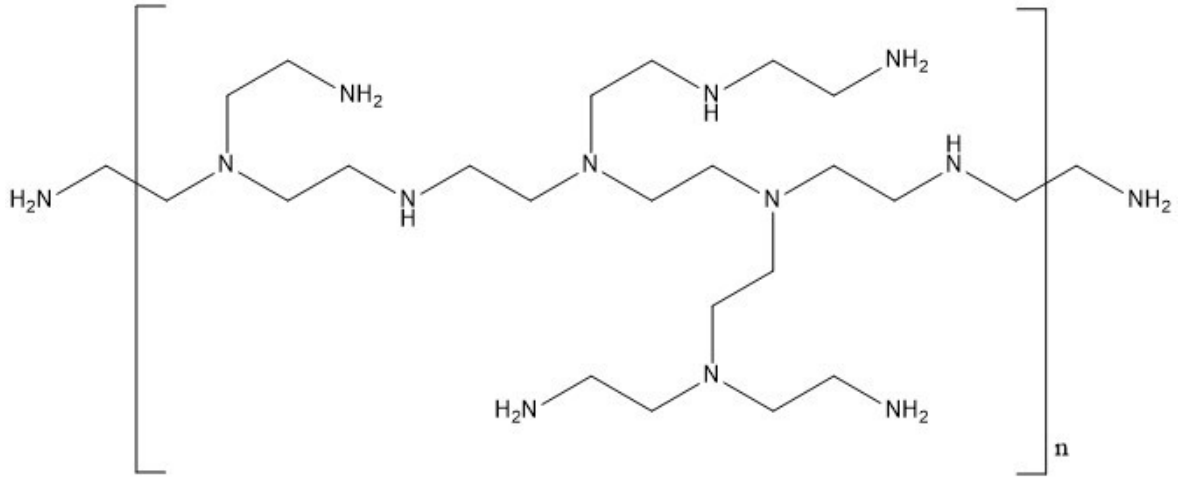

Figure 2.2: Structure of PEI.

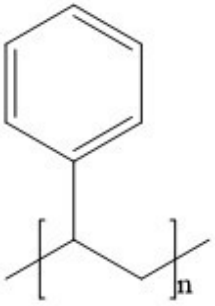

Figure 2.3: Structure of Sty.

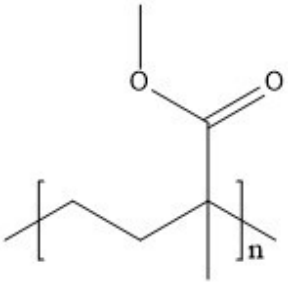

Figure 2.4: Structure of MMA.

Cross-Linking:

Enzymes are commonly very labile and thus a method of stabilisation will need to be employed - this is where cross-linking is involved [35]. This stabilisation occurs via the binding of the biomolecule's non-active sites to a solid support, the transducer, with use of bifunctional agents like glutaraldehyde (GA) [36] (see Figure 2.5). Cross-linking is very harsh on the enzyme, limits the diffusion of the substrate and has poor rigidity. For these reasons, cross-linking is more often applied alongside another method. A very effective coupling for this method is with entrapment, such as in the instance of GA and PEI coupled immobilisation. The carbonyl groups of GA covalently cross-link the amino groups of PEI in order to stabilise the immobilised biomolecule [37].

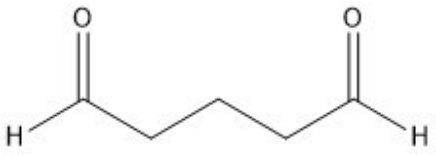

Figure 2.5: Structure of GA.

Covalent bonding:

This technique is the irreversible binding of an enzyme to the transducer with the use of hydrophobic linkers [38]. The non-active nucleophilic groups present in the amino acids of the enzyme are used to form the covalent bond to the transducer, as to not subvert the biological function of the enzyme. This can often have adverse effects on the enzyme activity, so the reaction must be carried out under specific working conditions, like low temperature, neutral pH and low ionic strength [39]. For the most part, this technique is undertaken in two steps. The first is depositing some useful compound on the otherwise inert electrode and, the second is bonding the enzyme to the newly activated electrode surface. The exact mechanism occurring will be dictated by the type of electrode used. Many of the covalent bonds are not entirely stable in use, with 60% loss in activity observed regularly [38]. Immobilisation by means of covalent bonding has demonstrated promise in improving the lifetime of a biosensor [40].

Each method of immobilisation has its own strengths and weaknesses, leading to a large degree of specialisation for each unique biosensor developed [24]. It is often more of an art form to design the optimum method given a particular biological recognition unit and transducer.

2.3 Electroanalysis

Electroanalysis refers to methods of chemical analysis involving the use of electrodes which make electrical contact with an analyte solution. Various electrical parameters of the solution can be measured and which parameter is measured defines the technique. The major methods include: amperometry, voltammetry, potentiometry, conductivity, electrogravimetry and, coulometry [41]. This body of work contains experimental data using amperometry and voltammetry techniques.

Amperometry measures electric current while applying a constant potential. Amperometric testing involves measuring the current that flows, due to the analyte being oxidised or reduced (see Equation 2.1), between an indicator electrode (*i.e.* working electrode) and a second electrode (*i.e.* auxiliary electrode) in reference to a third electrode (*i.e.* reference electrode) (see Figure2. 6). The measured current is correlated to the concentration of the analyte in the solution. A plot of current versus analyte concentration can be generated from these results. Amperometry techniques

include: constant potential amperometry (CPA), chronoamperometry and pulsed Amperometric detection (PAD). [42].

Voltammetry measures current while applying a varied potential. In essence, the set up operates much like amperometry apart from the varying potential (see Figure 2.7). Voltammetry deviates among each other based on the regularly varied potential, which include: cyclic voltammetry (CV), fast cyclic voltammetry (FCV), linear sweep voltammetry (LSV), staircase voltammetry (SCV), normal pulse voltammetry (NPV), differential pulse voltammetry (DPV) and differential normal pulse amperometry (DNPV) [43].

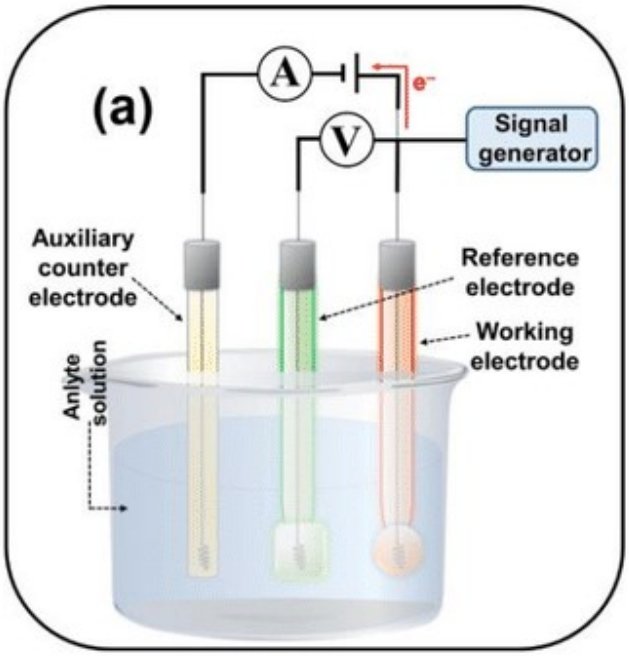

Figure 2.6: Schematic of a typical constant potential amperometry (CPA) set-up [44].

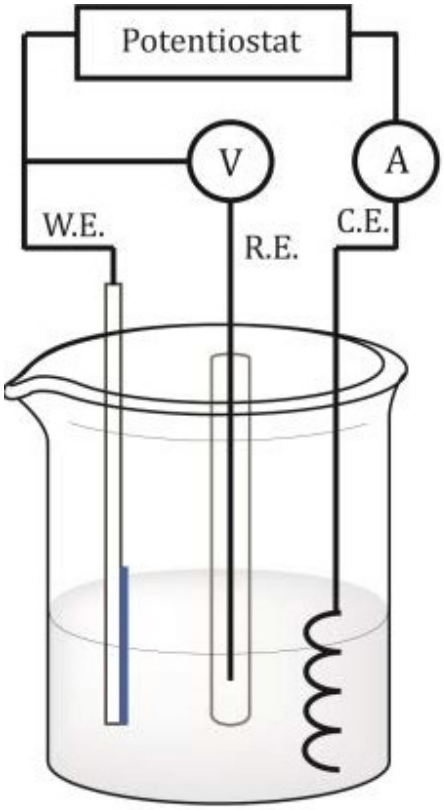

Figure 2.7: Schematic of a typical cyclic voltammetry (CV) set-up [45]. Where W.E. represents the working electrode, R.E. is the reference electrode and C.E. is the counter electrode or auxiliary electrode.

In both amperometry and voltammetry techniques, the species of interest is involved in a redox reaction according to:

$$O + ne^- \rightarrow R \qquad \textbf{(Equation 2.1)}$$

where O represents the oxidised species, ne^- presents the number of electrons transferred and R represents the reduced species.

The Nernst equation [46] (Equation 2.2) must be used to ascertain the concentration of the species of interest and, is as follows:

$$E_{eq} = E^* + \frac{RT}{nF} ln \frac{[O]}{[R]} \qquad \textbf{(Equation 2.2)}$$

where E^* represents the standard electrode potential, R represents the gas constant, T represents the temperature, n represents the number of electrons transferred, F is the Faraday constant, [O] is the concentration of the oxidised species and, [R] is the concentration of the reduced species [46].

2.4 Mass Transport and Interfacial Region

The overall rate of an electrochemical cell reaction is controlled by two factors: the rate of the electron transfer at the working electrode surface and the rate of the analyte's diffusion from the bulk solution to the active surface of the electrode. Mass transfer refers to the processes responsible for the movement of analyte through the system or electrochemical cell. This may occur via three processes: migration, convection and diffusion.

Migration only affects charged species and causes movement of hydrated cations and anions under the influence of an applied potential. In the context of constant potential amperometry, migration's effect is negligible due to the addition of a large excess of the electrolyte. Convection is the transfer of mass through mechanical motion by thermal effects or forced agitation by stirring or other methods. Often a steady-state system is coupled with stirring.

Diffusion is the process of moving an analyte from a region of high concentration to one of a low concentration. The simplest process of diffusion was developed by A. Fick in the 19th century and condensed into Fick's two laws (see Equation 2.3 and 2.4), which state: the molar flux due to diffusion is proportional to the concentration gradient, and the rate of change of concentration at a point in space is proportional to the second derivative of concentration with space.

Fick's first law defines diffusion as:

$$J = - D \frac{\delta c}{\delta x} \qquad \textbf{(Equation 2.3)}$$

Where J represents the flux of the species in question, $\frac{\delta c}{\delta x}$ represents the concentration gradient in the direction of x and D represents the diffusion coefficient.

Fick's second law is concerned with the variation of concentration due to the effect of time. It is defined as:

$$\frac{\delta c}{\delta x} = D\ \frac{\delta^2 c}{\delta x^2} \qquad \textbf{(Equation 2.4)}$$

At the surface of microelectrodes where the currents are small and the analyte does not deplete, conditions found during a constant potential amperometry calibration, the concentration gradient equals zero or in other words is constant with time, *i.e.* a steady-state current is achieved.

Fick's second law was adapted to describe the case for planar electrodes, such as disk geometry, and is referred to as Cottrell's equation [47] (Equation 2.5). Cottrell's equation is given by:

$$I = nFAJ = \frac{nFAD^{1/2}c_{\infty}}{(\pi t)^{1/2}} \qquad \textbf{(Equation 2.5)}$$

where I represents current, n represents the number of electrons transferred, A represents the area of the planar electrode, J represents the flux, D represents the diffusion coefficient, c_{∞} represents the concentration of the analyte in the bulk and, t represents the time. This can be simplified to:

$$I = kt^{-1/2} \qquad \textbf{(Equation 2.6)}$$

where k is just the collection of constants.

The influence of the applied potential occurs in an area between the electrode and bulk solution called the interfacial region. This region is an inherent phenomenon of applying charge to a solution with unique properties such as, charge separation between the electrode and bulk solution with one layer acquiring an excessive positive charge while the other layer acquires a counter charge of the same magnitude and opposite sign [48] (*i.e.* the double layer) which affect diffusion and thus, diffusion coefficient. For this reason, it is vital to minimise the interfacial region. The charge separation in this region is the cause of the capacitance current *i.e.* the background current.

2.5 Microelectrodes

Microelectrodes have been around since the 1920's [49]. There use in electrophysiology enables the recording of neural signals or the electrical stimulation of nervous tissue [50, 51]. There construction typically comprise of insulated inert metal wires, with high Young modulus, such as: tungsten, stainless steel or, platinum-iridium alloy with an exposed conductive tip [52]. The most common geometries of the exposed conductive tips are disks, cylinders, ring and line. This work predominantly used disk geometries with platinum-iridium alloy metal, unless expressly stated otherwise. Cottrell's equation deviation (Equation 2.7) can give the steady-state current in the limiting region for a disk via:

$$I = \frac{nFAD^{1/2}c_{\infty}}{r} = 2\pi nFDc_{\infty} \qquad \textbf{(Equation 2.7)}$$

where r represents the radius, and all over variables follow the representation of Equation 2.5.

2.6 Enzyme Kinetics

Many sophisticated mathematical models have been used to detail the kinetics of enzymes in membranes in use with biosensors with thick and/or conducting layers [3]. Established models like that described by Paul V. Bernhardt [53] and R. Baronas *et al* [54] are beneficial in terms of optimising biosensors incorporating these thick and/or conducting layers due to an advanced insight into the enzymes activities. The pioneers of such research into enzyme kinetics were Leonor Michaelis and Maud Menten, who conducted a fundamental experimental approach undertaken in 1913 [55], in which they demonstrated that the rate of an enzyme-catalysed reaction is proportional to the concentration of the enzyme-substrate complex described by their own Michaelis-Menten equation [56]. This model of enzyme kinetics holds true for biosensors incorporating thin layers [57] . The origin of the concept of enzyme saturation came from Adrian Brown with derivation of the equations for enzyme kinetics from Victor Henri [58]. Chemical reactions and enzyme-catalysed reactions are differentiated from one another via Brown's concept of enzyme saturation: when an enzyme-catalysed reaction reaches its maximum velocity, it is no longer dependent on the concentration of its substrate.

The Michaelis-Menten model is aptly described for a system where a substrate (S) binds reversibly to an enzyme (E), forming an enzyme-substrate complex (ES) and a following irreversible reaction producing the product (P) and regenerating the free enzyme (E). Such a system can be presented as:

$$E + S \rightleftharpoons ES \rightarrow E + P \qquad \textbf{(Equation 2.8)}$$

The Michaelis-Menten equation for the system detailed above is given by

$$v = \frac{V_{max}[S]}{K_M + [S]} \qquad \textbf{(Equation 2.9)}$$

Where; v represents the initial rate observed at total substrate concentration [S], V_{max} denotes maximum velocity of enzyme turnover (this is the limiting rate) and K_M is the concentration at half V_{max}[64].

Arguably the most proficient derivation of this Michaelis-Menten equation originates in 1925 by renowned scientists of their day, George Briggs and J. B. Haldane [59]. A form of it is given by:

$$E + S \underset{k_{off}}{\overset{k_{on}}{\rightleftharpoons}} ES \xrightarrow{k_{cat}} E + P \qquad \textbf{(Equation 2.10)}$$

where, k_{on} symbolises the association rate constant of the binding of the substrate to the enzyme, k_{off} is the reverse of this, the dissociation and k_{cat} is the rate constant of the irreversible generation of the product and return of the free enzyme. The dissociation binding constant (K_D) of the enzyme-substrate is by definition:

$$K_D = \frac{k_{off}}{k_{on}} \qquad \textbf{(Equation 2.11)}$$

In order to progress this derivation, the rate constants are defined, allowing differential rate equations of each chemical species to be defined;

For the substrate:

$$\frac{d[S]}{dt} = -k_{on}[E][S] + k_{off}[ES] \qquad \textbf{(Equation 2.12)}$$

For the free enzyme:

$$\frac{d[E]}{dt} = -k_{on}[E][S] + (k_{off} + k_{cat})[ES] \quad \textbf{(Equation 2.13)}$$

For the enzyme-substrate complex:

$$\frac{d[ES]}{dt} = k_{on}[E][S] - (k_{off} + k_{cat})[ES] \quad \textbf{(Equation 2.14)}$$

Finally, for the product:

$$\frac{d[P]}{dt} = k_{cat}[ES] \quad \textbf{(Equation 2.15)}$$

In the vast majority of systems, the rate equation for ES can be described with a steady-state approximation. This means that the substrate is readily binding to the available sites of the enzyme at the start of the reaction due to low substrate concentration and, the ES concentration will remain relatively constant until a substantial amount of the substrate is consumed. This is observed in the linear relationship found on a graph of substrate concentration *vs.* the rate of the reaction. This is the first of the implicit assumptions in the Michaelis-Menten model of enzyme kinetics [55]. A consequence of this being that the linear region of the graph, in which the product is formed linearly with time, is used to compute the reaction velocities. In terms of biosensors, this can be referred to as the biosensor operating range of concentration [60]. Considering only the initial reaction velocities, [ES] can be assumed constant;

$$\frac{d[ES]}{dt} = 0 \quad \textbf{(Equation 2.16)}$$

$$\Rightarrow k_{on}[E][S] = (k_{off} + k_{cat})[ES] \quad \textbf{(Equation 2.17)}$$

Now, to calculate the rate equation of the product, the concentration of ES must be established. This is achieved through configuration of the equation above, with the understanding that the free enzyme is simply

$$[E] = [E_T] - [ES] \quad \textbf{(Equation 2.18)}$$

With E_T being the total enzyme concentration. Making these adjustments gives

$$k_{on}([E_T] - [ES])[S] = (k_{off} + k_{cat})[ES] \quad \textbf{(Equation 2.19)}$$

$$k_{on}[E_T][S] - k_{on}[ES][S] = (k_{off} + k_{cat})[ES] \quad \textbf{(Equation 2.20)}$$

$$k_{on}[E_T][S] = (k_{off} + k_{cat})[ES] + k_{on}[ES][S] \quad \textbf{(Equation 2.21)}$$

Thus, [ES] can be calculated via

$$[ES] = \frac{k_{on}[E_T][S]}{(k_{off} + k_{cat}) + k_{on}[S]} = \frac{[E_T][S]}{\left(\frac{k_{off}+k_{cat}}{k_{on}}\right)+[S]} \qquad \textbf{(Equation 2.22)}$$

So, the initial rate observed at total substrate concentration is

$$v = k_{cat}[ES] = \frac{k_{cat}[E_T][S]}{(\frac{k_{off} + k_{cat}}{k_{on}})+[S]} \qquad \textbf{(Equation 2.23)}$$

Redefining some of the terms in the Briggs and Haldane derivation, yields the Michaelis-Menten equation. As V_{max} denotes the maximum velocity of enzyme turnover, it is the same as $k_{cat}[ES]$ when the enzyme-substrate complex concentration is equal to the total concentration of the enzyme. K_M can be used to represent the rate constants, thus:

$$V_{max} = k_{cat}[E_T] \; ; \; K_M = \frac{k_{off} + k_{cat}}{k_{on}} \qquad \textbf{(Equation 2.24)}$$

$$\Rightarrow v = \frac{V_{max}[S]}{K_M+[S]} \qquad \textbf{(Equation 2.25)}$$

It should be noted that [S] here represents the free substrate concentration. However, this is usually assumed to be close to the total concentration of the substrate. This is the second of the implicit assumptions, known as the free ligand approximation. This approximation relies on the K_M of a system being much larger than the total enzyme concentration. When this isn't the case, such as a very high-affinity substrate, the Morrison equation [61] must be implemented instead. Michaelis and Menten postulated that the reasoning behind the K_M value always being larger than the K_D value results from the substrate binding and dissociation occurring a lot quicker than the product forming, $k_{cat} << k_{off}$, this being the third and final implicit assumption, the rapid equilibrium assumption. The Briggs and Haldane derivation didn't include an assumption towards the relative k_{cat} and k_{off}, meaning the Michaelis-Menten kinetics are a special specific case of this derivation. Van Slyke and Cullen details the inverse of these conditions [62].

The Michaelis-Menten equation is accompanied by a quintessential graph (see Figure 2.10), with distinct regions as described above.

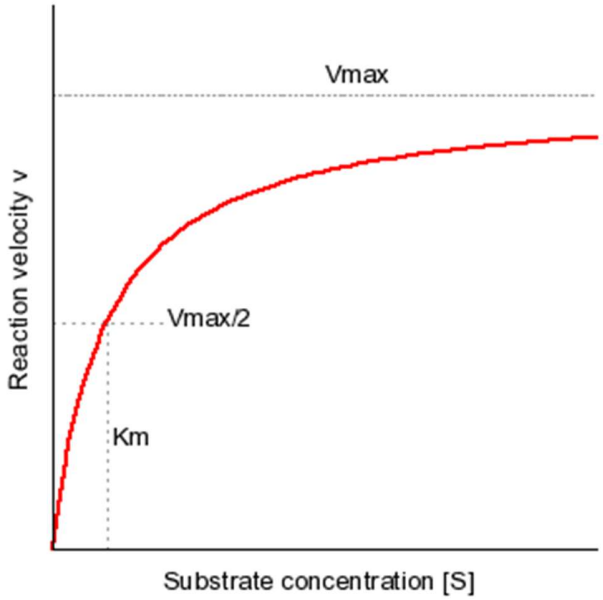

Figure 2.10: A graph of substrate concentration *vs.* the rate of reaction depicting the function predicted by the Michaelis-Menten equation with the kinetic parameters V_{max} and K_M.

From the origin of the plot, the linear region is present. In this region, the reaction rate is proportional to the substrate concentration, as is the current produced. This is because the rate determining step is the electron-transfer event. The slope (m) of this region will yield the sensitivity, given by:

$$\mathrm{m} = \frac{V_{max}}{K_M} \qquad \textbf{(Equation 2.26)}$$

Once enough of the substrate is consumed, V_{max} is actualised, or the plot plateaus as all active sites of the enzyme are being used. Once this has been achieved, the concentration of the substrate will no longer have an effect on the reaction velocity as the enzyme is overwhelmed, unable to catalyse the reaction to a higher degree, and the system is said to be under diffusion-control [63]. This is also referred to as maximum enzyme turnover rate [55]. Here, the maximum current is received.

An insight into the enzyme-substrate affinity comes from the K_M value. More readily bound substrates to the enzyme active sites will yield lower K_M values. Thus, the efficiency of a process can be followed through this value. It will also dictate the limiting current.

2.7 References

1. Darsanaki, R., et al., *Biosensors: Functions and Applications.* J. Biol. Today's World, 2013. **2**(1): p. 53-61.
2. Clark, L.C., Jr. and C. Lyons, *Electrode systems for continuous monitoring in cardiovascular surgery.* Ann N Y Acad Sci, 1962. **102**: p. 29-45.
3. O'Neill, R.D., et al., *Designing sensitive and selective polymer/enzyme composite biosensors for brain monitoring in vivo.* TrAC Trends in Analytical Chemistry, 2008. **27**(1): p. 78-88.
4. Jolly, P., N. Formisano, and P. Estrela, *DNA aptamer-based detection of prostate cancer.* Chemical Papers, 2015. **69**(1): p. 77-89.
5. Grayson, A.C.R., et al., *A BioMEMS review: MEMS technology for physiologically integrated devices.* Proceedings of the IEEE, 2004. **92**(1): p. 6-21.
6. Scognamiglio, V., et al., *Biosensors for effective environmental and agrifood protection and commercialization: from research to market.* Microchimica Acta, 2010. **170**(3): p. 215-225.
7. Zhang, Y., N. Jiang, and A. Yetisen, *Brain Neurochemical Monitoring.* Biosensors and Bioelectronics, 2021. **189**: p. 113351.
8. Micheli, L., D. Moscone, and G. Palleschi, *10 - Biosensors for non-invasive measurements*, in *Biosensors for Medical Applications*, S. Higson, Editor. 2012, Woodhead Publishing. p. 263-300.
9. Andrade, C., et al., *Biosensors for detection of Low-Density Lipoprotein and its modified forms*, in *Biosensors for Health, Environment and Biosecurity*. 2011.
10. Murugaiyan, S.B., et al., *Biosensors in clinical chemistry: An overview.* Adv Biomed Res, 2014. **3**: p. 67.
11. Updike, S.J. and G.P. Hicks, *The enzyme electrode.* Nature, 1967. **214**(5092): p. 986-8.
12. Karyakin, A.A., E.E. Karyakina, and L. Gorton, *Amperometric biosensor for glutamate using prussian blue-based "artificial peroxidase" as a transducer for hydrogen peroxide.* Anal Chem, 2000. **72**(7): p. 1720-3.
13. Putzbach, W. and N. Ronkainen, *ChemInform Abstract: Immobilization Techniques in the Fabrication of Nanomaterial-based Electrochemical Biosensors: A Review.* Sensors (Basel, Switzerland), 2013. **13**: p. 4811-40.

14. Wang, J., *Electrochemical glucose biosensors.* Chem Rev, 2008. **108**(2): p. 814-25.
15. Zhu, Z., et al., *A critical review of glucose biosensors based on carbon nanomaterials: carbon nanotubes and graphene.* Sensors (Basel), 2012. **12**(5): p. 5996-6022.
16. Scheller, F.W., et al., *Second generation biosensors.* Biosens Bioelectron, 1991. **6**(3): p. 245-53.
17. Harper, A. and M.R. Anderson, *Electrochemical glucose sensors--developments using electrostatic assembly and carbon nanotubes for biosensor construction.* Sensors (Basel), 2010. **10**(9): p. 8248-74.
18. Zhang, W. and G. Li, *Third-generation biosensors based on the direct electron transfer of proteins.* Anal Sci, 2004. **20**(4): p. 603-9.
19. Qiu, J.-D., H. Huang, and R.-P. Liang, *Biocompatible and label-free amperometric immunosensor for hepatitis B surface antigen using a sensing film composed of poly (allylamine)-branched ferrocene and gold nanoparticles.* Microchimica Acta, 2011. **174**(1): p. 97-105.
20. Liang, R.P., et al., *A Label-Free Amperometric Immunosensor Based on Redox-Active Ferrocene-Branched Chitosan/Multiwalled Carbon Nanotubes Conductive Composite and Gold Nanoparticles.* Electroanalysis, 2011. **23**(3): p. 719-727.
21. Shi, W. and Z. Ma, *A novel label-free amperometric immunosensor for carcinoembryonic antigen based on redox membrane.* Biosensors and Bioelectronics, 2011. **26**(6): p. 3068-3071.
22. Sin, M.L., et al., *Advances and challenges in biosensor-based diagnosis of infectious diseases.* Expert Rev Mol Diagn, 2014. **14**(2): p. 225-44.
23. Saxena, S., *Applied Microbiology*. 2015. p. 179 - 190.
24. Sassolas, A., L.J. Blum, and B.D. Leca-Bouvier, *Immobilization strategies to develop enzymatic biosensors.* Biotechnol Adv, 2012. **30**(3): p. 489-511.
25. Hanefeld, U., L. Cao, and E. Magner, *Enzyme immobilisation: fundamentals and application.* Chem Soc Rev, 2013. **42**(15): p. 6211-2.
26. Cao, L., *Covalent Enzyme Immobilization*, in *Carrier-bound Immobilized Enzymes*. 2005. p. 169-316.
27. Ambrózy, A., L. Hlavatá, and J. Labuda, *Protective membranes at electrochemical biosensors.* Acta Chimica Slovaca, 2013. **6**(1): p. 35-41.

28. Kanyong, P., et al., *Development of an amperometric screen-printed galactose biosensor for serum analysis.* Anal Biochem, 2013. **435**(2): p. 114-9.
29. Yuan, C.-J., et al., *Eliminating the Interference of Ascorbic Acid and Uric Acid to the Amperometric Glucose Biosensor by Cation Exchangers Membrane and Size Exclusion Membrane.* Electroanalysis, 2005. **17**(24): p. 2239-2245.
30. Rüdel, U., O. Geschke, and K. Cammann, *Entrapment of enzymes in electropolymers for biosensors and graphite felt based flow-through enzyme reactors.* Electroanalysis, 1996. **8**(12): p. 1135-1139.
31. Malitesta, C., et al., *Glucose fast-response amperometric sensor based on glucose oxidase immobilized in an electropolymerized poly(o-phenylenediamine) film.* Analytical chemistry, 1990. **62**(24): p. 2735-2740.
32. Bahulekar, R., N.R. Ayyangar, and S. Ponrathnam, *Polyethyleneimine in immobilization of biocatalysts.* Enzyme Microb Technol, 1991. **13**(11): p. 858-68.
33. Doran, M.M., N.J. Finnerty, and J.P. Lowry, *In–Vitro Development and Characterisation of a Superoxide Dismutase-Based Biosensor.* ChemistrySelect, 2017. **2**(14): p. 4157-4164.
34. Ngounou, B., et al., *Combinatorial synthesis of a library of acrylic acid-based polymers and their evaluation as immobilisation matrix for amperometric biosensors.* Electrochimica Acta, 2004. **49**(22): p. 3855-3863.
35. Gibson, T.D., *Biosensors : the stabilité problem.* Analusis, 1999. **27**(7): p. 630-638.
36. Häring, D. and P. Schreier, *Cross-linked enzyme crystals.* Curr Opin Chem Biol, 1999. **3**(1): p. 35-8.
37. Cerdeira Ferreira, L., et al., *Miniaturized flow system based on enzyme modified PMMA microreactor for amperometric determination of glucose.* Biosensors & bioelectronics, 2013. **47C**: p. 539-544.
38. Trevan, M.D., *Enzyme immobilization by covalent bonding.* Methods in molecular biology (Clifton, N.J.), 1988. **3**: p. 495-510.
39. Rocchitta, G., et al., *Enzyme Biosensors for Biomedical Applications: Strategies for Safeguarding Analytical Performances in Biological Fluids.* Sensors (Basel), 2016. **16**(6).

40. Eggins, B.R., *Chemical Sensors and Biosensors*. Analytical Techniques in the Sciences (AnTs). 2002: Wiley.
41. Dahmen, E.A.M.F., *Electroanalysis: Theory and Applications in Aqueous and Non-Aqueous Media and in Automated Chemical Control*. ISSN. 1986: Elsevier Science.
42. Adeloju, S.B., *AMPEROMETRY*, in *Encyclopedia of Analytical Science (Second Edition)*, P. Worsfold, A. Townshend, and C. Poole, Editors. 2005, Elsevier: Oxford. p. 70-79.
43. Venton, B.J. and D.J. DiScenza, *Chapter 3 - Voltammetry*, in *Electrochemistry for Bioanalysis*, B. Patel, Editor. 2020, Elsevier. p. 27-50.
44. Curulli, A., *Electrochemical Biosensors in Food Safety: Challenges and Perspectives.* Molecules, 2021. **26**: p. 2940.
45. Zeglio, E., *Self-doped Conjugated Polyelectrolytes for Bioelectronics Applications*. 2016.
46. Grimnes, S. and Ø.G. Martinsen, *Chapter 7 - Electrodes*, in *Bioimpedance and Bioelectricity Basics (Third Edition)*, S. Grimnes and Ø.G. Martinsen, Editors. 2015, Academic Press: Oxford. p. 179-254.
47. Bard, A.J. and L.R. Faulkner, *Electrochemical Methods: Fundamentals and Applications*. 2000: Wiley.
48. Schmickler, W., *Electrochemical Theory: Double Layer*, in *Reference Module in Chemistry, Molecular Sciences and Chemical Engineering*. 2014, Elsevier.
49. Hyde, I.H., *A MICRO-ELECTRODE AND UNICELLULAR STIMULATION.* The Biological Bulletin, 1921. **40**(3): p. 130-133.
50. Mendelson, Y., *Chapter 10 - Biomedical Sensors*, in *Introduction to Biomedical Engineering (Third Edition)*, J.D. Enderle and J.D. Bronzino, Editors. 2012, Academic Press: Boston. p. 609-666.
51. Zeuthen, T., *MICROELECTRODES*, in *Encyclopedia of Analytical Science (Second Edition)*, P. Worsfold, A. Townshend, and C. Poole, Editors. 2005, Elsevier: Oxford. p. 25-32.
52. Cogan, S.F., *Neural stimulation and recording electrodes.* Annu Rev Biomed Eng, 2008. **10**: p. 275-309.

53. Rais, R., et al., *Pharmacokinetics of Oral D-Serine in D-Amino Acid Oxidase Knockout Mice.* Drug metabolism and disposition: the biological fate of chemicals, 2012. **40**: p. 2067-73.
54. Baronas, R., F. Ivanauskas, and J. Kulys, *The Effect of Diffusion Limitations on the Response of Amperometric Biosensors with Substrate Cyclic Conversion.* Journal of Mathematical Chemistry, 2004. **35**(3): p. 199-213.
55. Michaelis, L. and M.M. Menten, *The kinetics of invertin action. 1913.* FEBS Lett, 2013. **587**(17): p. 2712-20.
56. Michaelis, L., et al., *The original Michaelis constant: translation of the 1913 Michaelis-Menten paper.* Biochemistry, 2011. **50**(39): p. 8264-9.
57. Zain, Z.M., et al., *Development of an implantable d-serine biosensor for in vivo monitoring using mammalian d-amino acid oxidase on a poly (o-phenylenediamine) and Nafion-modified platinum–iridium disk electrode.* Biosensors and Bioelectronics, 2010. **25**(6): p. 1454-1459.
58. Cornish-Bowden, A., *The origins of enzyme kinetics.* FEBS Letters, 2013. **587**(17): p. 2725-2730.
59. Briggs, G.E. and J.B. Haldane, *A Note on the Kinetics of Enzyme Action.* Biochem J, 1925. **19**(2): p. 338-9.
60. Thévenot, D.R., et al., *Electrochemical biosensors: recommended definitions and classification.* Biosens Bioelectron, 2001. **16**(1-2): p. 121-31.
61. Morrison, J.F., *Kinetics of the reversible inhibition of enzyme-catalysed reactions by tight-binding inhibitors.* Biochim Biophys Acta, 1969. **185**(2): p. 269-86.
62. Van Slyke, D.D. and G.E. Cullen, *THE MODE OF ACTION OF UREASE AND OF ENZYMES IN GENERAL.* Journal of Biological Chemistry, 1914. **19**(2): p. 141-180.
63. Baes, C.F., R.A. Zingaro, and C.F. Coleman, *The Extraction of Uranium(VI) from Acid Perchlorate Solutions by Di-(2-ethyl-hexyl) -Phosphoric Acid in n-Hexane.* The Journal of Physical Chemistry, 1958. **62**(2): p. 129-136.

CHAPTER THREE

Experimental

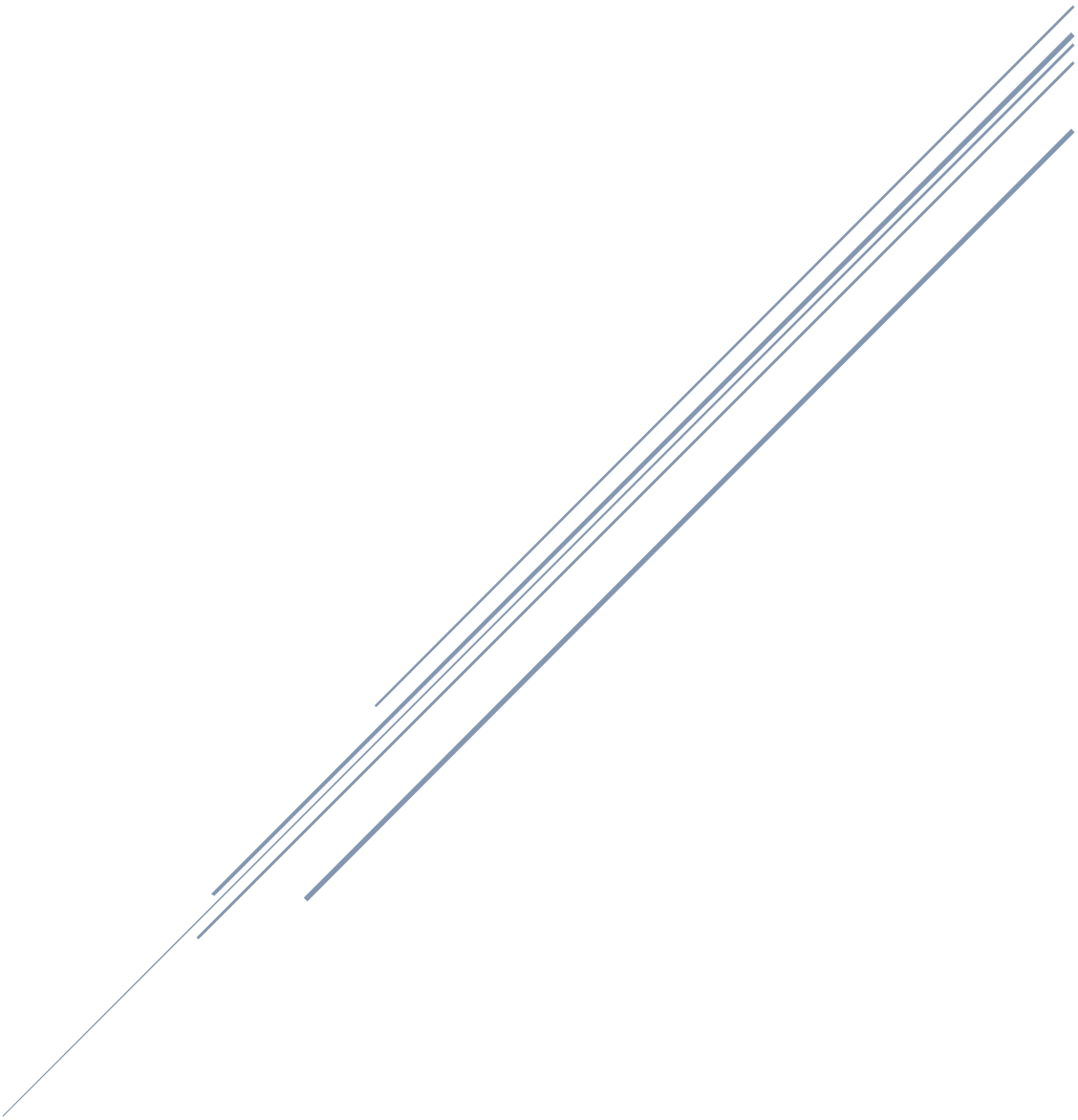

Chapter Three – Experimental

3.1 Reagents and solutions

All reagents were supplied by Sigma-Aldrich Ireland Ltd. (Dublin), unless otherwise stated. General chemicals included (γ)-Aminobutyric acid (99%), L-glutamic acid (monosodium salt, 99%), NADP (disodium salt, ≥ 97%) dopamine (hydrochloride), 5-hydroxytryptamine (5-HT), L-glutathione (oxidised form), dehydroascorbic acid (DHAA), uric acid (UA, potassium salt), 3,4-dihydroxyphenylacetic acid (DOPAC), homovanillic acid (HVA), 5-hydroxyindoleacetic acid (5-HIAA), L-tyrosine, L-cysteine, L-tryptophan and ascorbic acid (AA). Specific reagents used in biosensor manufacture were the immobiliser styrene (Sty, 99%), the enzymes GABase (GAB, lyophilized powder, from *Pseudomonas fluorescens*), L-glutamate oxidase (GluOx, EC 1.4.3.11, recombinant *E. coli*, 2B Scientific Ltd., Oxford, UK), the cross-linking agent glutaraldehyde (GA, Grade 1, 25%), and the stabilisers bovine serum albumin (BSA, fraction V from bovine plasma) and polyethylenimine (PEI, 80% ethoxylated). Poly (*ortho*-phenylenediamine) (P*o*PD, 1,2-diaminobenzene, ≥ 99%) was used to create a thin self-sealing permselective underlayer (see Biosensor fabrication).

All solutions were prepared in Milli-Q® water (18.2 MΩ cm). In-vitro experiments were performed in phosphate buffered saline (PBS, 1000 mL stock), pH 7.4 (137 mM NaCl, 2.7 mM KCl and 10 mM phosphate buffer solution, prepared from commercial tablets), except for pH studies where adjustments were made using either NaH_2PO_4 or NaOH and, addition of L-glutameric acid, α-ketoglutarate and NADP to the bulk (see Section 4.2 for details). Solutions used in biosensor manufacture (*o*-PD monomer, 300 mM in N_2-saturated PBS; GAB 5 U/mL, GAB 50 U/mL, GAB 100 U/mL in 75 mM phosphate buffer, pH 7.2, containing 25% (v/v) glycerol; GluOx, 100 U/mL in 0.02 M potassium phosphate buffer, pH 7.4; BSA, 1%; GA, 0.1%; PEI, 1%) and, calibration (GABA, 0.1 M) and (L-glutamic acid, 0.1 M) were prepared fresh on the day of use. Interferent solutions were prepared as required, and depending on stability either used fresh (e.g. AA) or stored frozen (−80 °C) between use.

3.2 Biosensor Fabrication

Pt/Ir disc (Pt/Ir_D) and cylinder (Pt/Ir_C) electrodes were constructed using 5 cm lengths of Teflon®-coated Pt/Ir (90%/10%) wire (127-μm bare diameter, 203-μm coated diameter, Science Products GmbH, Hofheimer Straße 63, D-65719 Hofheim, Germany). Using a new scalpel blade a section of the Teflon® insulation was striped back under a stereo microscope (Olympus SZ51, Mason Technology Ltd., Dublin), exposing approximately 2 mm of wire which was then soldered into a gold clip (*In vitro* - Fine Science Tools GmbH, 69115 Heidelberg, Germany; *In vivo* - Plastics One, Roanoke, VA, USA). This provides both electrical contact and rigidity to allow connection to the potentiostat. The active surface was then created by carefully cutting the opposite end of the wire to create a disc surface. Cylinder electrodes were prepared by subsequently removing a 1 mm or 4 mm portion of the insulation. A macroelectrode platinum (Pt_D) with a 1.6 mm diameter were also utilised (MF2013 - BASi® Research Products, 2701 Kent Avenue, West Lafayette, USA). These electrodes were polished prior to each use, starting with 15-μm coarse diamond polish for approx. 20 minutes, then a 3-μm fine diamond polish for approx. 20 minutes, and finally finished with a 1-μm very fine diamond polish for approx. 20 minutes. Electrodes were subsequently rinsed with purified water.

Various chemical layers were then used to modify this surface in order to facilitate enzyme immobilisation, interference rejection, etc. The first of these was P*o*PD which was electrochemically grown from a solution of *o*-PD monomer (300 mM in N_2 saturated PBS) following a previously reported procedure [1, 2]. This layer was allowed to dry for a minimum of 3 h at room temperature (*ca.* 21 °C) before proceeding with the sequential layering of the other reagents using a dip-adsorption method [3]. Briefly, the Pt/P*o*PD electrodes were first dipped into the immobiliser Sty (*ca.* 0.5 s), and then consecutively dipped (*ca.* 0.5 s each) into GluOx (100 U/mL), GAB (5 U/mL, 50 U/mL, 100 U/mL), a BSA:GA (1.0:0.1%) mixed solution, and PEI (1%), with 4 min drying between each GluOx/GAB/BSA:GA/PEI or differing sequential (see Section 4.2 for further details) coatings. Further drying and/or layering was performed in order to optimise the design in terms of sensitivity and ease of construction (see Section 4.2 (GAB) & Section 5.2 (Glu)). All sensors were stored overnight at 4 °C before being calibrated [3, 4].

3.3 Calibrations, stability and biocompatibility

GABA (0-10 μM, 0-60 μM, 0-10 mM) and L-Glutamate (0–10 mM) calibrations were performed using constant potential amperometry (CPA) in a standard three-electrode glass cell containing 15 mL of air-equilibrated PBS at room temperature (21–23 °C), unless otherwise stated. Reference and auxiliary electrodes were a saturated calomel electrode (SCE) and Pt wire respectively. A potential of +700 mV (*vs.* SCE) was used for monitoring H_2O_2 oxidation [1]. Sensors were allowed to settle for *ca.* 3 h before commencing calibrations. These were performed by injecting aliquots of the analyte into the buffer solution every 4 min (arbitrarily chosen). Each injection was followed by immediate stirring/mixing (*ca.* 5 s), with the current change measured immediately prior to the next injection. A GABA cyclic voltammetry (CV) investigation was performed under similar conditions. Scan rate was set to 50 mV/s for 10 scans. Potential window was set to -0.25 – 1 V.

Interferent testing typically commenced with AA (the principal endogenous interferent [5, 6]) and differed from GABA and glutamate calibrations in that the injection of aliquots of the respective chemicals was generally performed every 10 min with stirring/mixing lasting *ca*. 10 s. A similar protocol was followed for interferent testing in the presence of glutamate (100 μM).

The oxygen-dependence study was performed in PBS which was de-aerated by vigorously purging with N_2 for at least 30 min before commencing recording. Thereafter a N_2 cloud was maintained above the solution. An aliquot of L-glutamate was introduced into the cell to produce the desired concentration (10, 100, 200 or 500 μM), followed by the addition of standard aliquots (+313 μL, +319 μL, etc.) of a saturated O_2 solution (100%, 1200 μM), yielding 25 μM O_2 increments over the range 0–200 μM every 4 min, with a brief stirring/mixing period (*ca*. 5 s) after each addition.

Temperature controlled experiments were performed in a jacketed cell (ALS Ltd, IJ Cambria Scientific Ltd, Llanelli, UK), attached to a thermostatically controlled circulating water bath (Julabo Corio CD-BC4, Fisher Scientific, Dublin, Ireland). The temperature of the PBS was continuously recorded throughout the calibration using a commercial T-type thermocouple (AD Instruments Ltd., Oxford, UK) connected to a temperature pod (ADInstruments Ltd.) and interface system (eDAQ eCorder®, Green-Leaf Scientific, Dublin, Ireland). If required, adjustments were made to the bath temperature controller to maintain the desired temperature in the cell.

Stability/shelf-life was determined by comparing the response of the same and different batches of biosensors stored dry at 4 °C between calibrations performed on days 1, 14 and 28. For biocompatibility testing sensors were carefully placed in moist brain tissue and stored at 4 °C between calibrations on days 1 and 14.

3.4 Instrumentation, software and data analysis

A custom designed low-noise potentiostat (Biostat IV, ACM Instruments, Cumbria, UK) was used for all electrochemical experiments. Data acquisition was performed with a Dell notebook PC (*in vitro*) or Apple iMac® (*in vivo*), a PowerLab® 8/30 (ADInstruments Ltd) or eDAQ e-corder (Green-Leaf Scientific) interface system, and LabChart® for Windows (Version 6, ADInstruments Ltd.), eChem (v2.1.16, eDaq Ltd., Sydney, Australia) or eDAQ Chart (Version 5.5.23, eDAQ Pty Ltd., NSW 2112, Australia). GraphPad Prism (Version 8.2.0; GraphPad Software Inc., CA, USA) was used for all data analysis and graphical presentations. Data is expressed as mean ± SEM, where n denotes the number of sensors. All signals were baseline subtracted and calibration curves were analysed to calculate the enzyme kinetic parameters V_{MAX} and K_M using either Michaelis-Menten or Michaelis-Menten Hill-type equations [1, 7], as determined by the best non-linear regression fit. The linear range was defined by $K_M/2$ [8, 9] and sensitivity (Linear Region Slope, LRS) was determined using linear regression analysis. Biosensor efficiency (BE%) normalises the biosensor response with respect to H_2O_2 sensitivity and was calculated as LRS x 100/Slope(H_2O_2). It reflects the major enzyme parameters determining the biosensor response to glutamate (*i.e.* loading of active enzyme and enzyme affinity) independent of H_2O_2 sensitivity [8, 10]. K_MO_2 and $[O_2]_{90\%}$ were calculated based on previously defined criteria [9, 10]. Statistical significance tests were performed using t-tests (two-tailed paired or unpaired where appropriate) or one-way ANOVA (with Tukey's post-hoc analysis). Values of $P < 0.05$ were considered to indicate statistical significance.

3.5 Surgical procedures

Male Wistar rats (data from 10 animals, typically 250–350 g; Charles River Laboratories International, Inc., UK) were anesthetised with Isoflurane (4% in air for induction, 1.5–3% for

maintenance; Bioresource Unit (BRU), Maynooth University) using a Univentor 400 Anaesthetic Unit (AgnTho's AB, Sweden). Once surgical anaesthesia was established the animals were placed in a stereotaxic frame and the biosensors implanted following a previously reported method [11, 12]. The level of anaesthesia was checked regularly (pedal withdrawal reflex). Coordinates for striatum and prefrontal cortex, with the skull levelled between bregma and lambda, were AP + 1.0, M/L ± 2.5 and D/V −5 and AP + 3.2, M/L ± 0.8 and D/V −4.2 respectively. A reference electrode (8T Ag, 200-μm diameter; Advent Research Materials, Suffolk, UK) was implanted in the cortex and an auxiliary electrode (8T Ag wire) wrapped around a stainless steel support screw (Fine Science Tools GmbH) placed in the skull. All electrode connectors (gold clips) were placed in a six pin multi-channel electrode pedestal (MS363, Plastics One, Roanoke, VA, USA), which was secured to the skull using dental acrylate (Dentalon Plus, AgnTho's AB) and four support screws. Saline (0.9%) and analgesic (Buprecare®; BRU, Maynooth University) were administered immediately following surgery. Animals were then allowed to recover for several hours in a thermostatically controlled cage (Thermacage MkII, Datesand Ltd, Manchester, UK), and assessed for good health according to published guidelines [13], regularly throughout the day of surgery, and subsequently at the beginning of every day. All *in vivo* work was carried out with approval from Maynooth University Research Ethics Committee (BSRESC-2017-019), and under license (B100/2205 and HPRA AE19124/PO19) in accordance with the European Communities Regulations 2002 (Irish Statutory Instrument 566/2002 – Amendment of Cruelty to Animals Act 1876), and Part 5 of the European Union (Protection of Animals Used for Scientific Purposes) Regulations 2012 (S.I. No. 543 of 2012).

3.6 Experimental Conditions *In Vivo*

For experiments, animals were singly housed in Raturn® sampling cage systems (BASi, West Lafayette, IN, USA) which allowed free movement of the animal during recording (see Figure 3.1). All experiments were performed in the animal's home bowl in a temperature-controlled experimental facility with a 12 h light/dark cycle (lights on at 07:00) with access *ad libitum* to food and water. The implanted sensors in each animal were connected directly to the potentiostat in the late afternoon *via* the six pin electrode pedestal using a flexible screened six core cable (363-363 6TCM, Plastics One). The potential (+700 mV) was then applied and each animal was given at least 12 hours before experiments were started to allow them to become

reaccustomed to being tethered. A low-pass digital filter (50 Hz cut-off) was used to eliminate mains AC noise and all data was recorded at either 4 or 40 Hz depending on the experiment. Movement was registered using a PIR detector (Gardscan QX PIR, Gardiner Technology, Queensway, Rochdale, OL11 1TQ, UK) modified in-house with a microprocessor to enable enhancement of the resolution of the sensor thereby registering more movement. Restraint stress was carried out using a form of wrap restraint which involved using a hand towel to immobilise the animal in the home bowl for a period of 5 min.

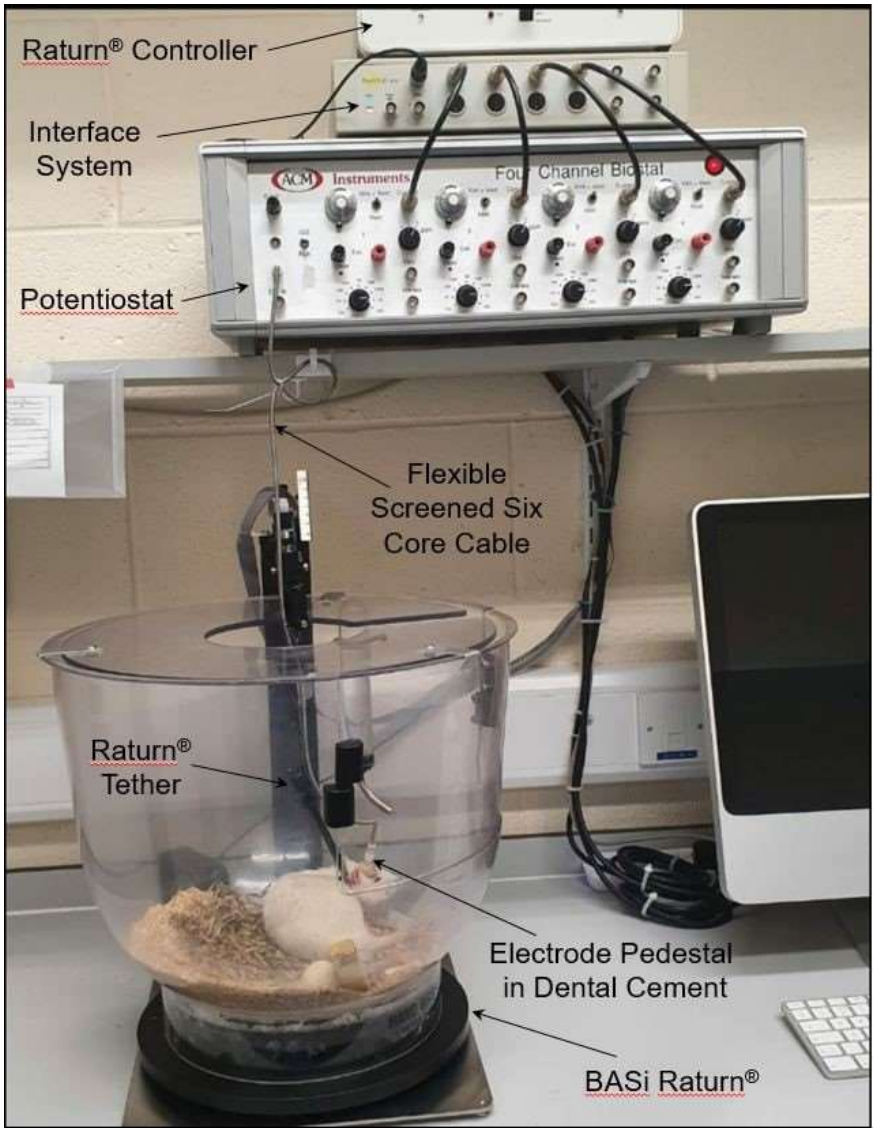

Figure 3.1: Picture showing an implanted tethered animal housed in its home bowl (Raturn® sampling cage system) and connected to the potentiostat (Biostat IV) and data acquisition interface system (PowerLab® 8/30).

3.7 References

1. Lowry, J.P., *Partial characterization in vitro of glucose oxidase-modified poly(phenylenediamine)-coated electrodes for neurochemical analysis in vivo.* Electroanalysis, 1994. **6**(5-6): p. 369-379.
2. Killoran, S.J. and R.D. O'Neill, *Characterization of permselective coatings electrosynthesized on Pt–Ir from the three phenylenediamine isomers for biosensor applications.* Electrochimica Acta, 2008. **53**(24): p. 7303-7312.
3. Baker, K.L., et al., *Characterisation of a Platinum-based Electrochemical Biosensor for Real-time Neurochemical Analysis of Choline.* Electroanalysis, 2019. **31**(1): p. 129-136.
4. Doran, M.M., N.J. Finnerty, and J.P. Lowry, *In–Vitro Development and Characterisation of a Superoxide Dismutase-Based Biosensor.* ChemistrySelect, 2017. **2**(14): p. 4157-4164.
5. Brown, F.O. and J.P. Lowry, *Microelectrochemical sensors for in vivo brain analysis: an investigation of procedures for modifying Pt electrodes using Nafion®.* Analyst, 2003. **128**(6): p. 700-705.
6. Kulagina, N.V., L. Shankar, and A.C. Michael, *Monitoring glutamate and ascorbate in the extracellular space of brain tissue with electrochemical microsensors.* Analytical Chemistry, 1999. **71**(22): p. 5093-5100.
7. Chou, T.-C., *Derivation and properties of Michaelis-Menten type and Hill type equations for reference ligands.* Journal of Theoretical Biology, 1976. **59**(2): p. 253-276.
8. Ford, R., S.J. Quinn, and R.D. O'Neill, *Characterization of Biosensors Based on Recombinant Glutamate Oxidase: Comparison of Crosslinking Agents in Terms of Enzyme Loading and Efficiency Parameters.* Sensors (Basel), 2016. **16**(10).
9. McMahon, C.P., et al., *Oxygen tolerance of an implantable polymer/enzyme composite glutamate biosensor displaying polycation-enhanced substrate sensitivity.* Biosensors and Bioelectronics, 2007. **22**(7): p. 1466-1473.
10. O'Neill, R.D., et al., *Designing sensitive and selective polymer/enzyme composite biosensors for brain monitoring in vivo.* TrAC Trends in Analytical Chemistry, 2008. **27**(1): p. 78-88.

11. Baker, K.L., F.B. Bolger, and J.P. Lowry, *A microelectrochemical biosensor for real-time in vivo monitoring of brain extracellular choline.* Analyst, 2015. **140**(11): p. 3738-3745.
12. Finnerty, N.J., et al., *An investigation of hypofrontality in an animal model of schizophrenia using real-time microelectrochemical sensors for glucose, oxygen, and nitric oxide.* ACS Chemical Neuroscience, 2013. **4**(5): p. 825-831.
13. Carstens, E. and G.P. Moberg, *Recognizing pain and distress in laboratory animals.* Ilar Journal, 2000. **41**(2): p. 62-71.

CHAPTER FOUR

In Vitro Development of Gamma-Aminobutyric Acid (GABA) Biosensor

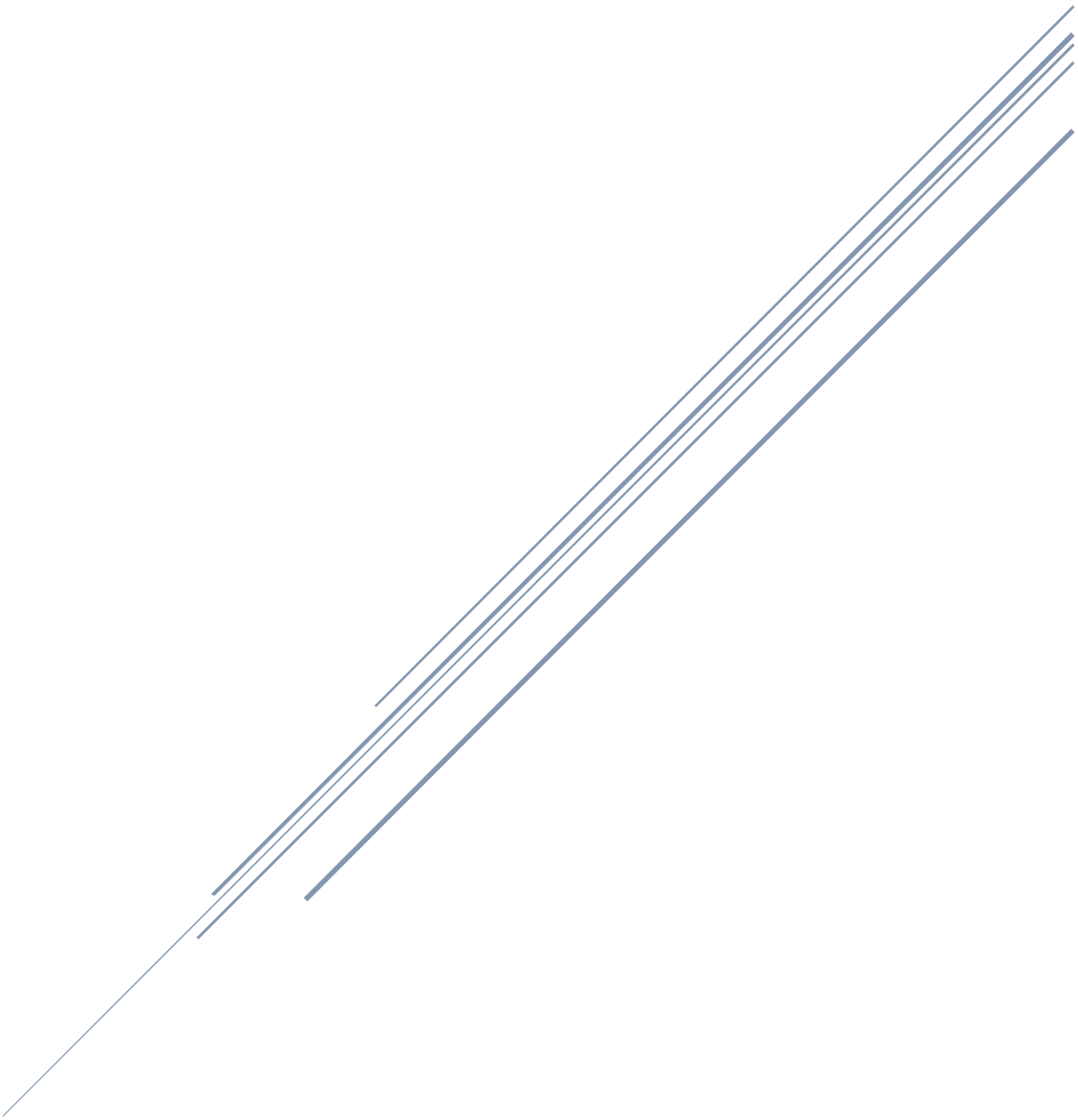

4.1 Introduction

Initially synthesised in 1883, gamma-aminobutyric acid (GABA) was identified as purely a metabolic product of plants and microbes. It wasn't until nearly 70 years later that GABA was found to be an integral part of the mammalian central nervous system (CNS) [1]. A mere nine years following this discovery, GABA was first seen at an inhibitory synapse of crayfish/lobster muscle fibres stimulating the inhibitor nerve [2]. While some research has gone into understanding GABA in terms of its chemistry and function as a neurotransmitter (previously discussed in Section 1.3), it hasn't received anywhere as much investigation in the scientific community as melatonin which may be one of the reasons it's not largely known in the public's eye. There does however seem to be a shift in the public's perception of GABA, such as adding it to food [3]. However, research has confirmed it to be the major inhibitory neurotransmitter acting on approximately one third of all neurosynapses of mature mammalians [4, 5]. GABA basal concentration has been previously reported at levels up to 0.5 μM [6, 7], but not at all, or only in trace amounts, in peripheral nerve tissue such as sciatica nerve, splenic nerve, and sympathetic nerve, or in any other peripheral tissue such as the liver, spleen and heart [8]. The importance of this vital biosynthesised chemical and its associated mechanisms has been linked to sleep [9], mood [10], pain perception [11] and overall health. Dysregulation of GABA has been linked to temporal lobe epilepsy [12, 13], Parkinson's disease [14], Huntington's disease [15] and an array of psychiatric diseases such as depression , anxiety disorders [16-18], alcohol use disorder, spastic diseases and idiopathic hypersomnia [18], and schizophrenia [19, 20]. A further insight to GABA and its mechanisms could enhance treatments of these various illnesses, or possibly assist in the development of new pain management regimens.

Interestingly, GABA acts primarily as an excitatory neurotransmitter in the immature mammalian brain development [21-24]. Prior to the formation of synaptic contacts, GABA synthesised by neurons assumes the role of both autocrine and paracrine signalling mediators [25]. During this stage of development GABA is responsible for the growth of progenitor cells [26, 27], the migration [28], differentiation [29, 30], the elongation of neurites [31], the formation of synapses [32], and the growth of embryonic and neural stem cells [33].

With such importance on this neurotransmitter, various methods have been employed to detect and monitor it, for instance; colorimetric [34], on-line sensor in a flow cell [35], an acoustic biosensor [36], carbon film electrode [37], microdialysis [38, 39], and amperometric biosensors [40]. There have been several publications with the use of immunosensors (*i.e.* biosensors using

antibodies as the biological recognition unit) to detect GABA [41-43]. The development of immunosensors offer potential but they all suffer for a lack of temporal response, on the order of seconds and sometimes minutes when sub-second responses are required for real-time neurochemical insight of neurotransmitters. The biggest challenge facing the development of an accurate and timely method of detection and monitoring of GABA is the lack of a direct *in vivo* detection method and consequently, a lack in temporal and spatial resolution for its function as a neurotransmitter. The table below illustrates the limitations of previously release work for neurochemical monitoring of a neurotransmitter.

Table 4.1: Detailing the research efforts of various groups to develop a sensor capable of monitoring GABA and highlighting the shortcomings for *in vivo* monitoring.

Author	Year	Technique	Limit of Detection	Temporal Resolution	*In Vivo* Application
F. Mazzei, et. al	1996	Amperometric biosensor	20 μM	2 min	Not viable
O. Niwa, et. al	1998	On-line sensor in flow cell	0.1 μM	Approx. 7 min	Not viable
A. Zhou & J. Muthuswamy	2004	Acoustic biosensor	38 μM	N/A	Not viable
N. Sekioka, et. al	2008	Electron cyclotron resonance	30 nM	2 min	Not viable
I. Kagen, et. al	2008	Gas chromatography	0.2 nM	28 min	Not viable
A. Jinnarak & S. Teerasong	2016	Colorimetric method based on silver nanoparticles	$\approx$ 560 μM	1 min	Not viable

GABase and Glutamate Oxidase working in tandem, suggests a potential elimination of these limitations. This body of work details the aim of producing a first generation biosensor *i.e.* involves the consumption of O_2 or production of H_2O_2. While there has been previous reports of

GABA oxidase isolation from Prof. Mastumoto's research group (Department of Applied Biology, Kanagawa Institute of Technology, Japan) [44], it is not commercially available. Additionally, Dr. Hitoshi Kusakabe (Enzyme-Sensor Co. Ltd.), an enzyme expert and the person who originally isolated glutamate oxidase, has little faith in the currently published works regarding GABA oxidase isolation (personal communication with Prof. Lowry). In his view it has neither the stability nor specific activity required for biosensor development. He also found that with other potential sources it could not be found in sufficient quantities. Due to this, a triple enzyme system was utilised. GABase, a commercially available dual enzyme was employed for the initial steps in the system. The reaction scheme was as follows:

$$GABA + \alpha\text{-}ketoglutarate \xrightarrow{GABase} L\text{-}glutamate + succinic\ semialdehyde \qquad (1)$$

After this reaction has taken place, an underlying glutamate biosensor is capable of converting the glutamate produced into hydrogen peroxide, which can be oxidised to produce an output signal.

$$L\text{-}glutamate + O_2 + H_2O \xrightarrow{GluOx} \alpha\text{-}ketoglutarate + NH_3 + H_2O_2 \qquad (2)$$

$$H_2O_2 \xrightarrow{+700\ mV\ vs.SCE} O_2 + 2H+ + 2e^- \qquad (3)$$

An alternative method also exists following equation (1):

$$Succinic\ semialdehyde + NADP^+ + H_2O \xrightarrow{ALDH5A1} succinate + NADPH \qquad (4)$$

$$NADPH \xrightarrow{+700\ mV\ vs.\ SCE} NADP^+ + 2H^+ + 2e^- \qquad (5)$$

This development of a first generation biosensor for neurochemical monitoring of GABA relies on earlier work targeting glutamate [45, 46] and further development in Chapter 5.

4.2 Results and Discussion

This section details the different steps involved in the design and development of the GABase-based biosensor. The aim was to find an optimal design which maximised the biosensor's sensitivity.

4.2.1 Unit Activity

The unit activity of an enzyme solution has been shown to have a significant effect on the operation of a biosensor [47]. This was the first issue to be addressed in the development of a biosensor capable of monitoring GABA. In order to tackle this issue, an arbitrary biosensor design needed to be selected. The design was based on previously published work by Prof. Lowry's research group targeting glutamate [45, 46], various other neurochemicals [47-51] and further refinement of a glutamate biosensor (detailed development presented in Section 5.2.1). The design chosen was:

Pt/Ir_D (90:10) - Sty-[Glu (100 U/mL –GAB (Figure 1) –BSA (1.0%):GA(0.1%) –PEI (1%)]$_{15}$

All other component concentrations remain as stated above, unless stated otherwise (this denotation is laid out in Section 3.2) and the unit activity of the GAB solution was varied (see Figure 4.1). Glutamate was required in the bulk in order to facilitate the production of glutamate to generate the signal (see reaction scheme (*1-3*) in Section 4.1). No signal output from the altered unit activities was observed (see Figure 4.2). No significant difference was observed across the varied unit activity ($P = 0.1935$ for 5 U/mL *vs.* 50 U/mL, $P = 0.0511$ for 5 U/mL *vs.* 100 U/mL, $P = 0.9738$ for 50 U/mL *vs.* 100 U/mL, one-way ANOVA). Negative values can be attributed to baseline drift or random noise [49, 52] and applies to all figures going forward. It was concluded that perhaps the order of the GAB in the underlying Glu biosensor was hindering the operation of the biosensor. The unit activity was to be investigated again once an appropriate order of GAB in the sequence was determined.

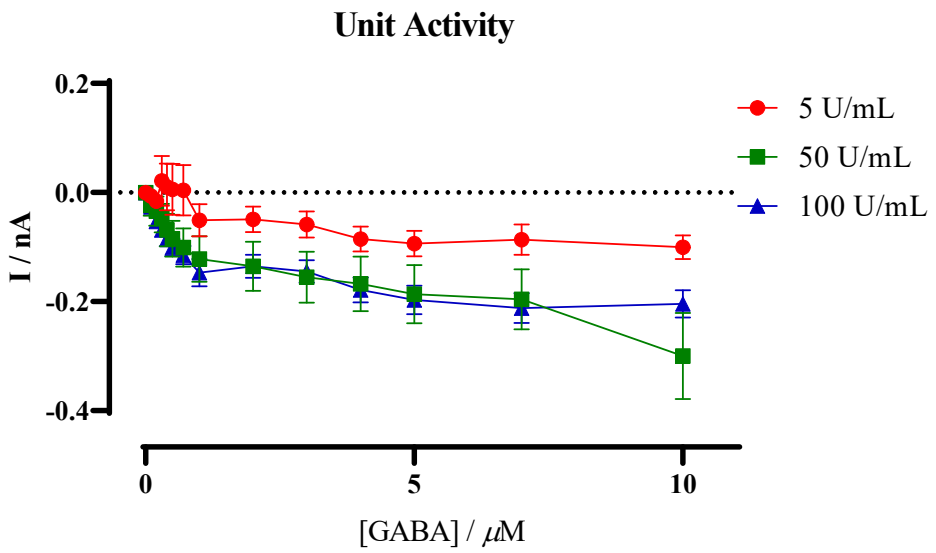

Figure 4.1: The mean current-concentration profiles for GABA [0-10 μM] calibrations carried out in PBS (pH 7.4, containing glutamate [10 μM]) using the design Sty-(GluOx-GAB-BSA:GA-PEI)$_{15}$, where the concentration of GABase was varied (5 U/mL, 50 U/mL, 100 U/mL). CPA was carried out at +700 mV *vs.* SCE.

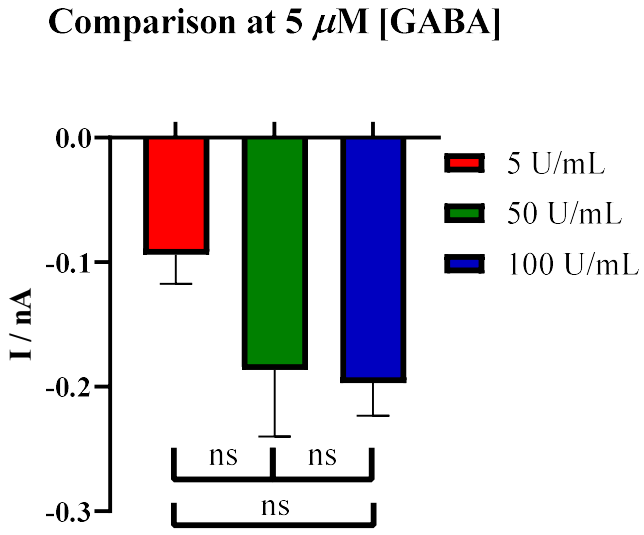

Figure 4.2: A comparison of the signal generated at 5 μM [GABA] for Figure 1. Ordinary one-way ANOVA with multiply comparisons was performed. No significant difference was found, *P*

= 0.1935 for 5 U/mL *vs.* 50 U/mL, $P = 0.0511$ for 5 U/mL *vs.* 100 U/mL, $P = 0.9738$ for 50 U/mL *vs.* 100 U/mL, one-way ANOVA.

4.2.2 GABase Position in Biosensor Design

The ordering of components in a composite design format have been seen to have an effect on the output of a biosensor [47, 49]. As no obvious unit activity of the GAB solution was found to have an observable reaction (see Figure 4.2), an arbitrary unit activity needed to be elected. 100 U/mL was chosen as this is the same unit activity of the Glu solution. The unit activity of the GAB solution was maintained at 100 U/mL, unless stated otherwise. The results shown in Figure 4.3 found that there was again no signal generated from altering the position of GAB. A comparison at 5 μM [GABA] using an ordinary one-way Anova analysis with multiply comparisons was also performed (see Figure 4.4). No significant difference was present ($P = 0.4025$ for Red *vs.* Green, $P = 0.5890$ for Red *vs.* Blue, $P = 0.9191$ for Red *vs.* Purple, $P = 0.9991$ for Green *vs.* Blue, $P = 0.1389$ for Green *vs.* Purple, $P = 0.2990$ for Blue *vs.* Purple, one-way ANOVA).

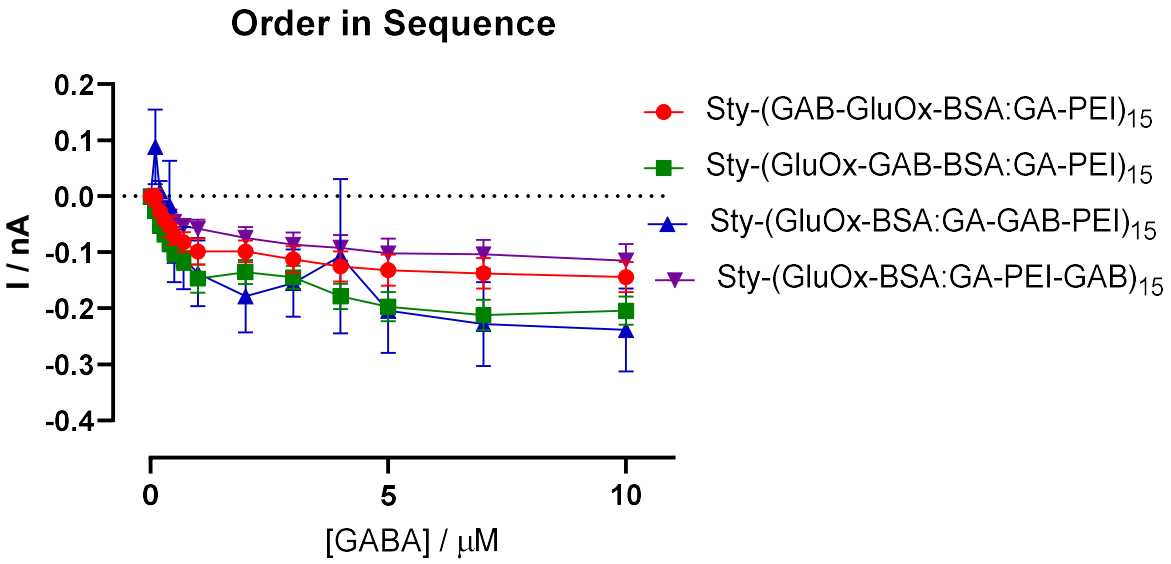

Figure 4.3: The mean current-concentration profiles for GABA [0-10 μM] calibrations carried out in PBS (pH 7.4, containing glutamate [10 μM]) using the design Sty-(GluOx-BSA:GA-PEI)$_{15}$.

Where the position of GABase in this sequence of components was varied. CPA was carried out at +700 mV *vs.* SCE.

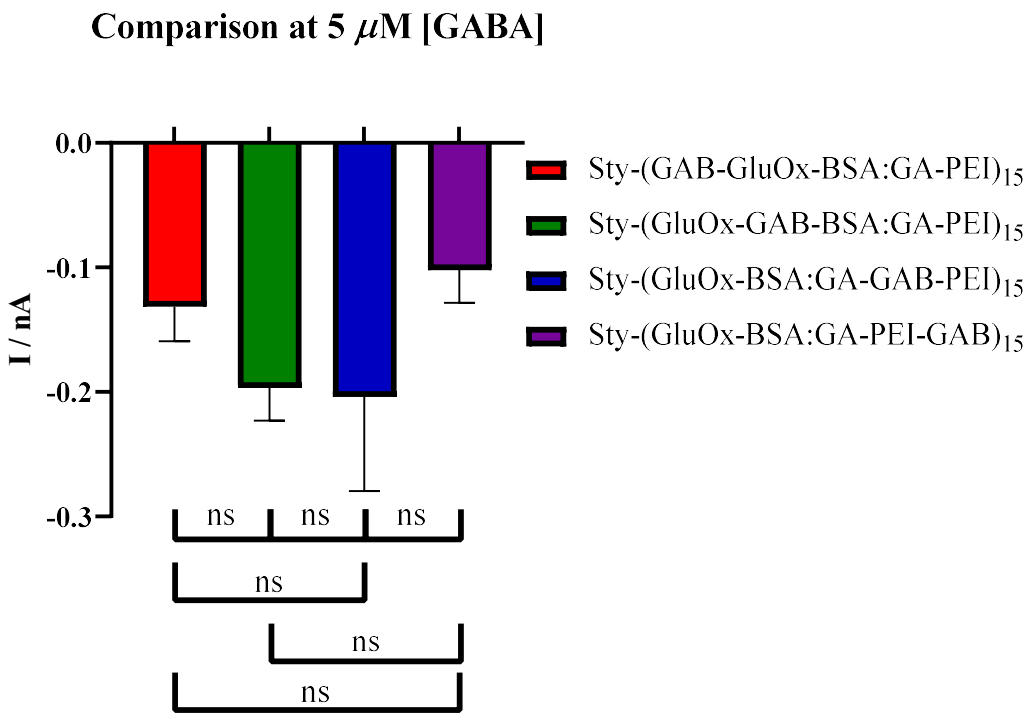

Figure 4.4: A comparison of the signal generated at 5 μM [GABA] for Figure 3. Ordinary one-way Anova with multiply comparisons was performed. No significant difference was found. P = 0.4025 for Red *vs.* Green, P = 0.5890 for Red *vs.* Blue, P = 0.9191 for Red *vs.* Purple, P = 0.9991 for Green *vs.* Blue, P = 0.1389 for Green *vs.* Purple, P = 0.2990 for Blue *vs.* Purple, one-way ANOVA

4.2.3 Post Glutamate Biosensor Layering

Another possible reason for the lack of a response may have been due to GAB being incorporated into the biosensor. It could be a case of over-loading the active surface which could hinder the analyte's ability to reach it. In order to investigate this hypothesis following the construction of the glutamate biosensor the GABase was then layered as per the design below:

Pt/Ir_D - Sty – $(GluOx\text{-}BSA:GA\text{-}PEI)_{15}\text{-}GAB_X$

Where, X is the number of layers of GABase. Experiments were performed using 5, 10 or 15 layers of GABase (see Figure 4.5). Unfortunately, the post-layering of GABase proved to have no discernible impact on the biosensor's ability to detect GABA.

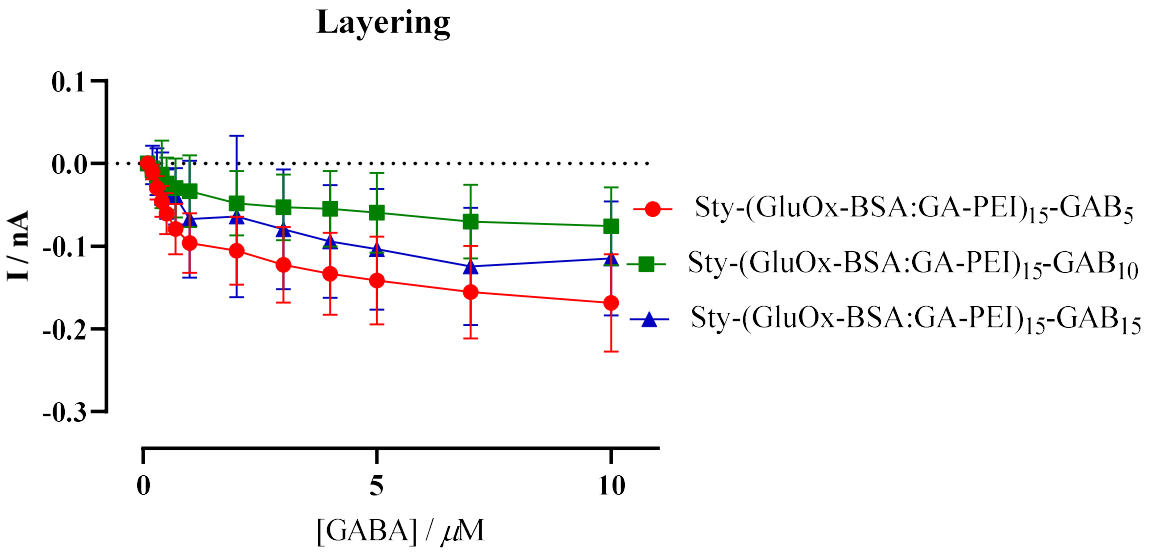

Figure 4.5: The mean current-concentration profiles for GABA [0-10 μM] calibrations carried out in PBS (pH 7.4, containing glutamate [10 μM]) using the design Sty-$(GluOx\text{-}GAB\text{-}BSA:GA\text{-}PEI)_{15}\text{-}GAB_X$. Where the number of layers of GABase is varied (5, 10 or 15). CPA was carried out at +700 mV *vs.* SCE.

5.2.4 Active Surface Response

Over-loading of the triple enzyme on the active surface could still be the potential problem. To investigate this complication further, various experiments were performed. Firstly, an aliquot of glutamate was added to a GABA calibration method (see Figure 4.6) and the concentration of GABA for the calibration was expanded slightly to ensure no signal output. The design used to investigate this was:

Pt/Ir_D - Sty-$(GluOx\text{-}GAB\text{-}BSA:GA\text{-}PEI)_{15}$

Secondly, the concentration of the GABA calibration was significantly increased to ensure that the parameters previously operated under weren't too restrictive (see Figure 4.7). The same design detailed above was used for this investigation. Thirdly, the geometry could potentially affect the ability of H_2O_2 to reach the active surface. To eliminate this, the same biosensor design was deposited on a 4 mm cylinder (see Figure 4.8). The design used for this was:

$$Pt/Ir_{C\ 4\ mm} - Sty\text{-}(GluOx\text{-}GAB\text{-}BSA{:}GA\text{-}PEI)_{15}$$

From these various experiments, a few insights were garnered. Any produced H_2O_2 can reach the active surface and be oxidised. The concentration of GABA during calibrations was not the problem as even outside any physiologically relevant concentrations there was still no response. The area of the active surface also was not the issue as responses are seen on both discs and 4 mm cylinders where H_2O_2 produced from the glutamate-glutamate oxidase reaction generates a signal output.

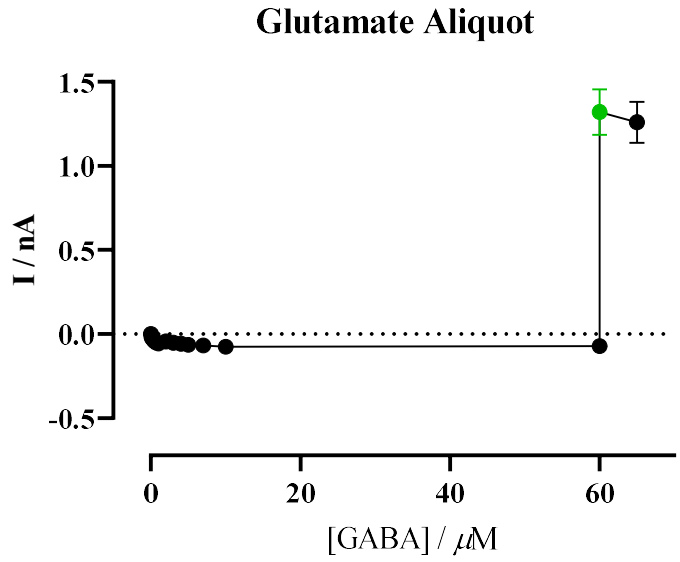

Figure 4.6: The mean current-concentration profiles for GABA [0-60 μM] calibrations carried out in PBS (pH 7.4, containing 1 mM α-ketoglutarate) using the design Sty-(GluOx-BSA:GA-PEI)$_{15}$. Where the green data point presents an aliquot of 300 μM glutamate. CPA was carried out at +700 mV *vs.* SCE.

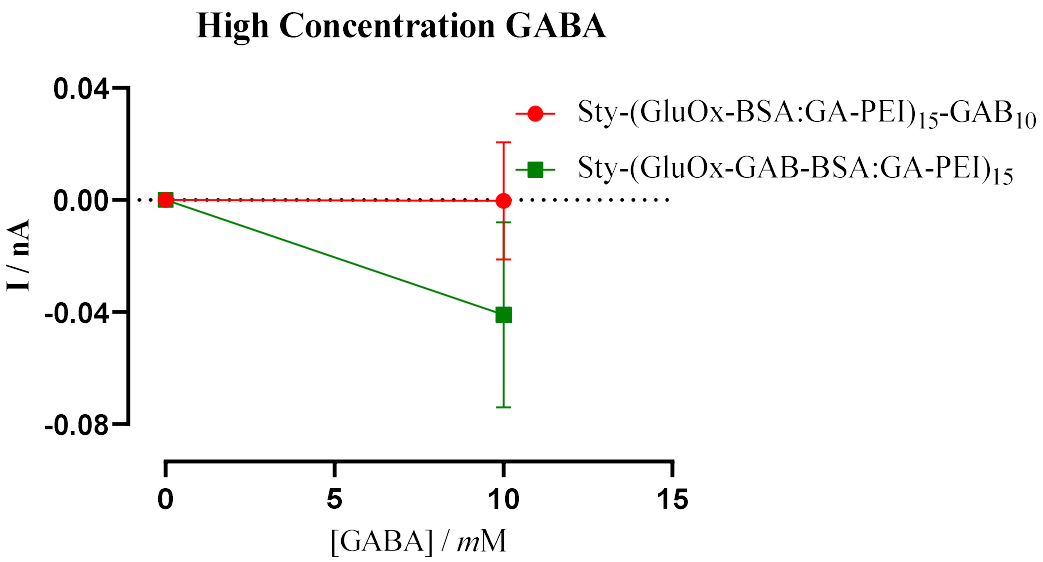

Figure 4.7: The mean current-concentration profiles for GABA [0-10 *m*M] calibrations carried out in PBS (pH 7.4, containing 100 mM *α*-ketoglutarate) using the design Sty-(GluOx-BSA:GA-PEI)$_{15}$. CPA was carried out at +700 mV *vs.* SCE.

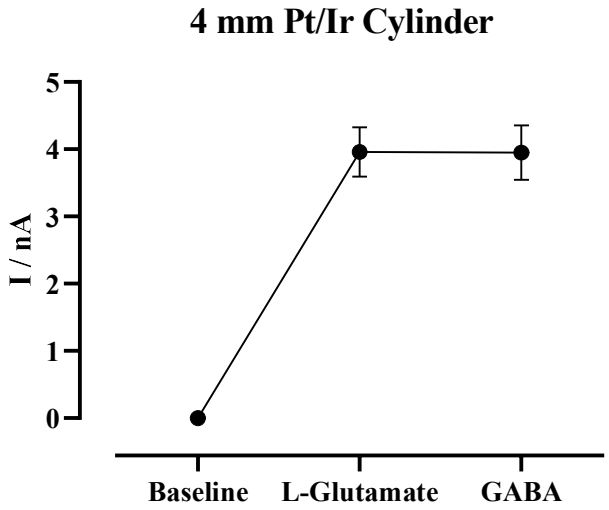

Figure 4.8: The current-analyte profile for glutamate [0.1 mM] and GABA [0.1 mM] carried out in PBS (pH 7.4) using the design Sty-(GluOx-GAB-BSA:GA-PEI)$_{15}$ on a 4 mm Pt/Ir cylinder active surface. CPA carried out at + 700 mV *vs.* SCE.

4.2.5 Alternative Detection Method

Previously published work by another research group demonstrated a response for GABA using a macroelectrode while using CV [35]. No previous augmentations had generated a GABA signal so a new starting point was to try and replicate these results. A platinum macroelectrode with a diameter of 1 mm, was used with the design:

$$Pt_{D\ 1\ mm}\text{ - Sty-(GluOx-GAB-BSA:GA-PEI)}_{15}$$

The scan rate was set at 50 mV/s for 10 scans. The eight scan is taken as the result (see Figure 4.9). The first scans were of PBS. The second scans were PBS containing an aliquot of 36.1 mM α-ketoglutarate. The third scans were PBS containing aliquots of 36.1 mM α-ketoglutarate and 9.1 mM GABA. Unlike the published work, no reaction was observed here.

As mentioned in Section 4.1, an alternative reaction scheme exists potentially producing a signal proportional to the concentration of GABA present. The reaction scheme (see *1, 4, 5*). This would remove the need for GluOx in the biosensor design. This would however, mean it is no longer classified as a first generation biosensor. The design used a Pt/Ir_D as before with the deposited design being:

$$Pt/Ir_D\text{ - Sty-(GAB-BSA:GA-PEI)}_{15}$$

As glutamate has been removed α-ketoglutarate must be added to the bulk. In this case 1 mM of α-ketoglutarate was added to ensure sufficient concentrations would be present if required (see Figure 4.10). One of the genes (ALDH5A1) present in the succinic semialdehyde dehydrogenase enzyme, which makes up GABase, breaks down succinic semialdehyde producing NADPH [53]. NADPH is electroactive, has been utilised in biosensors before [54-56] and can be oxidised at the electrode surface (at 700 mV/s *vs.* SCE) to regenerate $NADP^+$ which theoretically means no additionally $NADP^+$ is required when present in sufficient concentrations. For the experiments reported here, it was present in excess, at 5 mM.

Both the alternative technique and alternative reaction scheme again produced no signal output. As such, no further exploration into the development of a first generation biosensor was conducted.

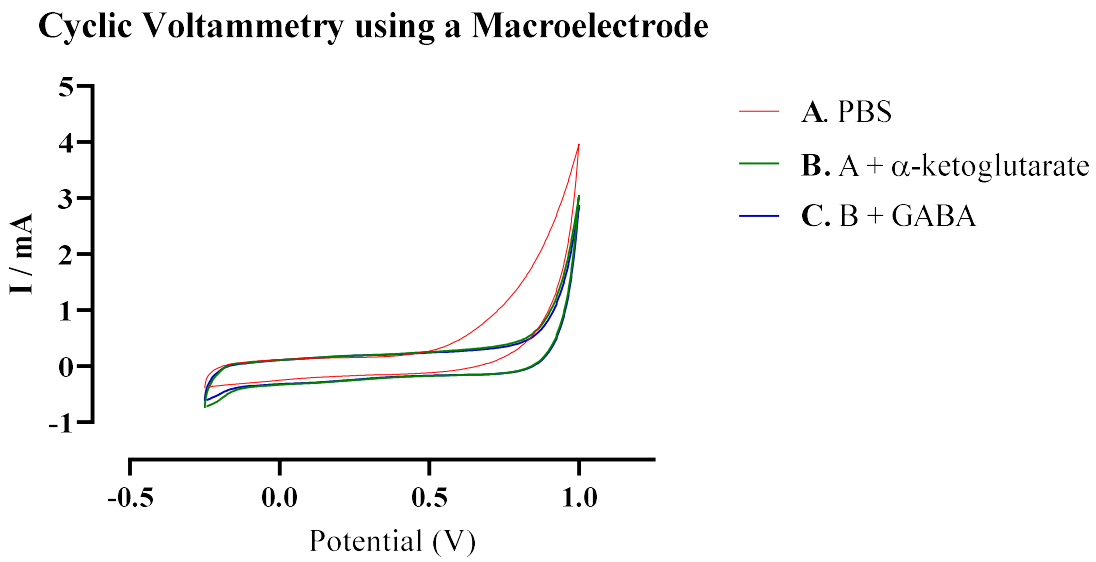

Figure 4.9: Cyclic voltammograms of a Sty-(GluOx-GAB-BSA:GA-PEI)$_{15}$ of a Pt electrode (d = 1 mm) in (**A**) PBS, (**B**) PBS containing 36.1 mM α-ketoglutarate and, (**C**) PBS containing 36.1 mM α-ketoglutarate and 9.1 mM GABA. The scan rate was 50 mV/s *vs.* SCE.

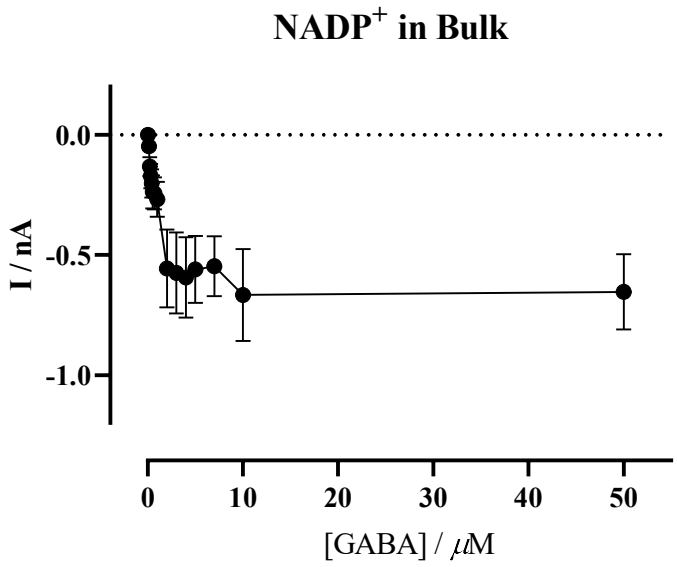

Figure 4.10: The mean current-concentration profiles for GABA [0-60 μM] calibrations carried out in PBS (pH 7.4, containing 1 mM α-ketoglutarate) using the design Sty-(BSA:GA-PEI)$_{15}$. CPA was carried out at +700 mV *vs.* SCE.

4.3 Conclusion

The exploration into various designs and parameters in this body of work can be briefly summarised as a study into unit activity, sequencing order, post-glutamate biosensor layering, additives to the bulk, active surface response and, alternative methods for the development of a biosensor capable of monitoring GABA. Unfortunately, there was no true indication present that any of the varied designs or parameters had the potential to generate a signal for refinement. It is most likely enzyme overloading causing the lack of signal (discussed in further detail in Section 6.1). It was concluded that efforts would be best spent on the development and characterisation of the glutamate biosensor.

4.4 References

1. Cooper, J.R., F.E. Bloom, and R.H. Roth, *The Biochemical Basis of Neuropharmacology*. STAT!Ref electronic medical library. 2003: Oxford University Press.
2. Van Der Kloot, W.G. and J. Robbins, *The effects of gamma-aminobutyric acid and picrotoxin on the junctional potential and the contraction of crayfish muscle.* Experientia, 1959. **15**(1): p. 35-6.
3. Boonstra, E., et al., *Neurotransmitters as food supplements: the effects of GABA on brain and behavior.* Front Psychol, 2015. **6**: p. 1520.
4. Hampel, L. and T. Lau, *Neurobiological Principles: Neurotransmitters*, in *NeuroPsychopharmacotherapy*, P. Riederer, et al., Editors. 2020, Springer International Publishing: Cham. p. 1-21.
5. de Leon, A.S. and P. Tadi, *Biochemistry, Gamma Aminobutyric Acid*. 2021: StatPearls Publishing, Treasure Island (FL).
6. Nyitrai, G., K.A. Kékesi, and G. Juhász, *Extracellular level of GABA and Glu: in vivo microdialysis-HPLC measurements.* Curr Top Med Chem, 2006. **6**(10): p. 935-40.
7. Peña, F. and R. Tapia, *Relationships among seizures, extracellular amino acid changes, and neurodegeneration induced by 4-aminopyridine in rat hippocampus: a microdialysis and electroencephalographic study.* J Neurochem, 1999. **72**(5): p. 2006-14.
8. Erdö, S.L. and J.R. Wolff, *γ-Aminobutyric Acid Outside the Mammalian Brain.* Journal of Neurochemistry, 1990. **54**(2): p. 363-372.
9. Gottesmann, C., *GABA mechanisms and sleep.* Neuroscience, 2002. **111**(2): p. 231-9.
10. Petty, F., *GABA and mood disorders: a brief review and hypothesis.* J Affect Disord, 1995. **34**(4): p. 275-81.
11. Sawynok, J., *GABAergic mechanisms of analgesia: an update.* Pharmacol Biochem Behav, 1987. **26**(2): p. 463-74.
12. Fritschy, J.M., et al., *GABAergic neurons and GABA(A)-receptors in temporal lobe epilepsy.* Neurochem Int, 1999. **34**(5): p. 435-45.
13. Bradford, H.F., *Glutamate, GABA and epilepsy.* Progress in Neurobiology, 1995. **47**(6): p. 477-511.
14. Błaszczyk, J.W., *Parkinson's Disease and Neurodegeneration: GABA-Collapse Hypothesis.* Front Neurosci, 2016. **10**: p. 269.

15. Rosas-Arellano, A., et al., *Huntington's disease leads to decrease of GABA-A tonic subunits in the D2 neostriatal pathway and their relocalization into the synaptic cleft.* Neurobiol Dis, 2018. **110**: p. 142-153.
16. Möhler, H., *The GABA system in anxiety and depression and its therapeutic potential.* Neuropharmacology, 2012. **62**(1): p. 42-53.
17. Kalueff, A.V. and D.J. Nutt, *Role of GABA in anxiety and depression.* Depress Anxiety, 2007. **24**(7): p. 495-517.
18. Petroff, O.A., *GABA and glutamate in the human brain.* Neuroscientist, 2002. **8**(6): p. 562-73.
19. Chiapponi, C., et al., *GABA System in Schizophrenia and Mood Disorders: A Mini Review on Third-Generation Imaging Studies.* Frontiers in Psychiatry, 2016. **7**.
20. O'Connor, W.T. and S.D. O'Shea, *Clozapine and GABA transmission in schizophrenia disease models: establishing principles to guide treatments.* Pharmacol Ther, 2015. **150**: p. 47-80.
21. Rivera, C., et al., *The K+/Cl− co-transporter KCC2 renders GABA hyperpolarizing during neuronal maturation.* Nature, 1999. **397**(6716): p. 251-255.
22. Cherubini, E., J.L. Gaiarsa, and Y. Ben-Ari, *GABA: an excitatory transmitter in early postnatal life.* Trends in Neurosciences, 1991. **14**(12): p. 515-519.
23. Li, K. and E. Xu, *The role and the mechanism of gamma-aminobutyric acid during central nervous system development.* Neuroscience bulletin, 2008. **24**(3): p. 195-200.
24. Ben-Ari, Y., et al., *GABA: a pioneer transmitter that excites immature neurons and generates primitive oscillations.* Physiol Rev, 2007. **87**(4): p. 1215-84.
25. Jelitai, M. and E. Madarasz, *The Role of GABA in the Early Neuronal Development*, in *International Review of Neurobiology*. 2005, Academic Press. p. 27-62.
26. LoTurco, J.J., et al., *GABA and glutamate depolarize cortical progenitor cells and inhibit DNA synthesis.* Neuron, 1995. **15**(6): p. 1287-98.
27. Haydar, T.F., et al., *Differential modulation of proliferation in the neocortical ventricular and subventricular zones.* The Journal of neuroscience : the official journal of the Society for Neuroscience, 2000. **20**(15): p. 5764-5774.

28. Behar, T.N., et al., *Differential response of cortical plate and ventricular zone cells to GABA as a migration stimulus.* The Journal of neuroscience : the official journal of the Society for Neuroscience, 1998. **18**(16): p. 6378-6387.
29. Ganguly, K., et al., *GABA Itself Promotes the Developmental Switch of Neuronal GABAergic Responses from Excitation to Inhibition.* Cell, 2001. **105**(4): p. 521-532.
30. Barbin, G., et al., *Involvement of GABAA receptors in the outgrowth of cultured hippocampal neurons.* Neurosci Lett, 1993. **152**(1-2): p. 150-4.
31. Maric, D., et al., *GABA expression dominates neuronal lineage progression in the embryonic rat neocortex and facilitates neurite outgrowth via GABA(A) autoreceptor/Cl- channels.* The Journal of neuroscience : the official journal of the Society for Neuroscience, 2001. **21**(7): p. 2343-2360.
32. Ben-Ari, Y., *Excitatory actions of gaba during development: the nature of the nurture.* Nature Reviews Neuroscience, 2002. **3**(9): p. 728-39.
33. Wang, D.D., A.R. Kriegstein, and Y. Ben-Ari, *GABA regulates stem cell proliferation before nervous system formation.* Epilepsy currents, 2008. **8**(5): p. 137-139.
34. Jinnarak, A. and S. Teerasong, *A novel colorimetric method for detection of gamma-aminobutyric acid based on silver nanoparticles.* Sensors and Actuators B: Chemical, 2016. **229**: p. 315-320.
35. Niwa, O., et al., *Small-Volume On-Line Sensor for Continuous Measurement of γ-Aminobutyric Acid.* Analytical Chemistry, 1998. **70**(1): p. 89-93.
36. Zhou, A. and J. Muthuswamy, *Acoustic biosensor for monitoring antibody immobilization and neurotransmitter GABA in real-time.* Sensors and Actuators B: Chemical, 2004. **101**(1): p. 8-19.
37. Sekioka, N., et al., *Improved detection limit for an electrochemical γ-aminobutyric acid sensor based on stable NADPH detection using an electron cyclotron resonance sputtered carbon film electrode.* Sensors and Actuators B: Chemical, 2008. **129**(1): p. 442-449.
38. Smith, S. and T. Sharp, *Measurement of GABA in rat brain microdialysates using o-phthaldialdehyde—sulphite derivatization and high-performance liquid chromatography with electrochemical detection.* Journal of Chromatography B: Biomedical Sciences and Applications, 1994. **652**(2): p. 228-233.

39. Ferraro, L., et al., *Striatal NTS1, dopamine D2 and NMDA receptor regulation of pallidal GABA and glutamate release - a dual-probe microdialysis study in the intranigral 6-hydroxydopamine unilaterally lesioned rat.* The European journal of neuroscience, 2011. **35**: p. 207-20.
40. Mazzei, F., et al., *Peroxidase based amperometric biosensors for the determination of γ-aminobutyric acid.* Analytica Chimica Acta, 1996. **328**(1): p. 41-46.
41. Wang, T. and J. Muthuswamy, *Immunosensor for detection of inhibitory neurotransmitter gamma-aminobutyric acid using quartz crystal microbalance.* Anal Chem, 2008. **80**(22): p. 8576-82.
42. Wang, T. and J. Muthuswamy. *Acoustic immunosensor for real-time sensing of neurotransmitter GABA*. in *Proceedings of the 25th Annual International Conference of the IEEE Engineering in Medicine and Biology Society (IEEE Cat. No.03CH37439)*. 2003.
43. Lee, J.-H., et al., *Label-free detection of γ-aminobutyric acid based on silicon nanowire biosensor.* Nano Convergence, 2019. **6**(1): p. 13.
44. Yamamura, A., et al., *Gamma-Aminobutyric acid (GABA) sensor using GABA oxidase from Penicillium sp. KAIT-M-117.* ECS Meeting Abstracts, 2008. **MA2008-02**(46): p. 2832-2832.
45. Ryan, M., J. Lowry, and R. O'Neill, *Biosensor for neurotransmitter L-glutamic acid designed for efficient use of L-glutamate oxidase and effective rejection of interference.* Analyst, 1997. **122**(11): p. 1419-1424.
46. McMahon, C.P. and R.D. O'Neill, *Polymer− enzyme composite biosensor with high glutamate sensitivity and low oxygen dependence.* Analytical chemistry, 2005. **77**(4): p. 1196-1199.
47. Doran, M.M., N.J. Finnerty, and J.P. Lowry, *In–Vitro Development and Characterisation of a Superoxide Dismutase-Based Biosensor.* ChemistrySelect, 2017. **2**(14): p. 4157-4164.
48. Baker, K.L., et al., *Characterisation of a Platinum-based Electrochemical Biosensor for Real-time Neurochemical Analysis of Choline.* Electroanalysis, 2019. **31**(1): p. 129-136.

49. Baker, K.L., F.B. Bolger, and J.P. Lowry, *Development of a microelectrochemical biosensor for the real-time detection of choline.* Sensors and Actuators B: Chemical, 2017. **243**: p. 412-420.
50. O'Brien, K.B., et al., *Development and characterization in vitro of a catalase-based biosensor for hydrogen peroxide monitoring.* Biosensors and Bioelectronics, 2007. **22**(12): p. 2994-3000.
51. O'Riordan, S.L. and J.P. Lowry, *In vivo characterisation of a catalase-based biosensor for real-time electrochemical monitoring of brain hydrogen peroxide in freely-moving animals.* Analytical Methods, 2017. **9**(8): p. 1253-1264.
52. Burmeister, J.J., et al., *Glutaraldehyde cross-linked glutamate oxidase coated microelectrode arrays: selectivity and resting levels of glutamate in the CNS.* ACS chemical neuroscience, 2013. **4**(5): p. 721-728.
53. Ippolito, J.E. and D. Piwnica-Worms, *A fluorescence-coupled assay for gamma aminobutyric acid (GABA) reveals metabolic stress-induced modulation of GABA content in neuroendocrine cancer.* PloS one, 2014. **9**(2): p. e88667-e88667.
54. Spielmann, A., et al., *NADPH biosensor-based identification of an alcohol dehydrogenase variant with improved catalytic properties caused by a single charge reversal at the protein surface.* AMB Express, 2020. **10**(1): p. 14.
55. Goldbeck, O., A.W. Eck, and G.M. Seibold, *Real Time Monitoring of NADPH Concentrations in Corynebacterium glutamicum and Escherichia coli via the Genetically Encoded Sensor mBFP.* Frontiers in Microbiology, 2018. **9**.
56. Zhang, J., et al., *Engineering an NADPH/NADP+ Redox Biosensor in Yeast.* ACS Synthetic Biology, 2016. **5**(12): p. 1546-1556.

CHAPTER FIVE

Design Optimisation and Characterisation of an Amperometric Glutamate Oxidase-based Composite Biosensor for Neurotransmitter L-Glutamic Acid

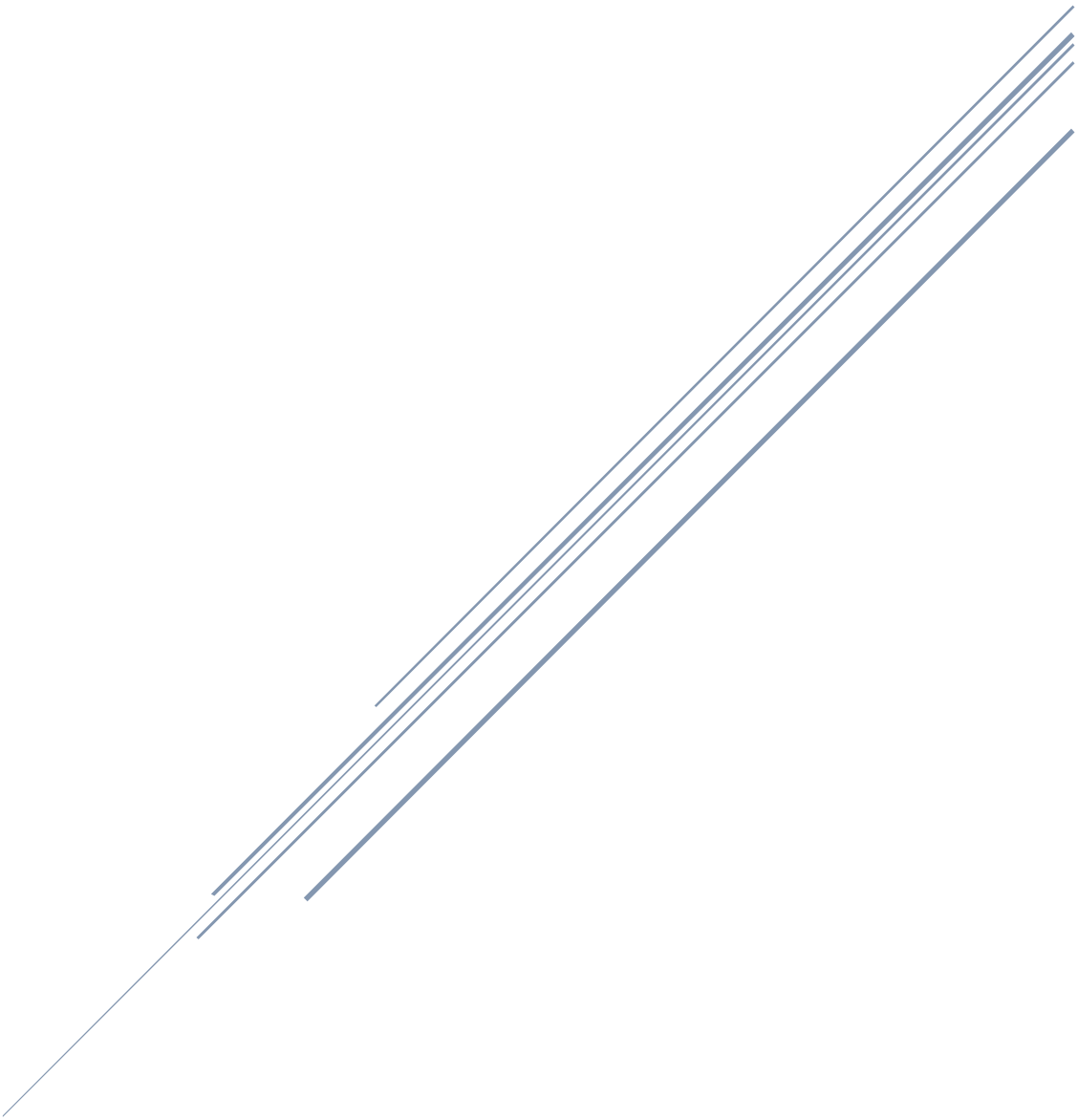

5.1 Introduction

The amino acid, L-Glutamate, is prevalent throughout the mammalian brain, with an estimated 60–70% of synapses using it as their neurotransmitter [1]. Consequently, it has been shown to be vital for normal brain functioning in areas such as development, plasticity, learning and memory, and sensory and motor systems [2]. Along with D-serine it is a co-agonist of the N-methyl-D-aspartate (NMDA) receptor [3], abnormal functioning of which has been linked to disorders such as epilepsy, stroke, and both neurodegenerative and psychiatric diseases [4-7]. Additionally, glutamate toxicity is also associated with neuronal death in ischemia, hypoglycaemia, and trauma [8]. Notwithstanding such extensive research there is still significant interest in improving and advancing our understanding of its neurochemical roles and mechanisms of action. Key to achieving this is the ability to perform rapid (of the order of seconds or less) highly sensitive measurements in the living brain. While this has proved challenging due to its low basal concentration, reported to be *ca.* 10 μM [9-11], several research groups have monitored L-glutamate levels using a variety of different analytical techniques, including brain microdialysis [12], capillary electrophoresis [13], and optical (e.g. chemiluminometric [14] and fluorescent [15]) sensors. However, depending on the method, limitations associated with temporal and spatial resolution, stability and biocompatibility, and interference, can hinder their suitability for *in situ* neurochemical monitoring.

The use of miniaturised enzyme-modified electrochemical biosensors offers the greatest potential of mitigating these shortcomings [9, 16, 17]. For glutamate monitoring such devices are typically first-generation devices operating by detecting electroactive H_2O_2 produced in an enzymatic (oxidase) reaction; for glutamate/glutamate oxidase (GluOx) the reaction scheme is:

$$L\text{-}Glutamate + H_2O + O_2 \xrightarrow{GluOx} 2\text{-}oxoglutarate + NH_3 + H_2O_2 \qquad (1)$$

$$H_2O_2 \xrightarrow{+7 \quad mV\ vs.\ SCE} 2H^+ + O_2 + 2e^- \qquad (2)$$

As such, they generally have fast response times but the high potential required for H_2O_2 oxidation can result in interfering signals from a variety of endogenous electroactive species including ascorbic acid (AA) and dopamine [16]. Second generation biosensors incorporate a low redox potential mediator [18] as a substitute for molecular O_2 in order to improve selectivity. However, these tend to have slow response times and poor stability/sensitivity due to mediator

leaching, in addition to potential toxicity issues, rendering them unsuitable for neurochemical monitoring [19]. Fortunately, for first generation biosensors the problem of selectivity has successfully been addressed through chemical modification of the electrode surface using a variety of polymeric permselective layers, including poly-*ortho*-phenylenediamine (P*o*PD) [20, 21], poly-*meta*-phenylenediamine (P*m*PD) [9, 22], polypyrrole [23], polyaniline [24] and Nafion® [25].

The research presented here builds on earlier biosensor development work targeting glutamate [10, 26], and involves the determination of the response characteristics of a sensitivity optimised polymer composite design format successfully applied previously in the development of devices for superoxide [27], choline [28, 29] and hydrogen peroxide [30, 31]. Functional considerations relevant to neurochemical monitoring were investigated *in vitro*, including stability, permselectivity and oxygen dependence, the effect of physiologically relevant temperature and pH changes, limit of detection, and response time. Finally, the sensor was employed successfully in preliminary *in vivo* experiments, demonstrating its ability to detect chronic real-time changes in glutamate.

5.2 Results and Discussion

This section details the refinement and characterisation of a glutamate oxidase (GluOx) based biosensor. The aim was to; optimise a design which maximised the biosensor's sensitivity, selectivity and reproducibility and; characterise the biosensor in the chemical and physiological constraints present in the brain extracellular fluid to ensure operation in such a harsh environment.

5.2.1 Biosensors Design

Building on previous glutamate biosensor development work , and more recent validation of biosensors for monitoring several other neurochemicals [10, 32, 33], the core constituents/drying periods have been optimised of the composite design to produce a sensitive biosensor for L-glutamate with a reproducible and efficient construction/assembly process. Each constituent, and their sequenced layering, is important to producing an appropriately viable sensor. Initial work focused on using a classic cylinder electrode design as employed successfully by Prof. Lowry's research group in the past [10, 31, 33, 34] and several other groups for monitoring a variety of neurochemicals *in vivo* [35-37]. Surface modification here involved electrodeposition of permselective P*o*PD, followed by dip coating of a styrene layer, and then 10 sequential layers of GluOx, BSA:GA, and PEI, applied consecutively, with 4 min drying between each complete coating sequence. The sensor was then left for 60 min at room temperature before applying a second styrene layer and a further 10 GluOx/BSA:GA/PEI layers as before (see Section 3.2). The resultant Pt_C(P*o*PD)[$(Sty)_1$($GluOx/BSA:GA/PEI)_{10}$]$_2$ biosensor (Design 14, Table 5.1) had comparable sensitivity (75.1 ± 1.5 nA·cm^{-2}·μM^{-1}, n = 8, $R^2 = 0.9965$) to previous designs developed by Prof. Lowry's research group (see *e.g*. 5 and 10, Table 5.1). The applied GluOx/BSA:GA/PEI layers were key to achieving this response. When used on its own glutaraldehyde can have a negative effect on enzyme activity due to modification of the enzyme by covalent bonding. As such, it was combined with BSA which preferentially binds to the glutaraldehyde reducing its negative influence, primarily by freeing enzyme active sites for substrate turnover. Additionally, PEI was incorporated to further enhance GluOx immobilisation

and stabilisation through the formation of polycationic/polyanionic complexes, and by decreasing the electrostatic repulsion between glutamate and the biosensor components.

Table 5.1: Comparison of V_{MAX}, K_M and sensitivies for different biosensors designed for neurochemical monitoring.

	Design	**Geometry**[a] **/ Dimensions** (μm)	V_{MAX} (μA.cm^{-2})	K_M (μM)	**Sensitivity** (nA.cm^{-2}.μM^{-1})
1	[10]	C, 60 x 1000	13 ± 2	250 ± 100	20 ± 7
2	[38]	C, 10 x 300-400	—	—	30.6 ± 8.5
3	[39]	D, 125	—	—	80 ± 10
4	[40]	D, 1600	—	—	85
5	[41]	C, 125 x 1000	74 ± 6	600 ± 100	100 ± 5
6	[18]	C, 25 x 500	—	—	29.9 ± 5.8
7	[42]	C, 15 x 333	—	—	101 ± 6
8	[17]	C, 50 x 500	173 ± 62	776	279 ± 2
9	[43]	C, 25 x 100	122 ± 16	790 ± 170	173 ± 62
10	[44]	D, 125	77	873	71 ± 1
11	[45]	C, 10 x 250	50 ± 6	1140 ± 60	135 ± 2
12	[46]	C, 125 x 1000	55 ± 9	310 ± 5	111 ± 34
13	[47]	C, 50 x 1000	—	—	61.0 ± 0.6
14	$Pt_C(PoPD)[(Sty)_1(GluOx/BSA:GA/PEI)_{10})]_2$	C, 127 x 1000	109 ± 2	849 ± 47	75.1 ± 1.5
15	$Pt_C(PoPD)(Sty)(GluOx/BSA:GA/PEI)_{15}$	C, 127 x 1000	77 ± 1	536 ± 20	82.0 ± 2.2
16	$Pt_D(PoPD)(Sty)(GluOx/BSA:GA/PEI)_{15}$	D, 127	139 ± 2	1069 ± 43	90.4 ± 2.0

[a] Geometry - Cylinder (C), Disc (D)

In order to reduce the manufacturing time, this design was further refined by only applying the initial styrene layer, removing the 60 min drying period, and optimising the total number of GluOx/BSA:GA/PEI layers at 15. This Pt_C(P*o*PD)(Sty)(GluOx/BSA:GA/PEI)$_{15}$ biosensor (see Figure 5.1) had increased sensitivity; LRS 82.0 ± 2.2 nA·cm^{-2}·μM^{-1} (n = 16; $t_{(22)} = 2.107$, $p = 0.0468$ *vs.* Design 14; $R^2 = 0.9943$, Figure 5.1 B). V_{MAX} and K_M values were 76.8 ± 1.0 μAcm^{-2} and 536 ± 20 μM (n = 16, Figure 5.1 A) respectively, and compare well with other reported values (see Table 5.1). The design was also tested using a disc geometry as GluOx-modified Pt_D electrodes (see Figure 5.2) have been reported to have higher sensitivity and less oxygen dependence compared to their cylinder counterparts [26], in addition to being more suitable for accessing smaller brain regions. The LRS was significantly increased (90.4 ± 2.0 nA·cm^{-2}·μM^{-1}, n = 16; $t_{(30)} = 2.837$, $p = 0.0081$, $R^2 = 0.9954$, Figure 5.1 B) compared to that observed with the cylinder geometry, as were both the V_{MAX} (139 ± 2 μAcm^{-2}; $t_{(30)} = 27.76$, $p < 0.0001$) and K_M values (1069 ± 43 μM; $t_{(30)} = 11.33$, $p < 0.0001$; Figure 5.1 A). A calculated biosensor efficiency, BE% (see Section 3.4), of 20.4 ± 1.0% (n = 16) for this Pt_D(P*o*PD)(Sty)(GluOx/BSA:GA/PEI)$_{15}$ biosensor indicates good diffusion-limited conversion of glutamate to H_2O_2 as BE% has an empirical maximum of *ca.* 60% [48, 49] given that the diffusion coefficient for glutamate will always be less than that for H_2O_2, coupled with the fact that a significant fraction of enzyme-generated H_2O_2 molecules are not oxidised at the electrode because of loss to the bulk solution [50].

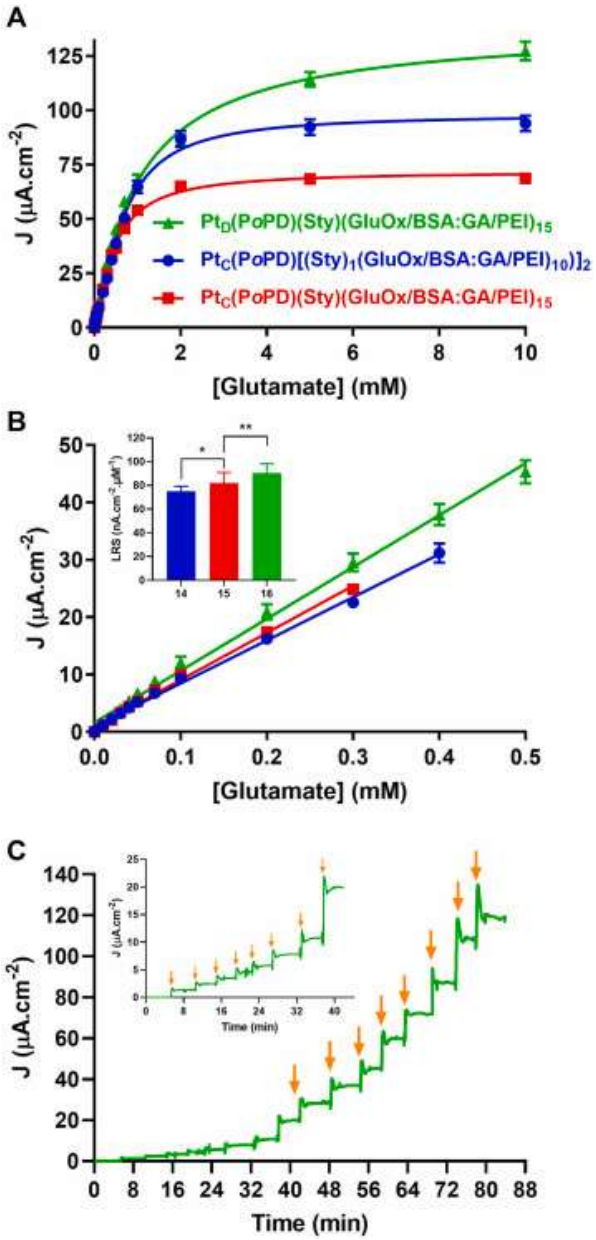

Figure 5.1: (**A**) Current-concentration profiles for glutamate calibrations (0–10 mM) for biosensor designs 14 (blue, n = 8), 15 (red, n = 16) and 16 (green, n = 16), performed using constant potential amperometry (CPA) at +700 mV (*vs.* SCE) in PBS (pH 7.4). (**B**) Linear regression analysis and comparison (*inset*) of sensitivities (Linear Region Slope, LRS); **p* < 0.05; ***p* < 0.01. (**C**) Typical raw data trace for design 16. Arrows indicate injections yielding concentrations of 0.3, 0.4, 0.5, 0.7, 1, 2, 5 and 10 mM glutamate. *Inset:* Close-up showing initial injections – arrows indicate concentrations of 0.01, 0.02, 0.03, 0.04, 0.05, 0.07, 0.1 and 0.2 mM.

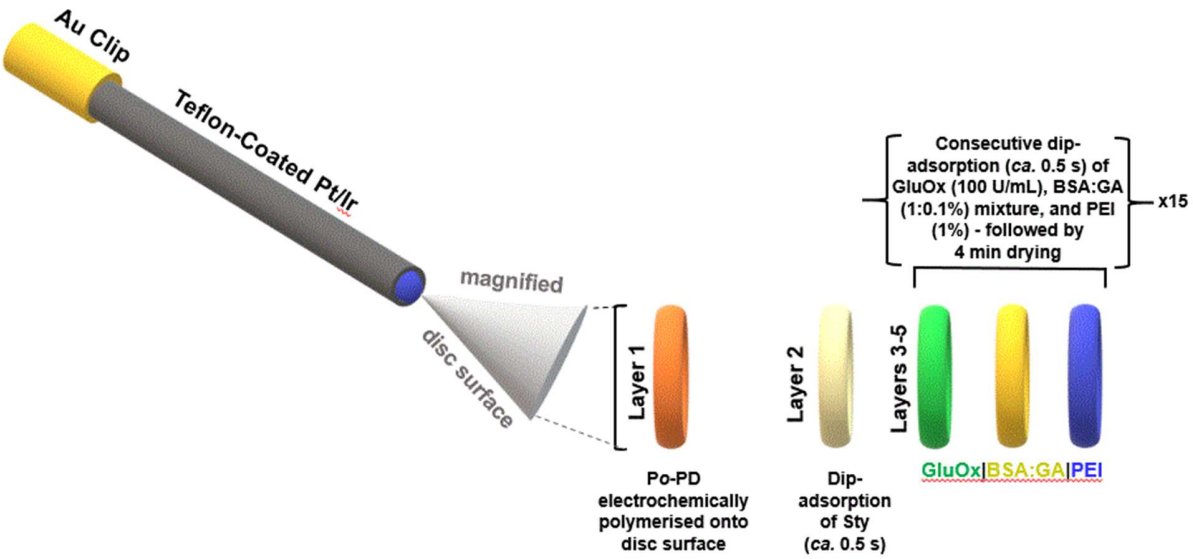

Figure 5.2: Schematic of the final design Pt_D(P*o*PD)(Sty)(GluOx/BSA:GA/PEI)$_{15}$ first-generation (H_2O_2 detecting) glutamate biosensor showing sequence of modifications made to the electrode surface using dip-coat layering. Details of reagents are given in Section 3.2.

5.2.2 Interference and Oxygen Dependence

One of the most important sensor characteristics is selectivity. This is particularly so for neurochemical applications due to the complex chemical matrix of the brain which consists of a multitude of electroactive species and surface modifying agents such as lipids and proteins, all of which can affect the performance of the implanted sensor. With respect to the former, the concentration of these endogenous species can often be greater than the concentration of the analyte of interest. For example, the basal concentration of L-glutamate has been estimated at *ca.* 10 μM using a variety of analytical techniques [10, 16, 51], while the most prevalent interferent, ascorbate (AA) [38, 52], has a concentration of *ca.* 400 μM [51, 53]. Thus, without appropriate exclusion strategies the current generated from AA oxidation would completely mask that of glutamate, as AA is readily oxidised at the biosensor operating potential required for H_2O_2 oxidation.

Interference from electroactive species can successfully be addressed by modifying the electrode surface with a permselective polymer layer. Here, P*o*PD was chosen due to its proficiency in eliminating potentially masking signals [21, 28, 50] and its superiority compared to polymers of other PD isomers [54], its high permeability to H_2O_2 [21, 48], in addition to its ability to improve biocompatibility [55]. An overlayer of monomeric styrene was used to protect the P*o*PD polymer from the immobilising agents used to entrap the glutamate oxidase on the electrode surface, and to improve binding [56] of the subsequent GluOx/BSA:GA/PEI layers. Figure 5.3 A compares the response for basal glutamate (*ca.* 10 μM), with that for AA, the principal interferent, and the other endogenous strong reducing agents [18] L-cysteine [38], uric acid [16] and dopamine [57], at their physiologically relevant concentrations. A series of other potential interferents [9, 17, 47] including the DA metabolites 3,4-dihydroxyphenylacetic acid (DOPAC) and homovanillic acid (HVA), 5-hydroxytryptamine (5-HT) and its metabolite 5-hydroxyindoleacetic acid (5-HIAA), the amino acids L-tyrosine and L-tryptophan, the antioxidant L-glutathione, and dehydroascorbic acid (DHAA), were also tested (Table 2). All signals recorded were found to be negligible compared to the current for physiological glutamate with the selectivity ratio [9, 58] for glutamate:AA calculated at 2326:1 ($nA \cdot cm^{-2} \cdot \mu M^{-1}$). In some cases where there was no detection of the interferent negative values attributable to baseline drift/random noise [9, 28] were observed.

Table 5.2: Response of the Pt_D(P*o*PD)(Sty)(GluOx/BSA:GA/PEI)$_{15}$ biosensor to various potential interferents at physiological levels found *in vivo,* where known.

Neurochemical	**n**	**[Interferent] (μM)**	**Current[e] ($nA \cdot cm^{-2}$)**	**% Change (*vs.* 10 μM Glutamate)[a]**
AA	21	500[b]	31 ± 110	2.1%
L-Cysteine	16	4[c]	41 ± 33	2.8%
Dopamine	16	0.05[b]	9 ± 34	0.6%
Uric Acid	15	10[d]	ND	–
DOPAC	19	20[b]	ND	–
HVA	16	10[b]	38 ± 71	2.6%

Neurochemical	n	[Interferent] (μM)	Current[e] (nA·cm^{-2})	% Change (*vs.* 10 μM Glutamate)[a]
5-HT	18	0.01[b]	74 ± 34	5.1%
5-HIAA	18	50[b]	14 ± 60	1.0%
L-Tyrosine	19	10[e]	ND	–
L-Tryptophan	16	20[f]	46 ± 46	3.2%
L-Glutathione	17	50[g]	57 ± 41	3.9%
DHAA	14	100[g]	26 ± 112	1.8%

a Approximate basal ECF concentration [9, 11].

b [16, 51].

c [38].

d [16].

e [16, 59].

f [16].

g ECF concentrations not known, high μM values chosen; ND – No detectable change.

The interference response in the presence of neurotoxic levels of glutamate (100 μM, see Section 5.2.3) was also profiled (see Figure 5.3 B), and again all signals were found to be negligible (pooled mean response −5.38 ± 2.23%) compared to the glutamate signal, which was not affected by the presence of any of the tested neurochemicals. Generally interference from unwanted enzymatic reactions is also not a concern for glutamate biosensors as GluOx is considered to be a very selective enzyme [18]. However, while glutamine has been reported to serve as a substrate for GluOx [38], no obtained results observed any detectable enzymatic activity for high micromolar glutamine concentrations, which is in line with other research group's publications [10, 38].

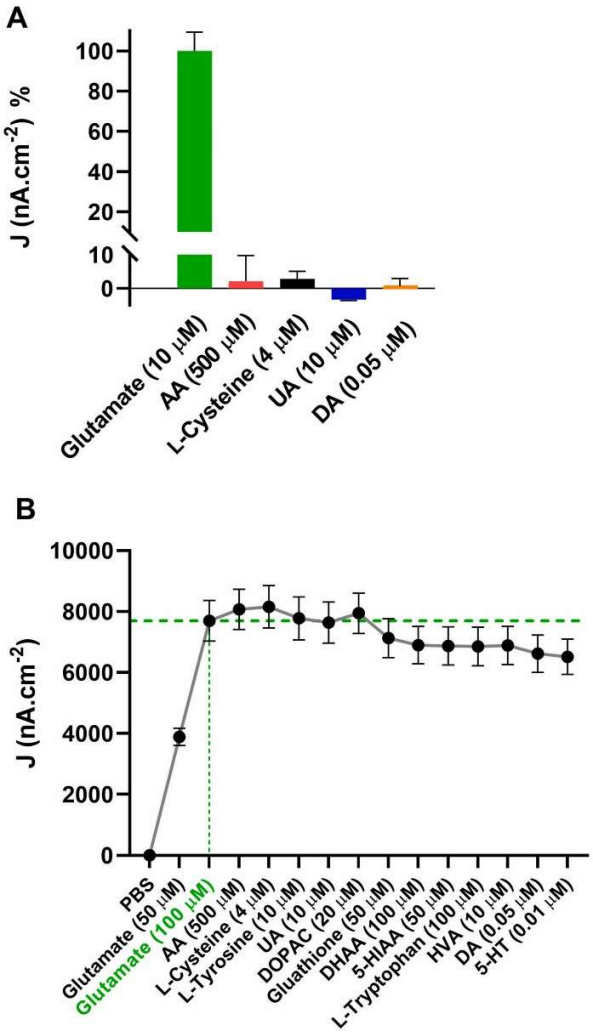

Figure 5.3: (**A**) Normalised Pt_D(P*o*PD)(Sty)(GluOx/BSA:GA/PEI)$_{15}$ biosensor signal (n = 16) for brain glutamate (10 μM) compared to the responses observed for the principal endogenous reducing agents [18] ascorbic acid (AA, n = 21), L-cysteine (n = 16), uric acid (UA, n = 15) and dopamine (DA, n = 16) at their physiologically relevant concentrations. (**B**) Mean (±SEM, n = 4) biosensor response to two 50 μM glutamate injections followed by sequential injections of a series of common potential interfering neurochemicals (see Section 5.2.2).

5.2.3 Oxygen Dependence

Oxygen dependence is another possible form of interference associated with first generation peroxide detecting biosensors as oxidase enzymes require the use of physiological O_2 as a cofactor (see Section 5.1). As such, it is important when characterising their properties for neurochemical monitoring to ensure that the enzymatic reaction in question can occur independently across all O_2 concentration ranges found *in vivo* under normal physiological conditions. For the mammalian brain this is typically between 40 and 80 μM [O_2] [16, 26, 60]. Figure 5.4 A shows the normalised glutamate versus O_2 (0–200 μM) correlation profile for the Pt_D(P*o*PD)(Sty)(GluOx/BSA:GA/PEI)$_{15}$ biosensor at a fixed glutamate concentration of 10 μM. Oxygen dependence was quantified as K_MO_2; small K_MO_2 values indicate low O_2 dependence because higher O_2 affinity leads to O_2 saturation at lower pO_2, thereby reducing biosensor dependency at higher pO_2 levels. The value of 2.60 ± 0.58 μM (n = 7) determined here is similar to previous estimates for Prof. Lowry's research group for other composite designs [26, 61], and suggests negligible O_2 interference (see Figure 5.4).

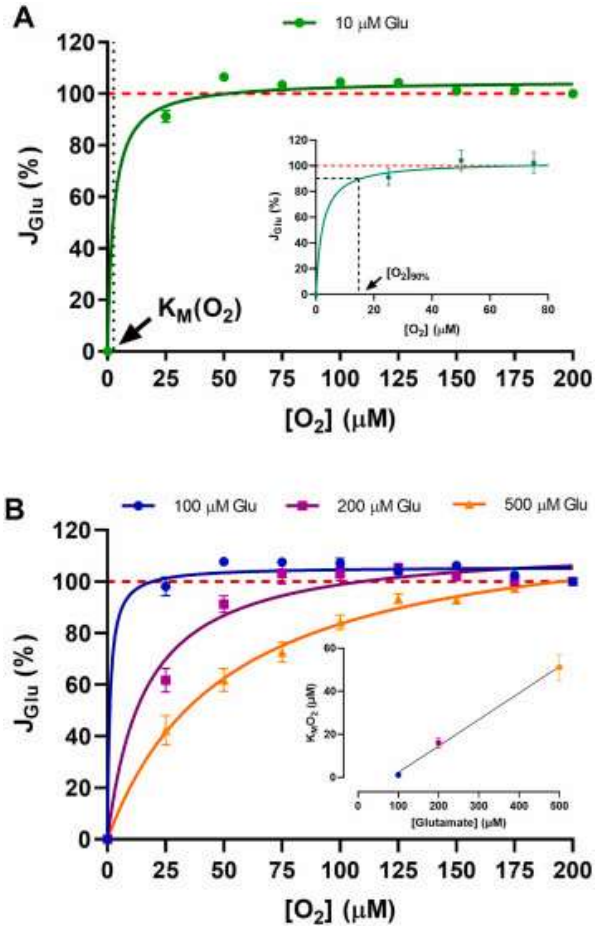

Figure 5.4: (**A**) The effect of changing oxygen levels (0–200 μM) on the averaged normalised Pt_D(P*o*PD)(Sty) (GluOx/BSA:GA/PEI)$_{15}$ biosensor signal for 10 μM glutamate (n = 7). Non-linear regression analysis [61, 62] yielded K_MO_2 = 2.60 ± 0.58 μM (R^2 = 0.984). *Inset:* Pooled data for 10 μM and 100 μM glutamate (see B) used to determine $[O_2]_{90\%}$ (*ca.* 15 μM). (**B**) Averaged normalised glutamate-oxygen correlation plots for 100 μM (n = 7), 200 μM (n = 7) and 500 μM (n = 8) glutamate. *Inset:* Linear regression analysis of K_MO_2 values determined from data in B (R^2 = 0.997).

However, the turnover of O_2 in the polymer/enzyme composite membrane depends on the rate at which glutamate binds to the enzyme, *i.e.*, on the concentration of glutamate. While glutamate concentrations under normal physiological conditions are typically 10 μM or lower for cerebrospinal fluid and brain ECF [11], concentrations are known to increase to high excitotoxic

micromolar levels (e.g. 100 μM) in acute neurological disorders including neurodegenerative diseases, stroke and trauma [63]. Additionally, Prof. Lowry's research group has previously shown that O_2 dependence typically becomes more acute at higher concentrations of analyte [26, 62]. As such, K_MO_2 values over a range of glutamate concentrations were determined for this biosensor. Unlike previous designs where K_MO_2 increased linearly with glutamate concentration in the range 5–150 μM [26, 61], the value for 100 μM (1.1 ± 0.7 μM, n = 7) here was not significantly different from that at 10 μM ($t_{(12)} = 1.63$, $p = 0.1295$; Figure 5.4 A and B). Concentrations above this showed increased values in line with previous results; 16.1 ± 2.3 μM (n = 7) and 51.2 ± 5.9 μM (n = 8) for 200 μM and 500 μM glutamate respectively (Figure 5.4 B *inset*). An alternative and more intuitive quantification of the level of O_2 dependence is $[O_2]_{90\%}$, which is the concentration of O_2 at which 90% of the air-saturated (200 μM) signal (100%) is observed [26]. Analysis of the pooled data for both 10 μM and 100 μM glutamate indicates that 90% of the air-saturated signal can be maintained for the Pt_D(P*o*PD)(Sty)(GluOx/BSA:GA/PEI)$_{15}$ biosensor in media where O_2 concentrations fall to values as low as 15 μM (Figure 5.4 A *inset*). This data suggests that physiological changes in pO_2 would have negligible impact on the biosensor signal recorded in brain ECF, and that decreases in pO_2 would only be significant if the tissue O_2 levels became severely depleted. This is a characteristic previously observed by Prof. Lowry's research with other similar composite biosensors designs for glucose [62], glutamate [61] and choline [29], and by other groups with devices for glutamate and ATP constructed using thin layers [17, 64]. The underlying mechanisms are most likely a combination of O_2 generation on the Pt surface from the electrolysis of water and O_2 regeneration/recycling at the electrode surface (see Section 5.1, *enzyme reaction 2*).

5.2.4 pH and Temperature

It is also important to establish the biosensor response characteristics associated with pH and temperature changes due to their well-documented potential effects on sensitivity. The dependence of the Pt_D(P*o*PD)(Sty)(GluOx/BSA:GA/PEI)$_{15}$ biosensor response to pH (Figure 5.5 A) was examined over the physiologically relevant range of 7.2–7.6 [17, 28]. No significant difference ($F_{(2,31)} = 0.6315$, $p = 0.5385$, one-way ANOVA) was observed in sensitivity: pH 7.2,

89.3 ± 4.3 nA·cm^{-2}·μM^{-1} (n = 8); pH 7.4, 89.5 ± 3.8 nA·cm^{-2}·μM^{-1} (n = 20); and pH 7.6, 81.9 ± 4.0 nA·cm^{-2}·μM^{-1} (n = 6).

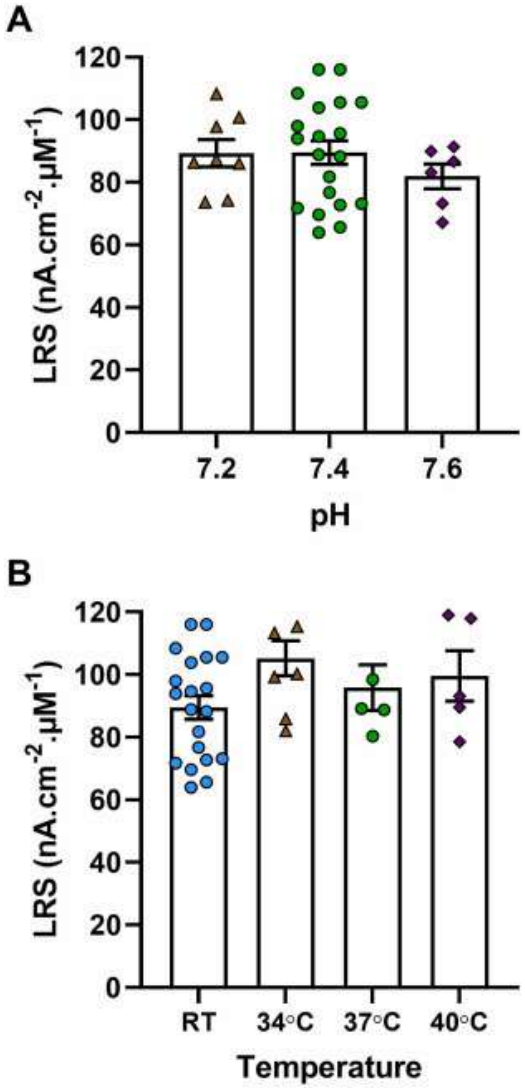

Figure 5.5: The effect of changing pH (**A**) and temperature (**B**) on the sensitivity (Linear Region Slope) of the Pt_D(P*o*PD)(Sty)(GluOx/BSA:GA/PEI)$_{15}$ biosensor over physiologically relevant ranges; 7.2 to 7.6 and room temperature (RT, 21 °C) to 40 °C respectively. Average current-concentration responses are shown in Figure 5.

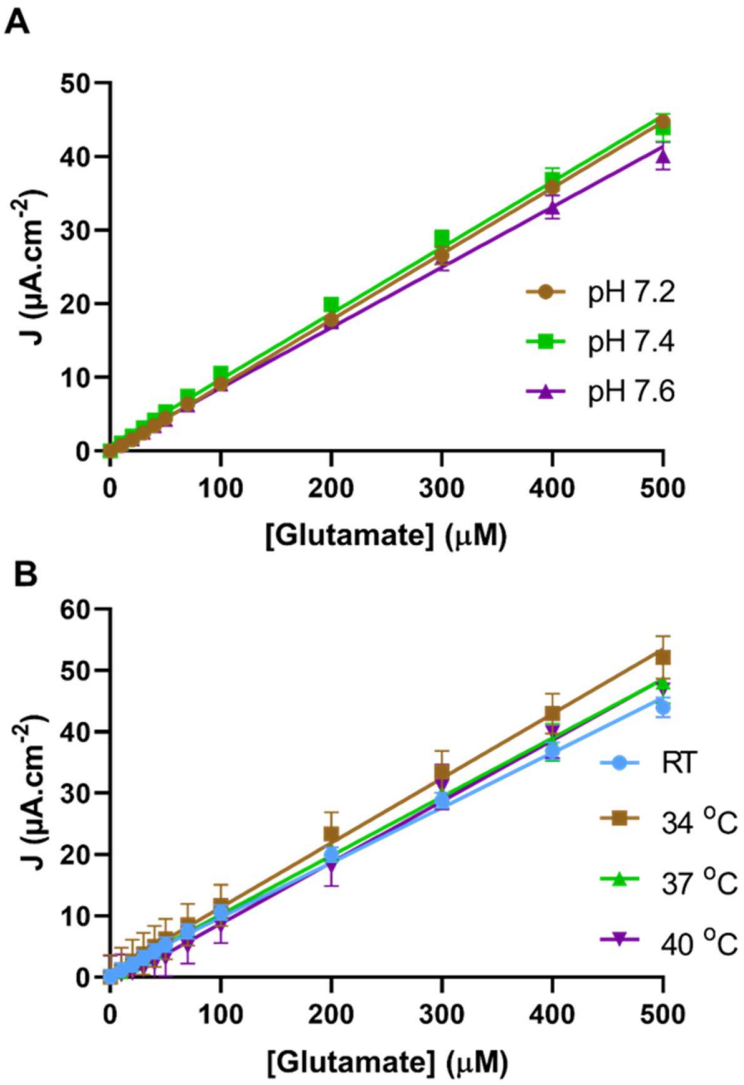

Figure 5.6: The effect of changing pH (**A**) and temperature (**B**) on the current-concentration (linear region) responses of the Pt_D(P*o*PD)(Sty)(GluOx/BSA:GA/PEI)$_{15}$ biosensor. Mean ± SEM: pH 7.2 (n = 8), 7.4 (n = 20), 7.6 (n = 6); Temperature - 21 ºC (Room Temperature, n = 20), 34 ºC (n = 8), 37 ºC (n = 5), 40 ºC (n = 5).

For temperature, variations between 35.5 °C and 38.8 °C, associated with behaviour and pharmacological interventions, have been reported in freely-moving animals [65]. Figure 5.6 B shows the effect of changing temperature over the range 21 °C–40 °C on the glutamate response.

Similar sensitivities ($F_{(3,34)} = 1.855$, $p = 0.1559$, one-way ANOVA) were observed at each of the temperatures tested indicating that the biosensor has the ability to accurately measure glutamate free from temperature induced bias: 21 °C, 89.5 ± 3.8 nA·cm^{-2}·μM^{-1} (n = 20); 34 °C, 105 ± 6 nA·cm^{-2}·μM^{-1} (n = 8); 37 °C, 95.9 ± 7.3 nA·cm^{-2}·μM^{-1} (n = 5); and 40 °C, 99.62 ± 8.06 nA·cm^{-2}·μM^{-1} (n = 5). Other groups have also reported temperature independence for chemically modified GluOx-based electrochemical sensors [66].

5.2.5 Limit of Detection, Response Time and Stability

A limit of detection (LOD) of 0.44 ± 0.05 μM (n = 4) was determined from three times the standard deviation of the baseline biosensor signal in background electrolyte divided by the LRS [48, 49]. The response time, defined as the time taken for the biosensor signal at a fixed concentration to rise from 10% to 90% of the maximum amplitude ($t_{10–90\%}$) was less than the mixing time (*ca.* 5 s); the signal change (Figure 5.7) was instantaneous following injection with $t_{10–90\%}$ estimated at 1.67 ± 0.06 s (n = 4) for 10 μM glutamate.

Stability is the study of the longevity of a biosensor [17, 28]. That is, whether the particular design gives accurate and reliable results over the required timeframe with respect to the intended application. Typically, a minimum of at least two weeks is needed for chronic *in vivo* neurochemical experiments. As the sensitivity of an implanted biosensor can be compromised immediately following biological implantation due to the presence of surface modifying agents (*e.g.* lipids) and electrode poisons (*e.g.* proteins) [67] we tested the biocompatibility of the Pt_D(P*o*PD)(Sty)(GluOx/BSA:GA/PEI)$_{15}$ sensor by calibrating a batch of sensors before and after storage for two weeks in moist brain tissue at 4 °C (Figure 5.8 A). A small decrease ($t_{(7)} = 1.17$, $p = 0.2804$, n = 8) of *ca.* 10% was observed in the sensitivity measured on Day 14 (70.8 ± 8.4 nA·cm^{-2}·μM^{-1}) compared to Day 1 (78.9 ± 4.0 nA·cm^{-2}·μM^{-1}), and compares favourably with other reports where reduced sensitivities of between 20% and 50% have been reported following implantation [37].The stability of the biosensor was also investigated by examining baseline *in vivo* data for recording periods out to 16 days following implantation (see Section 5.2.6).

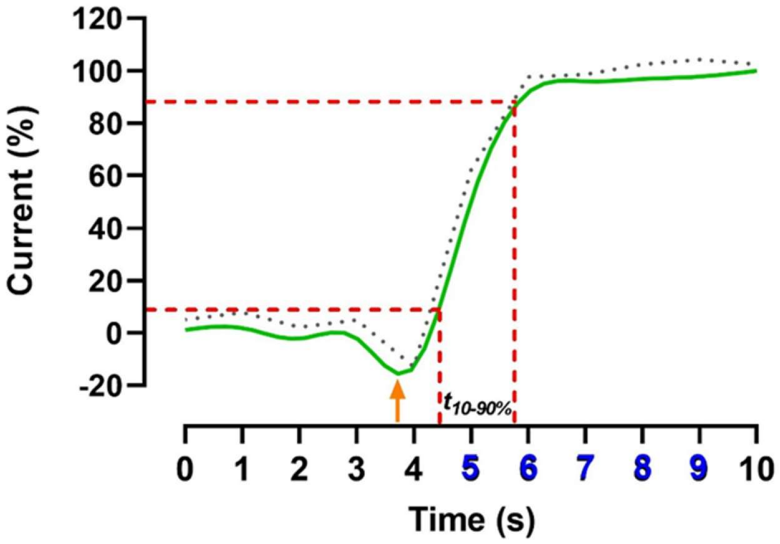

Figure 5.7: A typical example of the average (n = 4) and SEM (dotted line) normalised current change (response time, $t_{10–90\%}$) for the Pt_D(P*o*PD)(Sty)(GluOx/BSA:GA/PEI)$_{15}$ biosensor in response to a glutamate injection (10 μM, arrow) performed at room temperature. Blue numerals indicate mixing time.

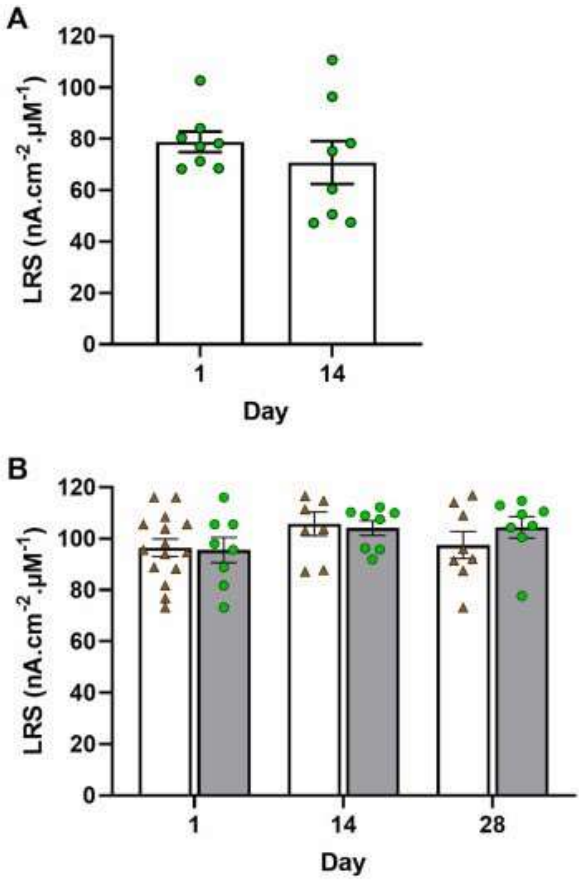

Figure 5.8: (**A**) The effect of two weeks storage in *ex vivo* rodent brain tissue at 4 °C on the $Pt_D(PoPD)(Sty)(GluOx/BSA:GA/PEI)_{15}$ biosensor sensitivity (Linear Region Slope; Mean ± SEM, n = 8). (**B**) Clear - comparison of sensitivities for biosensors stored dry at 4 °C until one-off calibration on Day 1 (n = 15), Day 14 (n = 8) and Day 28 (n = 8). Grey - comparison of sensitivities (n = 8) for a batch of biosensors measured following storage between initial calibration on Day 1, and repeated calibrations on Days 14 and 28. Average current-concentration responses are shown in Figure 5.9.

Appraisal of shelf-life (Figure 5.8 B), *i.e.*, the time under defined storage conditions during which the sensor remains viable, involved comparing the sensitivities of batches of biosensors which were stored dry at 4 °C until one-off calibration on Days 1, 14 and 28. Responses were similar ($F_{(2,28)} = 1.317$, $p = 0.2841$, one-way ANOVA) for all three days: Day 1, 96.4 ± 3.4 nA·cm^{-2}·μM^{-1} (n = 15); Day 14, 105.8 ± 4.6 nA·cm^{-2}·μM^{-1} (n = 8); and Day 28,

97.5 ± 5.2 nA·cm^{-2}·μM^{-1} (n = 8). As repeated calibrations can sometimes have a negative effect on the sensitivity of polymer-enzyme composite biosensors [28, 47] additional examination of the effect of calibrating the same batch of biosensors over the same time interval was performed (Figure 5.8 B). Again, no significant difference ($F_{(2,14)} = 1.412$, $p = 0.2764$, one-way repeated measures ANOVA, n = 8) in sensitivity was observed: Day 1, 95.6 ± 4.9 nA·cm^{-2}·μM^{-1}; Day 14, 104.1 ± 2. nA·cm^{-2}·μM^{-1}; and Day 28, 104.4 ± 4.2 nA·cm^{-2}·μM^{-1}.

Overall, these characteristics indicate good stability in terms of biocompatibility, storage and use, and compare favourably with other glutamate biosensors reported to retain their sensitivity following implantation [68], and for up to 5 [17, 48] months of storage. The calculated LOD and response time are also similar to previously reported values for glutamate biosensors [47], and when considered with the stability data suggest that the Pt_D(P*o*PD)(Sty)(GluOx/BSA:GA/PEI)$_{15}$ biosensor is ideally suited to performing neurochemical measurements associated with behavioural and/or pharmacological manipulations. While BSA:GA mixtures have been used extensively in biosensor designs to increase sensitivity/stability, it is most likely that the extended characteristics observed here can be attributed to the incorporation of the polycation PEI, through its ability to facilitate charge counterbalance with the polyanionic GluOx [61].

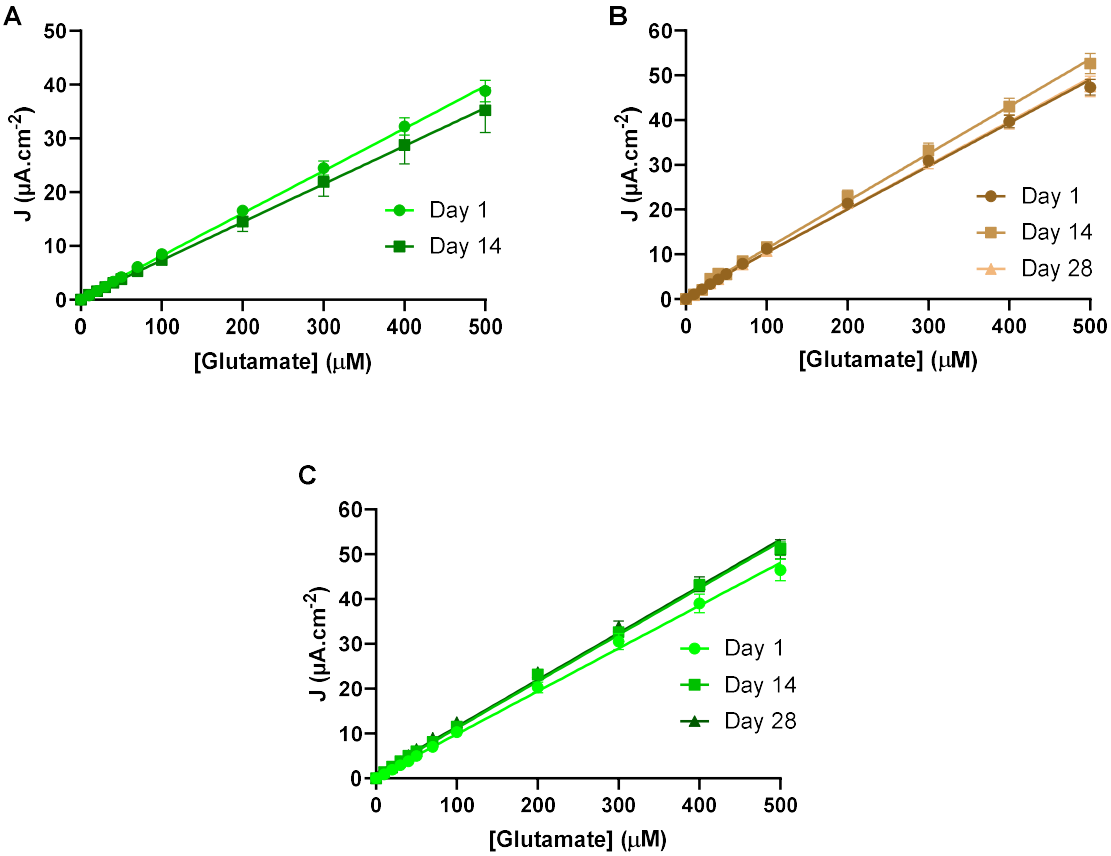

Figure 5.9: Current-concentration (linear region) responses (Mean ± SEM) of the Pt_D(P*o*PD)(Sty)(GluOx/BSA:GA/PEI)$_{15}$ biosensor: (**A**) before (Day 1) and after (Day 14) storage in *ex vivo* rodent brain tissue at 4 ºC (n = 8); (**B**) following dry storage at 4 ºC until one-off calibrations of different batches of biosensors on Day 1 (n = 15), Day 14 (n = 8) and Day 28 (n = 8) and; (**C**) following dry storage of the same batch of biosensors between initial calibration on Day 1, and repeated calibrations on Days 14 and 28.

5.2.6 *In Vivo* Recording

Preliminary *in vivo* experiments were performed to examine biocompatibility/stability and to validate the ability of the Pt_D(P*o*PD)(Sty)(GluOx/BSA:GA/PEI)$_{15}$ biosensor to detect extracellular changes in glutamate. Baseline signals were analysed over the same time interval (08:00–09:00), for recording phases between Day 6 and Day 16, and no significant variation in current was observed (Figure 5.10 A; $F_{(8,61)} = 0.1741$, $P = 0.9936$, one-way ANOVA). A sample continuous 12 h trace (dark phase) with simultaneously recorded motor activity clearly highlights periods of activity which are coincident with increases in glutamate (Figure 5.10 B). Such naturally occurring changes are often associated with behavioural phenomena such as grooming, feeding and locomotor activity [34, 69].

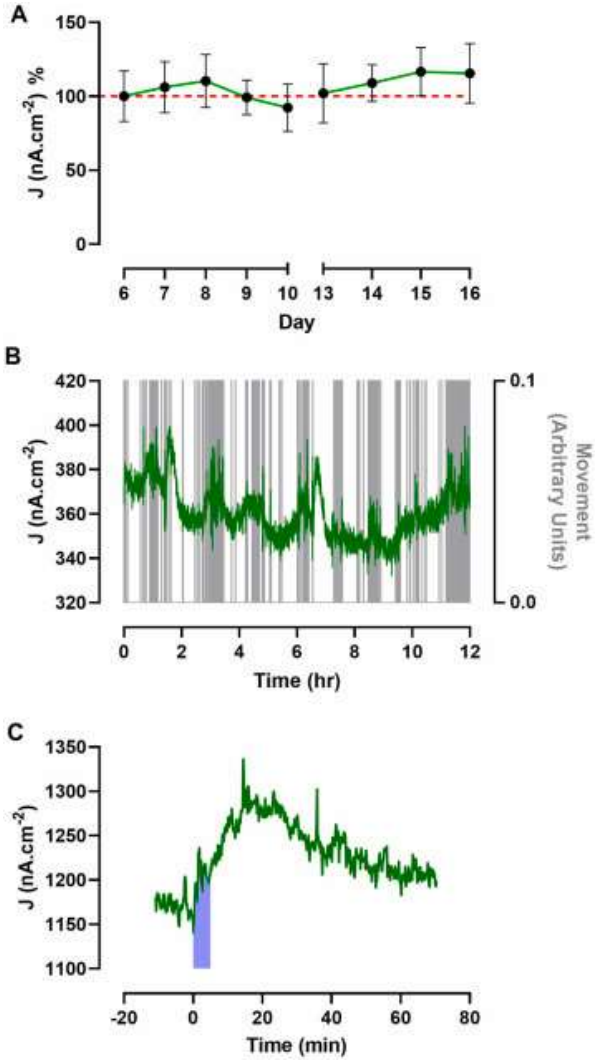

Figure 5.10: (**A**) Average (±SEM, n = 5–11) baseline *in vivo* data (pooled from 8 freely-moving animals) for the Pt_D(P*o*PD)(Sty)(GluOx/BSA:GA/PEI)$_{15}$ biosensor recorded from striatum using CPA at +700 mV over an 11 day period. All data taken from the same daily 1-h (08:00-09:00) period when the animals were mostly inactive and normalised to Day 6, (average = 106 ± 3). (**B**) A typical example of a continuous real-time *in vivo* recording from prefrontal cortex over a 12 h period (dark phase, 19:00 – 07:00). Grey lines represent simultaneously monitored motor activity. (**C**) Typical signal change associated with a period of restraint stress (5-min, shaded area).

Similarly, physiological stimulation induced in response to stress (e.g. tail-pinch), has previously been shown to elicitate neuronal activation with concomittant increases in glutamate

measured using both microdialysis [70] and biosensors [33, 68]. As such, we examined the effect of mild stress in the form of a 5 min restraint (see Section 3.6); the signal, recorded from prefrontal cortex, increased during the procedure with a return to baseline that was dependent on the activity/behaviour of the animal post stimulus (Figure 5.10 C).

Taken together, these preliminary results support the *in vitro* data indicating that the developed biosensor is capable of detecting brain extracellular glutamate, and is suitable for recording changes for at least three weeks following implantation

.

5.3 Conclusion

This research work set out to complete the development and *in vitro* characterisation of a glutamate oxidase-based microelectrode biosensor capable of *in vivo* measurements. The optimal Pt_D(P*o*PD)(Sty)(GluOx/BSA:GA/PEI)$_{15}$ design achieved a sensitivity comparable to previously reported sensors, a shelf-life of several weeks, and displayed no loss of sensitivity with repeated calibrations or exposure to *ex vivo* rodent brain tissue. Potential interference signal contributions from physiologically relevant electroactive species were tested for both basal and neurotoxic levels of glutamate and found to be negligible. Oxygen interference studies suggest that the biosensor signal should not suffer significantly from oxygen fluctuations in brain ECF under all but extreme anaerobic conditions. In addition, physiologically relevant pH and temperature changes had minimal effect on the biosensor performance, which, when taken with a calculated low μM detection limit and rapid response time, suggests that this composite sensor should reliably detect L-glutamate when used for neurochemical monitoring. These results were supported by preliminary *in vivo* experiments performed in freely-moving animals where expected signal changes were observed for both natural and induced behavioural/neuronal activation, from a baseline which was stable 16 days following implantation.

5.4 References

1. Victor Nadler, J., *Plasticity of glutamate synaptic mechanisms.* Epilepsia, 2010. **51**(s5): p. 17-17.
2. Meldrum, B.S., *Glutamate as a neurotransmitter in the brain: review of physiology and pathology.* J Nutr, 2000. **130**(4S Suppl): p. 1007s-15s.
3. Furukawa, H., et al., *Subunit arrangement and function in NMDA receptors.* Nature, 2005. **438**(7065): p. 185-192.
4. Bradford, H.F., *Glutamate, GABA and epilepsy.* Progress in Neurobiology, 1995. **47**(6): p. 477-511.
5. Coyle, J.T., *Glutamate and schizophrenia: beyond the dopamine hypothesis.* Cell Mol Neurobiol, 2006. **26**(4-6): p. 365-84.
6. Fern, R. and C. Matute, *Glutamate receptors and white matter stroke.* Neuroscience Letters, 2019. **694**: p. 86-92.
7. Lau, A. and M. Tymianski, *Glutamate receptors, neurotoxicity and neurodegeneration.* Pflügers Archiv - European Journal of Physiology, 2010. **460**(2): p. 525-542.
8. Choi, D.W., *Glutamate neurotoxicity and diseases of the nervous system.* Neuron, 1988. **1**(8): p. 623-634.
9. Burmeister, J.J., et al., *Glutaraldehyde cross-linked glutamate oxidase coated microelectrode arrays: selectivity and resting levels of glutamate in the CNS.* ACS chemical neuroscience, 2013. **4**(5): p. 721-728.
10. R. Ryan, M., J. P. Lowry, and R. D. O'Neill, *Biosensor for Neurotransmitter L-Glutamic Acid Designed for Efficient Use of L-Glutamate Oxidase and Effective Rejection of Interference.* Analyst, 1997. **122**(11): p. 1419-1424.
11. Miele, M., et al., *The determination of the extracellular concentration of brain glutamate using quantitative microdialysis.* Brain research, 1996. **707**(1): p. 131-133.
12. Galvan, A., Y. Smith, and T. Wichmann, *Continuous monitoring of intracerebral glutamate levels in awake monkeys using microdialysis and enzyme fluorometric detection.* Journal of Neuroscience Methods, 2003. **126**(2): p. 175-185.
13. Dawson, L.A., J.M. Stow, and A.M. Palmer, *Improved method for the measurement of glutamate and aspartate using capillary electrophoresis with laser induced fluorescence*

detection and its application to brain microdialysis. Journal of Chromatography B: Biomedical Sciences and Applications, 1997. **694**(2): p. 455-460.

14. Kiba, N., et al., *Chemiluminometric sensor for simultaneous determination of L-glutamate and L-lysine with immobilized oxidases in a flow injection system.* Analytical Chemistry, 2002. **74**(6): p. 1269-1274.
15. Doong, R.-a. and H.-m. Shih, *Glutamate optical biosensor based on the immobilization of glutamate dehydrogenase in titanium dioxide sol–gel matrix.* Biosensors and Bioelectronics, 2006. **22**(2): p. 185-191.
16. Chatard, C., A. Meiller, and S. Marinesco, *Microelectrode Biosensors for in vivo Analysis of Brain Interstitial Fluid.* Electroanalysis, 2018. **30**(6): p. 977-998.
17. Tian, F., et al., *A microelectrode biosensor for real time monitoring of l-glutamate release.* Analytica Chimica Acta, 2009. **645**(1): p. 86-91.
18. Qin, S., et al., *Microsensors for in vivo Measurement of Glutamate in Brain Tissue.* Sensors, 2008. **8**(11): p. 6860-6884.
19. Tan, C., et al., *Recent advances in in vivo neurochemical monitoring.* Micromachines, 2021. **12**(2): p. 208.
20. Kirwan, S.M., et al., *Modifications of Poly(o-phenylenediamine) Permselective Layer on Pt-Ir for Biosensor Application in Neurochemical Monitoring.* Sensors (Basel, Switzerland), 2007. **7**(4): p. 420-437.
21. Lowry, J.P., *Partial characterization in vitro of glucose oxidase-modified poly(phenylenediamine)-coated electrodes for neurochemical analysis in vivo.* Electroanalysis, 1994. **6**(5-6): p. 369-379.
22. Polcari, D., et al., *Disk-Shaped Amperometric Enzymatic Biosensor for in Vivo Detection of d-serine.* Analytical Chemistry, 2014. **86**(7): p. 3501-3507.
23. Singh, M., P.K. Kathuroju, and N. Jampana, *Polypyrrole based amperometric glucose biosensors.* Sensors and Actuators B: Chemical, 2009. **143**(1): p. 430-443.
24. Kausaite-Minkstimiene, A., et al., *Evaluation of amperometric glucose biosensors based on glucose oxidase encapsulated within enzymatically synthesized polyaniline and polypyrrole.* Sensors and Actuators B: Chemical, 2011. **158**(1): p. 278-285.
25. Liu, X., et al., *Amperometric glucose biosensor based on single-walled carbon nanohorns.* Biosensors and Bioelectronics, 2008. **23**(12): p. 1887-1890.

26. McMahon, C.P. and R.D. O'Neill, *Polymer−Enzyme Composite Biosensor with High Glutamate Sensitivity and Low Oxygen Dependence.* Analytical Chemistry, 2005. **77**(4): p. 1196-1199.
27. Doran, M.M., N.J. Finnerty, and J.P. Lowry, *In–Vitro Development and Characterisation of a Superoxide Dismutase-Based Biosensor.* ChemistrySelect, 2017. **2**(14): p. 4157-4164.
28. Baker, K.L., et al., *Characterisation of a Platinum-based Electrochemical Biosensor for Real-time Neurochemical Analysis of Choline.* Electroanalysis, 2019. **31**(1): p. 129-136.
29. Baker, K.L., F.B. Bolger, and J.P. Lowry, *Development of a microelectrochemical biosensor for the real-time detection of choline.* Sensors and Actuators B: Chemical, 2017. **243**: p. 412-420.
30. O'Brien, K.B., et al., *Development and characterization in vitro of a catalase-based biosensor for hydrogen peroxide monitoring.* Biosensors and Bioelectronics, 2007. **22**(12): p. 2994-3000.
31. O'Riordan, S.L. and J.P. Lowry, *In vivo characterisation of a catalase-based biosensor for real-time electrochemical monitoring of brain hydrogen peroxide in freely-moving animals.* Analytical Methods, 2017. **9**(8): p. 1253-1264.
32. Govindarajan, S., et al., *Highly selective and stable microdisc biosensors for l-glutamate monitoring.* Sensors and Actuators B: Chemical, 2013. **178**: p. 606-614.
33. Lowry, J.P., M.R. Ryan, and R.D. O'Neill, *Behaviourally induced changes in extracellular levels of brain glutamate monitored at 1 s resolution with an implanted biosensor.* Analytical Communications, 1998. **35**(3): p. 87-89.
34. Baker, K.L., F.B. Bolger, and J.P. Lowry, *A microelectrochemical biosensor for real-time in vivo monitoring of brain extracellular choline.* Analyst, 2015. **140**(11): p. 3738-3745.
35. Dash, M.B., et al., *Sleep/wake dependent changes in cortical glucose concentrations.* Journal of neurochemistry, 2013. **124**(1): p. 79-89.
36. Hu, Y. and G.S. Wilson, *A temporary local energy pool coupled to neuronal activity: fluctuations of extracellular lactate levels in rat brain monitored with rapid-response enzyme-based sensor.* Journal of neurochemistry, 1997. **69**(4): p. 1484-1490.

37. Hu, Y., et al., *Direct measurement of glutamate release in the brain using a dual enzyme-based electrochemical sensor.* Brain research, 1994. **659**(1-2): p. 117-125.
38. Kulagina, N.V., L. Shankar, and A.C. Michael, *Monitoring Glutamate and Ascorbate in the Extracellular Space of Brain Tissue with Electrochemical Microsensors.* Analytical Chemistry, 1999. **71**(22): p. 5093-5100.
39. Hamdi, N., J.J. Wang, and H.G. Monbouquette, *Polymer films as permselective coatings for H2O2-sensing electrodes.* Journal of Electroanalytical Chemistry, 2005. **581**(2): p. 258-264.
40. Zhang, M., C. Mullens, and W. Gorski, *Chitosan-Glutamate Oxidase Gels: Synthesis, Characterization, and Glutamate Determination.* Electroanalysis, 2005. **17**(23): p. 2114-2120.
41. McMahon, C.P., et al., *Oxygen tolerance of an implantable polymer/enzyme composite glutamate biosensor displaying polycation-enhanced substrate sensitivity.* Biosensors and Bioelectronics, 2007. **22**(7): p. 1466-1473.
42. Day, B.K., et al., *Microelectrode array studies of basal and potassium-evoked release of l-glutamate in the anesthetized rat brain.* Journal of Neurochemistry, 2006. **96**(6): p. 1626-1635.
43. Vasylieva, N., et al., *Covalent enzyme immobilization by poly(ethylene glycol) diglycidyl ether (PEGDE) for microelectrode biosensor preparation.* Biosensors and Bioelectronics, 2011. **26**(10): p. 3993-4000.
44. Govindarajan, S., et al., *Highly selective and stable microdisc biosensors for L-glutamate monitoring.* Sensors and Actuators B: Chemical, 2013. **178**: p. 606-614.
45. Salazar, P., et al., *Glutamate microbiosensors based on Prussian Blue modified carbon fiber electrodes for neuroscience applications: In-vitro characterization.* Sensors and Actuators B: Chemical, 2016. **235**: p. 117-125.
46. Ford, R., et al., *Carbon nanohorn modified platinum electrodes for improved immobilisation of enzyme in the design of glutamate biosensors.* Analyst, 2019. **144**(17): p. 5299-5307.
47. Ganesana, M., et al., *Development of a novel micro biosensor for in vivo monitoring of glutamate release in the brain.* Biosensors and Bioelectronics, 2019. **130**: p. 103-109.

48. Ford, R., S.J. Quinn, and R.D. O'Neill, *Characterization of Biosensors Based on Recombinant Glutamate Oxidase: Comparison of Crosslinking Agents in Terms of Enzyme Loading and Efficiency Parameters.* Sensors (Basel), 2016. **16**(10).
49. O'Neill, R.D., et al., *Designing sensitive and selective polymer/enzyme composite biosensors for brain monitoring in vivo.* TrAC Trends in Analytical Chemistry, 2008. **27**(1): p. 78-88.
50. Lowry, J.P., et al., *Characterization of glucose oxidase-modified poly (phenylenediamine)-coated electrodes in vitro and in vivo: homogeneous interference by ascorbic acid in hydrogen peroxide detection.* Analytical Chemistry, 1994. **66**(10): p. 1754-1761.
51. Miele, M. and M. Fillenz, *In vivo determination of extracellular brain ascorbate.* Journal of Neuroscience Methods, 1996. **70**(1): p. 15-19.
52. Brown, F.O. and J.P. Lowry, *Microelectrochemical sensors for in vivo brain analysis: an investigation of procedures for modifying Pt electrodes using Nafion®.* Analyst, 2003. **128**(6): p. 700-705.
53. Rebec, G.V. and R. Christopher Pierce, *A vitamin as neuromodulator: Ascorbate release into the extracellular fluid of the brain regulates dopaminergic and glutamatergic transmission.* Progress in Neurobiology, 1994. **43**(6): p. 537-565.
54. Killoran, S.J. and R.D. O'Neill, *Characterization of permselective coatings electrosynthesized on Pt–Ir from the three phenylenediamine isomers for biosensor applications.* Electrochimica Acta, 2008. **53**(24): p. 7303-7312.
55. Lowry, J.P., et al., *An amperometric glucose-oxidase/poly (o-phenylenediamine) biosensor for monitoring brain extracellular glucose: in vivo characterisation in the striatum of freely-moving rats.* Journal of neuroscience methods, 1998. **79**(1): p. 65-74.
56. Liebana, S. and G.A. Drago, *Bioconjugation and stabilisation of biomolecules in biosensors.* Essays in biochemistry, 2016. **60**(1): p. 59-68.
57. Lowry, J.P. and R.D. O'Neill, *Neuroanalytical chemistry in vivo using biosensors.* Encyclopedia of sensors, 2005: p. 501-524.
58. Walker, E., et al., *Selective detection of extracellular glutamate in brain tissue using microelectrode arrays coated with over-oxidized poly pyrrole.* Analyst, 2007. **132**(11): p. 1107-1111.

59. Breier, J.M., M.G. Bankson, and B.K. Yamamoto, *L-tyrosine contributes to (+)-3, 4-methylenedioxymethamphetamine-induced serotonin depletions.* Journal of Neuroscience, 2006. **26**(1): p. 290-299.
60. Nair, P.K., D.G. Buerk, and J.H. Halsey Jr, *Comparisons of oxygen metabolism and tissue PO2 in cortex and hippocampus of gerbil brain.* Stroke, 1987. **18**(3): p. 616-622.
61. McMahon, C.P., et al., *Oxygen tolerance of an implantable polymer/enzyme composite glutamate biosensor displaying polycation-enhanced substrate sensitivity.* Biosensors and Bioelectronics, 2007. **22**(7): p. 1466-1473.
62. Dixon, B.M., J.P. Lowry, and R. D O'Neill, *Characterization in vitro and in vivo of the oxygen dependence of an enzyme/polymer biosensor for monitoring brain glucose.* Journal of Neuroscience Methods, 2002. **119**(2): p. 135-142.
63. Vaarmann, A., et al., *Dopamine protects neurons against glutamate-induced excitotoxicity.* Cell death & disease, 2013. **4**(1): p. e455-e455.
64. Llaudet, E., et al., *Microelectrode biosensor for real-time measurement of ATP in biological tissue.* Analytical chemistry, 2005. **77**(10): p. 3267-3273.
65. Kiyatkin, E.A., *The hidden side of drug action: brain temperature changes induced by neuroactive drugs.* Psychopharmacology, 2013. **225**(4): p. 765-780.
66. Frey, O., et al., *Enzyme-based choline and L-glutamate biosensor electrodes on silicon microprobe arrays.* Biosensors and Bioelectronics, 2010. **26**(2): p. 477-484.
67. O'Neill, R.D., *Sensor–tissue interactions in neurochemical analysis with carbon paste electrodes in vivo.* Analyst, 1993. **118**(4): p. 433-438.
68. Tseng, T.T.C., C.-F. Chang, and W.-C. Chan, *Fabrication of implantable, enzyme-immobilized glutamate sensors for the monitoring of glutamate concentration changes in vitro and in vivo.* Molecules, 2014. **19**(6): p. 7341-7355.
69. Finnerty, N.J., et al., *An investigation of hypofrontality in an animal model of schizophrenia using real-time microelectrochemical sensors for glucose, oxygen, and nitric oxide.* ACS Chemical Neuroscience, 2013. **4**(5): p. 825-831.
70. Lupinsky, D., L. Moquin, and A. Gratton, *Interhemispheric regulation of the medial prefrontal cortical glutamate stress response in rats.* Journal of Neuroscience, 2010. **30**(22): p. 7624-7633.

CHAPTER SIX

Conclusions

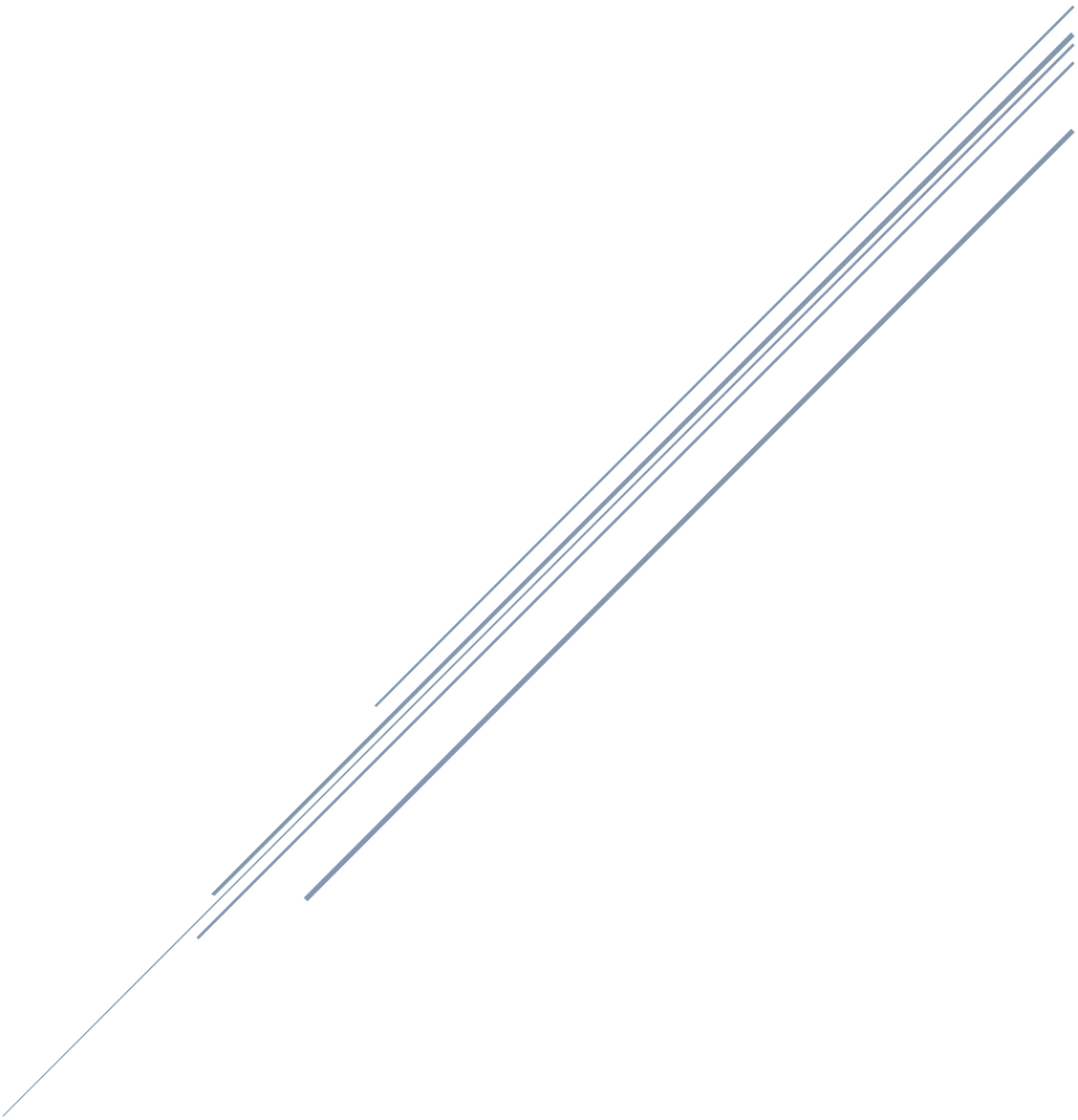

6.1 – Conclusions

This research began with a challenging goal, to develop and characterise a GABase-based *in vitro* first generation biosensor capable of monitoring GABA *in vivo*. Following this, dual detection and monitoring of GABA and L-glutamate was to be performed because of the associative nature of GABA as the major inhibitory neurotransmitter and L-glutamate as the major excitatory neurotransmitter. Unfortunately the development of the GABA biosensor proved to be too challenging a task to be completed. Focus was thus diverted to the refinement and full *in vitro* characterisation of the L-glutamate biosensor. Preliminary *in vivo* characterisation was then undertaken.

In developing a GABA biosensor, various parameters were examined. The parameters included: the unit activity of the enzyme solution; the position of GABase in the underlying L-glutamate biosensor and post L-glutamate biosensor deposition of the GABase solution; an investigation into ensuring the active surface was appropriate; and alternative methods of detection *i.e.* use of a different reaction scheme and a different electrochemical technique. There was no indication that any of these composite design changes would produce a signal. Three other research groups have developed GABase and glutamate oxidase-based biosensors for GABA monitoring [1-3] shortly after this work had concluded. This suggests there was an underlying issue never addressed in our development. All three groups' biosensors operated under the same reaction equations laid out in Section 4.1 (*enzyme reaction 1-3*). Multi-electrode set-ups were used, unlike the work presented here. These groups employed drop-casting of their matrix mixtures of the enzymes, GABase and GluOx, and the various components, BSA and GA. This work used individual solutions for each of the enzymes and components while employing dip-coating. The concentrations of the constituents of their matrices also differed - all matrices used significantly lower unit activities for the GluOx and GABase, compared to the experimental designs investigated herein (100 U/mL GluOx, and 5 U/mL, 50 U/mL, 100 U/mL GABase): Hossain *et. al.* matrix mixture (0.1 U/μL GluOx; 0.1 U/μL GABase; 0.8% BSA; 0.1% GA); Doughty *et al.* (0.1 U/mL GluOx; 0.1 U/mL GABase; 1% BSA; 0.125% GA); and Burmeister *et al.* (0.05 U/μL GluOx; 0.0125 GABase; 1% BSA; 0.1%); This could be a potential source preventing any H_2O_2 production from GABA due to enzyme over-loading (the constant potential remained at +700 mV *vs*. SCE as this is ideal for H_2O_2 detection). Also, none of the other groups incorporated PEI in their final designs.

Given the comparison to other research groups' design, it further supports the hypothesis that enzyme over-loading is, at least in part, responsible for the lack of a signal output. Refinement of the enzyme solution and concentrations used is needed. The publications suggest it may be required to derive a multi-electrode set-up using drop-casting of an enzyme matrix for biosensor fabrication to produce a viable biosensor for GABA monitoring.

A polymer/enzyme composite biosensor for monitoring neurochemical glutamate was performance optimised *in vitro* for sensitivity, selectivity and stability. This first generation Pt/glutamate oxidase-based sensor displayed appropriate sensitivity (90.4 ± 2.0 nA·cm^{-2}·μM^{-1}). It also has ideal stability/biocompatibility with no significant decrease in response observed for repeated calibrations, or following storage at 4 °C either dry (28 days) or in *ex-vivo* rodent brain tissue (14 days). Potential non-glutamate contributing signals, generated by extracellular levels of the principal endogenous electroactive interferents, were typically <5% of the basal (10 μM) glutamate response. Changes in molecular oxygen (the natural enzyme mediator) over the normal brain tissue range of 40 – 80 μM had minimal effect on the glutamate signal for concentrations of 10 and 100 μM (Mean $K_MO_2 = 1.86 \pm 0.74$ μM, $[O_2]_{90\%}$ = *ca.* 15 μM). Additionally, a low μM calculated limit of detection (0.44 ± 0.05) and rapid response time (*ca.* 1.67 ± 0.06 s), combined with no effect of pH and temperature changes over physiologically relevant ranges (7.2–7.6 and 34–40 °C respectively), collectively suggest that this composite biosensor should reliably detect L-glutamate when used for neurochemical monitoring. Preliminary experiments involving implantation in the striatum of freely moving rats demonstrated stable recording over several weeks, and reliable detection of physiological changes in glutamate in response to behavioural/neuronal activation (locomotor activity and restraint stress).

Future *in vivo* studies will focus on consolidating this conclusion, and identifying the sources (e.g. neuronal and/or glial) contributing to the recorded glutamate signal. Further investigation into the inter-related nature of D-serine and L-glutamate as co-agonists for the NMDA receptor is also planned.

6.2 References

1. Hossain, I., et al., *A Novel Microbiosensor Microarray for Continuous ex Vivo Monitoring of Gamma-Aminobutyric Acid in Real-Time.* Frontiers in Neuroscience, 2018. **12**.
2. Doughty, P.T., et al., *Novel microwire-based biosensor probe for simultaneous real-time measurement of glutamate and GABA dynamics in vitro and in vivo.* Scientific Reports, 2020. **10**(1): p. 12777.
3. Burmeister, J.J., et al., *Challenges of simultaneous measurements of brain extracellular GABA and glutamate in vivo using enzyme-coated microelectrode arrays.* Journal of Neuroscience Methods, 2020. **329**: p. 108435.

APPENDICES

Publications

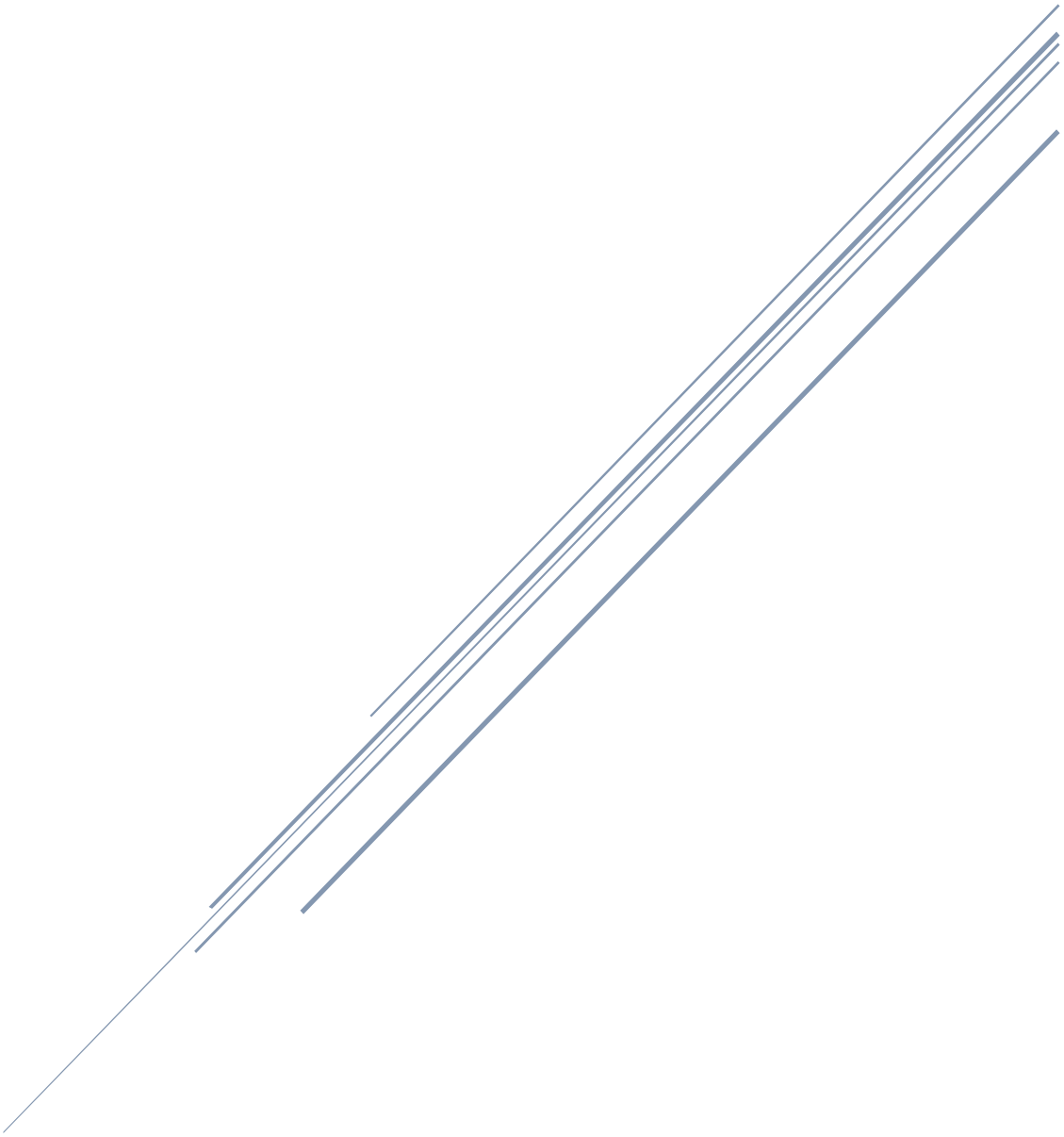

Appendix 1: Design optimisation and characterisation of an amperometric glutamate oxidase-based composite biosensor for neurotransmitter L-glutamic acid

Analytica Chimica Acta 1224 (2022) 340205

Contents lists available at ScienceDirect

Analytica Chimica Acta

journal homepage: www.elsevier.com/locate/aca

Design optimisation and characterisation of an amperometric glutamate oxidase-based composite biosensor for neurotransmitter L-glutamic acid

Kobi P. Bermingham [1], Michelle M. Doran [1], Fiachra B. Bolger, John P. Lowry [*,1]

Neurochemistry Laboratory, Maynooth University Department of Chemistry, Maynooth University, Maynooth, Co. Kildare, Ireland

HIGHLIGHTS

- *In vitro* performance optimisation of a composite biosensor for neurochemical glutamate.
- Reduced manufacturing time, low μM limit of detection and rapid response time.
- No effect of interferent, pH and temperature changes over physiologically relevant ranges.
- No loss of sensitivity following sterilisation and stable recording over several weeks *in vivo.*
- Reliable detection of physiological changes in response to behavioural/ neuronal activation.

GRAPHICALABSTRACT

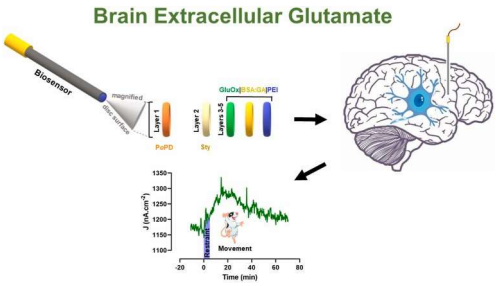

ARTICLEINFO

Keywords:
Glutamate
Biosensor
Amperometry
Neurochemistry
Rat brain

ABSTRACT

A polymer/enzyme composite biosensor for monitoring neurochemical glutamate was performance optimised *in vitro* for sensitivity, selectivity and stability. This first generation Pt/glutamate oxidase-based sensor displayed appropriate sensitivity (90.4 ± 2.0 nA cm^{-2} μM^{-1}). It also has ideal stability/biocompatibility with no significant decrease in response observed for repeated calibrations, exposure to electron beam sterilisation, or following storage at 4 °C either dry (28 days) or in *ex-vivo* rodent brain tissue (14 days). Potential non-glutamate contributing signals, generated by extracellular levels of the principal endogenous electroactive interferents, were typically <5% of the basal (10 μM) glutamate response. Changes in molecular oxygen (the natural enzyme mediator) over the normal brain tissue range of 40–80 μM had minimal effect on the glutamate signal for concentrations of 10 and 100 μM (Mean K_MO_2 = 1.86 ± 0.74 μM, $[O_2]_{90\%}$ = *ca.* 15 μM). Additionally, a low μM calculated limit of detection (0.44 ± 0.05) and rapid response time (*ca.* 1.67 ± 0.06 s), combined with no effect of pH and temperature changes over physiologically relevant ranges (7.2–7.6 and 34–40 °C respectively), collectively suggest that this composite biosensor should reliably detect L-glutamate when used for neurochemical monitoring. Preliminary experiments involving implantation in the striatum of freely moving rats demonstrated stable recording over several weeks, and reliable detection of physiological changes in glutamate in response to behavioural/neuronal activation (locomotor activity and restraint stress).

* Corresponding author.
E-mail address: John.Lowry@mu.ie (J.P. Lowry).
[1] These authors contributed equally. https://doi.org/10.1016/j.aca.2022.340205

Received 6 April 2022; Received in revised form 15 July 2022; Accepted 24 July 2022 Available online 31 July 2022

1. Introduction

The amino acid, L-Glutamate, is prevalent throughout the mammalian brain, with an estimated 60–70% of synapses using it as their neurotransmitter [1]. Consequently, it has been shown to be vital for normal brain functioning in areas such as development, plasticity, learning and memory, and sensory and motor systems [2]. Along with D-serine it is a co-agonist of the *N*-methyl-D-aspartate (NMDA) receptor [3], abnormal functioning of which has been linked to disorders such as epilepsy, stroke, and both neurodegenerative and psychiatric diseases [4–7]. Additionally, glutamate toxicity is also associated with neuronal death in ischemia, hypoglycaemia, and trauma [8]. Notwithstanding such extensive research there is still significant interest in improving and advancing our understanding of its neurochemical roles and mechanisms of action. Key to achieving this is the ability to perform rapid (of the order of seconds or less) highly sensitive measurements in the living brain. While this has proved challenging due to its low basal concentration, reported to be *ca.* 10 μM [9–11], several research groups have monitored L-glutamate levels using a variety of different analytical techniques, including brain microdialysis [12], capillary electrophoresis [13], and optical (e.g. chemiluminometric [14] and fluorescent [15]) sensors. However, depending on the method, limitations associated with temporal and spatial resolution, stability and biocompatibility, and interference, can hinder their suitability for *in situ* neurochemical monitoring.

The use of miniaturised enzyme-modified electrochemical biosensors offers the greatest potential of mitigating these shortcomings [9,16,17]. For glutamate monitoring such devices (see Table S1) are typically first-generation devices operating by detecting electroactive H_2O_2 produced in an enzymatic (oxidase) reaction; for glutamate/glutamate oxidase (GluOx) the reaction scheme is:

$$L-Glutamate + H_2O + O_2 \xrightarrow{GluOx} 2-oxoglutarate + NH_3 + H_2O_2 \quad (1)$$

$$H_2O_2 \xrightarrow{+700\ mV\ vs.\ SCE} 2H^+ + O_2 + 2e^- \quad (2)$$

As such, they generally have fast response times but the high potential required for H_2O_2 oxidation can result in interfering signals from a variety of endogenous electroactive species including ascorbic acid and dopamine [16]. Second generation biosensors incorporate a low redox potential mediator [18] as a substitute for molecular O_2 in order to improve selectivity. However, these tend to have slow response times and poor stability/sensitivity due to mediator leaching, in addition to potential toxicity issues, rendering them unsuitable for neurochemical monitoring [19]. Fortunately, for first generation biosensors the problem of selectivity has successfully been addressed through chemical modification of the electrode surface using a variety of polymeric permselective layers, including poly-*ortho*-phenylenediamine (P*o*PD) [20,21], poly-*meta*-phenylenediamine (P*m*PD) [9,22], polypyrrole [23], polyaniline [24] and Nafion® [25].

The research presented here builds on earlier biosensor development work targeting glutamate [11,26], and involves the determination of the response characteristics of a sensitivity optimised polymer composite design format successfully applied previously in the development of devices for superoxide [27], choline [28,29] and hydrogen peroxide [30, 31]. Functional considerations relevant to neurochemical monitoring were investigated *in vitro*, including stability, permselectivity and oxygen dependence, the effect of physiologically relevant temperature and pH changes, limit of detection, and response time. Finally, the sensor was employed successfully in preliminary *in vivo* experiments, demonstrating its ability to detect chronic real-time changes in glutamate.

2. Materials and methods

2.1. Reagents and solutions

All reagents were supplied by Sigma-Aldrich Ireland Ltd. (Dublin), unless otherwise stated. General chemicals included L-glutamic acid (monosodium salt, 99%), dopamine (hydrochloride), 5-hydroxytryptamine (5-HT), L-glutathione (oxidised form), dehydroascorbic acid (DHAA), uric acid (UA, potassium salt), 3,4-dihydroxyphenylacetic acid (DOPAC), homovanillic acid (HVA), 5-hydroxyindoleacetic acid (5- HIAA), L-tyrosine, L-cysteine, L-tryptophan and ascorbic acid (AA). Specific reagents used in biosensor manufacture were the immobiliser styrene (Sty, 99%), the enzyme L-glutamate oxidase (GluOx, EC 1.4.3.11, recombinant *E. coli*, 2B Scientific Ltd., Oxford, UK), the cross- linking agent glutaraldehyde (GA, Grade 1, 25%), and the stabilisers bovine serum albumin (BSA, fraction V from bovine plasma) and polyethylenimine (PEI, 80% ethoxylated). Poly(*ortho*-phenylenediamine) (P*o*PD, 1,2-diaminobenzene, ≥ 99%) was used to create a thin self- sealing permselective underlayer (see *Biosensor fabrication*).

All solutions were prepared in Milli-Q® water (18.2 MΩ cm). *In-vitro* experiments were performed in phosphate buffered saline (PBS, 1000 mL stock), pH 7.4 (137 mM NaCl, 2.7 mM KCl and 10 mM phosphate buffer solution, prepared from commercial tablets), except for pH studies where adjustments were made using either NaH_2PO_4 or NaOH. Solutions used in biosensor manufacture (*o*-PD monomer, 300 mM in N_2- saturated PBS; GluOx, 100 U/mL in 0.02 M potassium phosphate buffer, pH 7.4; BSA, 1%; GA, 0.1%; PEI, 1%) and calibration (L-glutamic acid, 0.1 M) were prepared fresh on the day of use. Interferent solutions were prepared as required, and depending on stability either used fresh (e.g. AA) or stored frozen (− 80 °C) between use.

2.2. Biosensor fabrication

Pt disc (Pt_D) and cylinder (Pt_C) electrodes were constructed using 5 cm lengths of Teflon®-coated Pt/Ir (90%/10%) wire (127-μm bare diameter, 203-μm coated diameter, Science Products GmbH, Hofheimer Straße 63, D-65719 Hofheim, Germany). Using a new scalpel blade a section of the Teflon® insulation was striped back under a stereo microscope (Olympus SZ51, Mason Technology Ltd., Dublin), exposing approximately 2 mm of wire which was then soldered into a gold clip (*In-vitro* - Fine Science Tools GmbH, 69115 Heidelberg, Germany; *In-vivo* - Plastics One, Roanoke, VA, USA). This provides both electrical contact and rigidity to allow connection to the potentiostat. The active surface was then created by carefully cutting the opposite end of the wire to create a disc surface. Cylinder electrodes were prepared by subsequently removing a 1 mm portion of the insulation. Various chemical layers were then used to modify this surface in order to facilitate enzyme immobilisation/stabilisation, interference rejection, etc. The first of these was P*o*PD which was electrochemically grown from a solution of *o*-PD monomer (300 mM in N_2 saturated PBS) following a previously reported procedure [21,32]. This layer was allowed to dry for a minimum of 3 h at room temperature (*ca.* 21 °C) before proceeding with the sequential layering of the other reagents using a dip-adsorption method [28]. Briefly, the Pt/P*o*PD electrodes were first dipped into the immobiliser Sty (*ca.* 0.5 s), and then consecutively dipped (*ca.* 0.5 s each) into GluOx (100 U/mL), a BSA:GA (1.0:0.1%) mixed solution, and PEI (1%), with 4 min drying between each GluOx/BSA:GA/PEI coating. Further drying and/or layering was performed in order to optimise the design in terms of sensitivity and ease of construction (see *Section 3.1 Biosensor design,* and Fig. 1S). All sensors were stored overnight at 4 °C before being calibrated [27,28].

2.3. Calibrations, stability and biocompatibility

L-Glutamate (0–10 mM) calibrations were performed using constant potential amperometry (CPA) in a standard three-electrode glass cell containing 15 mL of air-equilibrated PBS at room temperature (21–23 °C), unless otherwise stated. Reference and auxiliary electrodes were a saturated calomel electrode (SCE) and Pt wire respectively. A potential of +700 mV (*vs.* SCE) was used for monitoring H_2O_2 oxidation [21]. Sensors were allowed to settle for *ca.* 3 h before commencing calibrations. These were performed by injecting aliquots of the analyte into the buffer solution every 4 min (arbitrarily chosen). Each injection was followed by immediate stirring/mixing (*ca.* 5 s), with the current change measured immediately prior to the next injection. Interferent testing typically commenced with AA (the principal endogenous interferent [33,34]) and differed from glutamate calibrations in that the injection of aliquots of the respective chemicals was generally performed every 10 min with stirring/mixing lasting *ca.* 10 s. A similar protocol was followed for interferent testing in the presence of glutamate (100 μM).

The oxygen-dependence study was performed in PBS which was de-aerated by vigorously purging with N_2 for at least 30 min before commencing recording. Thereafter a N_2 cloud was maintained above the solution. An aliquot of L-glutamate was introduced into the cell to produce the desired concentration (10, 100, 200 or 500 μM), followed by the addition of standard aliquots (+313 μL, +319 μL, etc) of a saturated O_2 solution (100%, 1200 μM), yielding 25 μM O_2 increments over the range 0–200 μM every 4 min, with a brief stirring/mixing period (*ca.* 5 s) after each addition. Temperature controlled experiments were performed in a jacketed cell (ALS Ltd, IJ Cambria Scientific Ltd, Llanelli, UK), attached to a thermostatically controlled circulating water bath (Julabo Corio CD-BC4, Fisher Scientific, Dublin, Ireland). The temperature of the PBS was continuously recorded throughout the calibration using a commercial T-type thermocouple (AD Instruments Ltd., Oxford, UK) connected to a temperature pod (ADInstruments Ltd.) and interface system (eDAQ eCorder®, Green-Leaf Scientific, Dublin, Ireland). If required, adjustments were made to the bath temperature controller to maintain the desired temperature in the cell. Stability/shelf-life was determined by comparing the response of the same and different batches of biosensors stored dry at 4 °C between calibrations performed on days 1, 14 and 28. For biocompatibility testing sensors were carefully placed in moist brain tissue and stored at 4 °C between calibrations on days 1 and 14.

2.4. Biosensor sterilisation

Biosensors were carefully packaged in sealable Tyvek bags (Bemis Healthcare Packaging, Co. Offaly, Ireland) following construction and calibration (Day 1). They were then sent to a commercial sterilisation company (STERIS/Synergy Health, Co. Mayo, Ireland) and subjected to electron beam irradiation (50 kGy min^{-1}). On return, the sensors were calibrated (Day 8) to determine the effect, if any, of the sterilisation process on their performance.

2.5. Instrumentation, software and data analysis

A custom designed low-noise potentiostat (Biostat IV, ACM Instruments, Cumbria, UK) was used for all electrochemical experiments. Data acquisition was performed with a Dell notebook PC (*in-vitro*) or Apple iMac® (*in-vivo*), a PowerLab® 8/30 (ADInstruments Ltd) or eDAQ e-corder (Green-Leaf Scientific) interface system, and LabChart® for Windows (Version 6, ADInstruments Ltd.) or eDAQ Chart (Version 5.5.23, eDAQ Pty Ltd., NSW 2112, Australia). GraphPad Prism (Version 8.2.0; GraphPad Software Inc., CA, USA) was used for all data analysis and graphical presentations. Data is expressed as mean ± SEM, where *n* denotes the number of sensors. All signals were baseline subtracted and calibration curves were analysed to calculate the enzyme kinetic parameters V_{MAX} and K_M using either Michaelis-Menten or Michaelis- Menten Hill-type equations [21,35], as determined by the best non-linear regression fit. The linear range was defined by $K_M/2$ [36,37] and sensitivity (Linear Region Slope, LRS) was determined using linear regression analysis. Biosensor efficiency (BE%) normalises the biosensor response with respect to H_2O_2 sensitivity and was calculated as LRS x 100/Slope(H_2O_2). It reflects the major enzyme parameters determining the biosensor response to glutamate (i.e. loading of active enzyme and enzyme affinity) independent of H_2O_2 sensitivity [36,38]. K_MO_2 and $[O_2]_{90\%}$ were calculated based on previously defined criteria [26,38]. Statistical significance tests were performed using *t*-tests (two-tailed paired or unpaired where appropriate) or one-way ANOVA (with Tukey's post-hoc analysis). Values of $P < 0.05$ were considered to indicate statistical significance.

2.6. Surgical procedures

Male Wistar rats (data from 10 animals, typically 250–350 g; Charles River Laboratories International, Inc., UK) were anesthetised with Isoflurane (4% in air for induction, 1.5–3% for maintenance; Bioresource Unit (BRU), Maynooth University) using a Univentor 400 Anaesthetic Unit (AgnTho's AB, Sweden). Once surgical anaesthesia was established the animals were placed in a stereotaxic frame and the biosensors implanted following a previously reported method [39,40]. The level of anaesthesia was checked regularly (pedal withdrawal reflex). Coordinates for striatum and prefrontal cortex, with the skull levelled between bregma and lambda, were AP + 1.0, M/L ± 2.5 and D/V − 5 and AP + 3.2, M/L ± 0.8 and D/V − 4.2 respectively. A reference electrode (8T Ag, 200-μm diameter; Advent Research Materials, Suffolk, UK) was implanted in the cortex and an auxiliary electrode (8T Ag wire) wrapped around a stainless steel support screw (Fine Science Tools GmbH) placed in the skull. All electrode connectors (gold clips) were placed in a six pin multi-channel electrode pedestal (MS363, Plastics One, Roanoke, VA, USA), which was secured to the skull using dental acrylate (Dentalon Plus, AgnTho's AB) and four support screws. Saline (0.9%) and analgesic (Buprecare®; BRU, Maynooth University) were administered immediately following surgery. Animals were then allowed to recover for several hours in a thermostatically controlled cage (Thermacage MkII, Datesand Ltd, Manchester, UK), and assessed for good health according to published guidelines [41], regularly throughout the day of surgery, and subsequently at the beginning of every day. All *in-vivo* work was carried out with approval from Maynooth University Research Ethics Committee (BSRESC-2017-019), and under license (B100/2205 and HPRA AE19124/PO19) in accordance with the European Communities Regulations 2002 (Irish Statutory Instrument 566/2002 – Amendment of Cruelty to Animals Act 1876), and Part 5 of the European Union (Protection of Animals Used for Scientific Purposes) Regulations 2012 (S.I. No. 543 of 2012).

2.7. Experimental conditions in-vivo

For experiments, animals were singly housed in Raturn® sampling cage systems (BASi, West Lafayette, IN, USA; Fig. 2S) which allowed free movement of the animal during recording. All experiments were performed in the animal's home bowl in a temperature-controlled experimental facility with a 12 h light/dark cycle (lights on at 07:00) with access *ad libitum* to food and water. The implanted sensors in each animal were connected directly to the potentiostat in the late afternoon *via* the six pin electrode pedestal using a flexible screened six core cable (363-363 6TCM, Plastics One). The potential (+700 mV) was then applied and each animal was given at least 12 hours before experiments were started to allow them to become reaccustomed to being tethered. A low-pass digital filter (50 Hz cut-off) was used to eliminate mains AC noise and all data was recorded at either 4 or 40 Hz depending on the experiment. Movement was registered using a PIR detector (Gardscan QX PIR, Gardiner Technology, Queensway, Rochdale, OL11 1TQ, UK) modified in-house with a microprocessor to enable enhancement of the resolution of the sensor thereby registering more movement. Restraint stress was carried out using a form of wrap restraint which involved using a hand towel to immobilise the animal in the home bowl for a period of 5 min.

3. Results and discussion

3.1. Biosensor design

Building on previous glutamate biosensor development work [11,42, 43], and more recent validation of biosensors for monitoring several other neurochemicals [27,29,31,43], we have optimised the core

constituents/drying periods of our composite design to produce a sensitive biosensor for L-glutamate with a reproducible and efficient construction/assembly process. Each constituent, and their sequenced layering, is important to producing an appropriately viable sensor. Initial work focused on using a classic cylinder electrode design as employed successfully by ourselves [11,31,39,43] and several other groups for monitoring a variety of neurochemicals *in vivo* [44–46]. Surface modification here involved electrodeposition of permselective PoPD, followed by dip coating of a styrene layer, and then 10 sequential layers of GluOx, BSA:GA, and PEI, applied consecutively, with 4 min drying between each complete coating sequence. The sensor was then left for 60 min at room temperature before applying a second styrene layer and a further 10 GluOx/BSA:GA/PEI layers as before (see Section 2.2, *Biosensor fabrication*). The resultant Pt_C(PoPD)[(Sty)$_1$(GluOx/BSA:GA/PEI)$_{10}$]$_2$ biosensor (Design 14, Table S1) had comparable sensitivity (75.1 ± 1.5 nA cm^{-2} μM^{-1}, n = 8, R^2 = 0.9965) to our previous designs (*see* e.g. 5 and 10, Table S1). The applied GluOx/BSA:GA/PEI layers were key to achieving this response. When used on its own glutaraldehyde can have a negative effect on enzyme activity due to modification of the enzyme by covalent bonding. As such, it was combined with BSA which preferentially binds to the glutaraldehyde reducing its negative influence, primarily by freeing enzyme active sites for substrate turnover. Additionally, PEI was incorporated to further enhance GluOx immobilisation and stabilisation through the formation of polycationic/polyanionic complexes, and by decreasing the electrostatic repulsion between glutamate and the biosensor components.

In order to reduce the manufacturing time, this design was further refined by only applying the initial styrene layer, removing the 60 min drying period, and optimising the total number of GluOx/BSA:GA/PEI layers at 15. This Pt_C(PoPD)(Sty)(GluOx/BSA:GA/PEI)$_{15}$ biosensor (Fig. 1) had increased sensitivity; LRS 82.0 ± 2.2 nA cm^{-2} μM^{-1} (n = 16; $t_{(22)}$ = 2.107, p = 0.0468 *vs.* Design 14; R^2 = 0.9943, Fig. 1B). V_{MAX} and K_M values were 76.8 ± 1.0 μA cm^{-2} and 536 ± 20 μM (n = 16, Fig. 1A) respectively, and compare well with other reported values (see Table S1). The design was also tested using a disc geometry as GluOx- modified Pt_D electrodes have been reported to have higher sensitivity and less oxygen dependence compared to their cylinder counterparts [26], in addition to being more suitable for accessing smaller brain regions. The LRS was significantly increased (90.4 ± 2.0 nA cm^{-2} μM^{-1}, n = 16; $t_{(30)}$ = 2.837, p = 0.0081, R^2 = 0.9954, Fig. 1B) compared to that observed with the cylinder geometry, as were both the V_{MAX} (139 ± 2 μA cm^{-2}; t(30) = 27.76, p < 0.0001) and K_M values (1069 ± 43 μM; t(30) = 11.33, p < 0.0001; Fig. 1A). A calculated biosensor efficiency, BE% (see *Instrumentation, software and data analysis*), of 20.4 ± 1.0% (n = 16) for this Pt_D(PoPD)(Sty)(GluOx/BSA:GA/PEI)$_{15}$ biosensor indicates good diffusion-limited conversion of glutamate to H_2O_2 as BE% has an empirical maximum of *ca.* 60% [36,38] given that the diffusion coefficient for glutamate will always be less than that for H_2O_2, coupled with the fact that a significant fraction of enzyme-generated H_2O_2 molecules are not oxidised at the electrode because of loss to the bulk solution [47]. *3.2. Interference studies*

One of the most important sensor characteristics is selectivity. This is particularly so for neurochemical applications due to the complex chemical matrix of the brain which consists of a multitude of electroactive species and surface modifying agents such as lipids and proteins,

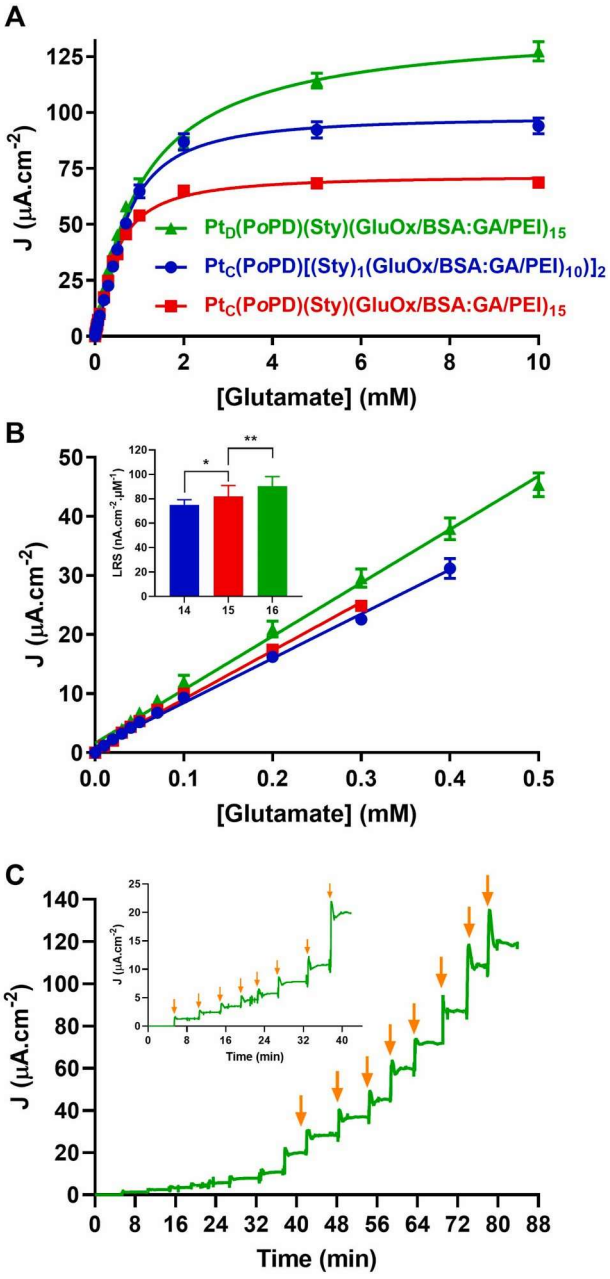

Fig. 1. (A) Current-concentration profiles for glutamate calibrations (0–10 mM) for biosensor designs 14 (blue, n = 8), 15 (red, n = 16) and 16 (green, n = 16), performed using constant potential amperometry (CPA) at +700 mV (*vs.* SCE) in PBS (pH 7.4). (B) Linear regression analysis and comparison (*inset*) of sensitivities (Linear Region Slope, LRS); *p < 0.05; **p < 0.01. (C) Typical raw data trace for design 16. Arrows indicate injections yielding concentrations of 0.3, 0.4, 0.5, 0.7, 1, 2, 5 and 10 mM glutamate. *Inset:* Close-up showing initial injections – arrows indicate concentrations of 0.01, 0.02, 0.03, 0.04, 0.05, 0.07, 0.1 and 0.2 mM. (For interpretation of the references to colour in this figure legend, the reader is referred to the Web version of this article.)

all of which can affect the performance of the implanted sensor. With respect to the former, the concentration of these endogenous species can often be greater than the concentration of the analyte of interest. For example, the basal concentration of L-glutamate has been estimated at *ca.* 10 μM using a variety of analytical techniques [10,11,16], while the most prevalent interferent, ascorbate (AA) [33,34], has a concentration of *ca.* 400 μM [48,49]. Thus, without appropriate exclusion strategies the current generated from AA oxidation would completely mask that of glutamate, as AA is readily oxidised at the biosensor operating potential required for H_2O_2 oxidation.

Interference from electroactive species can successfully be addressed by modifying the electrode surface with a permselective polymer layer. Here, PoPD was chosen due to its proficiency in eliminating potentially masking signals [21,28,47] and its superiority compared to polymers of other PD isomers [32], its high permeability to H_2O_2 [21,36], in addition to its ability to improve biocompatibility [50]. An overlayer of monomeric styrene was used to protect the PoPD polymer from the immobilising agents used to entrap the glutamate oxidase on the electrode surface, and to improve binding [51] of the subsequent GluOx/BSA: GA/PEI layers. Fig. 2A compares the response for basal glutamate (*ca.* 10 μM), with that for AA, the principal interferent, and the other endogenous strong reducing agents [18] L-cysteine [34], uric acid [16] and dopamine [52], at their physiologically relevant concentrations. A series of other potential interferents [9,17,53] including the DA metabolites 3,4-dihydroxyphenylacetic acid (DOPAC) and homovanillic acid (HVA), 5-hydroxytryptamine (5-HT) and its metabolite 5-hydroxyindoleacetic acid (5-HIAA), the amino acids L-tyrosine and L-tryptophan, the antioxidant L-glutathione, and dehydroascorbic acid (DHAA), were also tested (Table 1). All signals recorded were found to be negligible compared to the current for physiological glutamate with the selectivity ratio [9,54] for glutamate:AA calculated at 2326:1 (nA cm^{-2} μM^{-1}). In some cases where there was no detection of the interferent negative values attributable to baseline drift/random noise [9,28] were observed.

The interference response in the presence of neurotoxic levels of glutamate (100 μM, see *Section 3.3 Oxygen dependence*) was also profiled (see Fig. 2B), and again all signals were found to be negligible (pooled mean response − 5.38 ± 2.23%) compared to the glutamate signal, which was not affected by the presence of any of the tested neurochemicals. Generally interference from unwanted enzymatic reactions is also not a concern for glutamate biosensors as GluOx is considered to be a very selective enzyme [18]. However, while glutamine has been reported to serve as a substrate for GluOx [34], we and others [11,34] have not observed any detectable enzymatic activity for high micromolar glutamine concentrations.

3.3. Oxygen dependence

Oxygen dependence is another possible form of interference associated with first generation peroxide detecting biosensors as oxidase

Table 1
Response of the Pt_D(PoPD)(Sty)(GluOx/BSA:GA/PEI)$_{15}$ biosensor to various potential interferents at physiological levels found *in vivo,* where known.

Neurochemical	n	[Interferent] (μM)	Current[e] (nA. cm^{-2})	% Change (*vs.* 10 μM Glutamate)[a]
AA	21	500[b]	31 ± 110	2.1%
L-Cysteine	16	4[c]	41 ± 33	2.8%
Dopamine	16	0.05[b]	9 ± 34 ND	0.6%
Uric Acid	15	10[d] 20[b]	ND	–
DOPAC HVA	19	10[b]	38 ± 71	–
5-HT	16	0.01[b]	74 ± 34	2.6%
5-HIAA L-Tyrosine	18	50[b]	14 ± 60	5.1%
L-Tryptophan	18	10[e] 20[f]	ND	1.0%
L-Glutathione	19	50[g]	46 ± 46	–
DHAA	16	100[g]	57 ± 41	3.2%
	17		26 ± 112	3.9%
	14			1.8%

[a] Approximate basal ECF concentration [9,10].
[b] [16,48]. [c] [34]. [d] [16]. [e] [16,55]. [f] [16].
[g] ECF concentrations not known, high μM values chosen; ND – No detectable change.

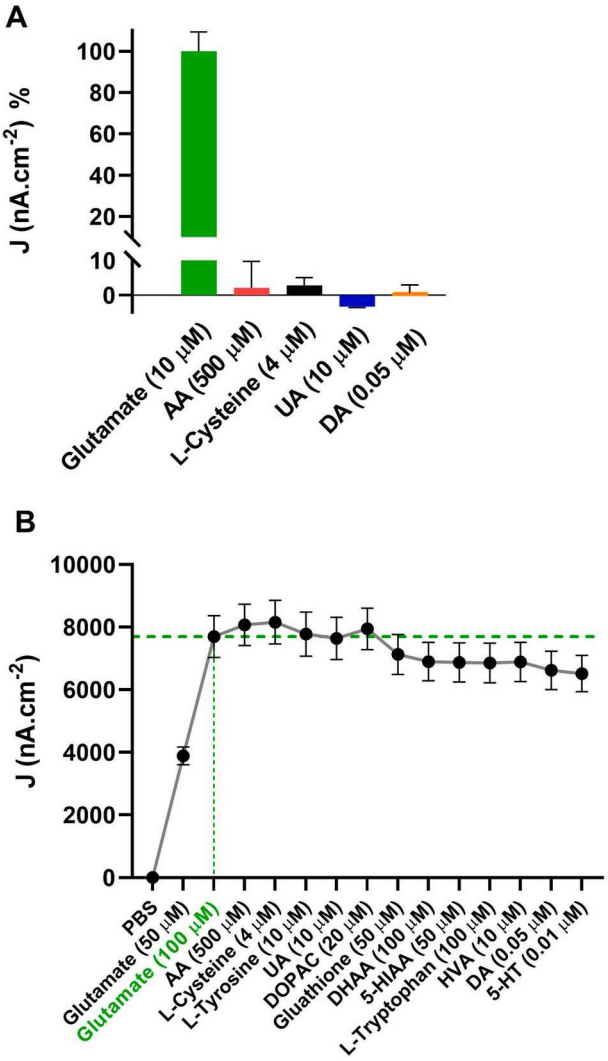

Fig. 2. (A) Normalised Pt_D(PoPD)(Sty)(GluOx/BSA:GA/PEI)$_{15}$ biosensor signal (n = 16) for brain glutamate (10 μM) compared to the responses observed for the principal endogenous reducing agents [18] ascorbic acid (AA, n = 21), L-cysteine (n = 16), uric acid (UA, n = 15) and dopamine (DA, n = 16) at their physiologically relevant concentrations. (B) Mean (±SEM, n = 4) biosensor response to two 50 μM glutamate injections followed by sequential injections of a series of common potential interfering neurochemicals (see Section 3.2).

enzymes require the use of physiological O_2 as a cofactor (see *Introduction*). As such, it is important when characterising their properties for neurochemical monitoring to ensure that the enzymatic reaction in question can occur independently across all O_2 concentration ranges found *in-vivo* under normal physiological conditions. For the mammalian brain this is typically between 40 and 80 μM O_2 [16,26,56]. Fig. 3A shows the normalised glutamate versus O_2 (0–200 μM) correlation profile for the Pt_D(PoPD)(Sty)(GluOx/BSA:GA/PEI)$_{15}$ biosensor at a fixed glutamate concentration of 10 μM. Oxygen dependence was quantified as K_MO_2; small K_MO_2 values indicate low O_2 dependence because higher O_2 affinity leads to O_2 saturation at lower pO_2, thereby reducing biosensor dependency at higher pO_2 levels. The value of 2.60 ± 0.58 μM (n = 7) determined here is similar to our previous estimates for other composite designs [26,37], and suggests negligible O_2 interference (see Fig. 3).

However, the turnover of O_2 in the polymer/enzyme composite membrane depends on the rate at which glutamate binds to the enzyme, i.e., on the concentration of glutamate. While glutamate concentrations under normal physiological conditions are typically 10 μM or lower for

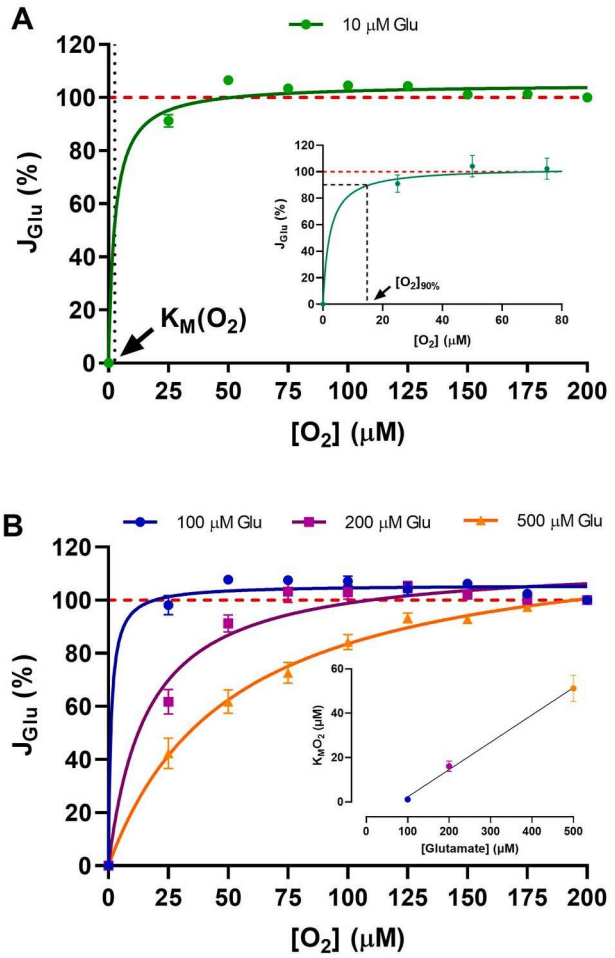

Fig. 3. (A) The effect of changing oxygen levels (0–200 μM) on the averaged normalised Pt_D(*Po*PD)(Sty) (GluOx/BSA:GA/PEI)$_{15}$ biosensor signal for 10 μM glutamate (n = 7). Non-linear regression analysis [37,58] yielded K_MO_2 = 2.60 ± 0.58 μM (R^2 = 0.984). *Inset:* Pooled data for 10 μM and 100 μM glutamate (see B) used to determine $[O_2]_{90\%}$ (*ca.* 15 μM). (B) Averaged normalised glutamate-oxygen correlation plots for 100 μM (n = 7), 200 μM (n = 7) and 500 μM (n = 8) glutamate. *Inset:* Linear regression analysis of K_MO_2 values determined from data in B (R^2 = 0.997).

cerebrospinal fluid and brain ECF [10], concentrations are known to increase to high excitotoxic micromolar levels (e.g. 100 μM) in acute neurological disorders including neurodegenerative diseases, stroke and trauma [57]. Additionally, we have previously shown that O_2 dependence typically becomes more acute at higher concentrations of analyte [26,58]. As such, we determined K_MO_2 values over a range of glutamate concentrations for this biosensor. Unlike previous designs where K_MO_2 increased linearly with glutamate concentration in the range 5–150 μM [26,37], the value for 100 μM (1.1 ± 0.7 μM, n = 7) here was not significantly different from that at 10 μM ($t_{(12)}$ = 1.63, p = 0.1295; Fig. 3A and B). Concentrations above this showed increased values in line with previous results; 16.1 ± 2.3 μM (n = 7) and 51.2 ± 5.9 μM (n = 8) for 200 μM and 500 μM glutamate respectively (Fig. 3B *inset*). An alternative and more intuitive quantification of the level of O_2 dependence is $[O_2]_{90\%}$, which is the concentration of O_2 at which 90% of the air-saturated (200 μM) signal (100%) is observed [26]. Analysis of the pooled data for both 10 μM and 100 μM glutamate indicates that 90% of the air-saturated signal can be maintained for the Pt_D(*Po*PD)(Sty) (GluOx/BSA:GA/PEI)$_{15}$ biosensor in media where O_2 concentrations fall to values as low as 15 μM (Fig. 3A *inset*). This data suggests that physiological changes in pO_2 would have negligible impact on the biosensor signal recorded in brain ECF, and that decreases in pO_2 would only be significant if the tissue O_2 levels became severely depleted. This is a characteristic we have observed previously with other similar composite biosensors designs for glucose [58], glutamate [37] and choline [29], and by other groups with devices for glutamate and ATP constructed using thin layers [17,59]. The underlying mechanisms are most likely a combination of O_2 generation on the Pt surface from the electrolysis of water and O_2 regeneration/recycling at the electrode surface (see *Introduction, enzyme reaction 2*).

3.4. pH and temperature

It is also important to establish the biosensor response characteristics associated with pH and temperature changes due to their well documented potential effects on sensitivity. The dependence of the Pt_D(*Po*PD)(Sty)(GluOx/BSA:GA/PEI)$_{15}$ biosensor response to pH (Fig. 4A) was examined over the physiologically relevant range of 7.2–7.6 [17,28]. No significant difference ($F_{(2,31)}$ = 0.6315, p = 0.5385, one-way ANOVA) was observed in sensitivity: pH 7.2, 89.3 ± 4.3 nA cm^{-2} μM^{-1} (n = 8); pH 7.4, 89.5 ± 3.8 nA cm^{-2} μM^{-1} (n = 20); and pH 7.6, 81.9 ± 4.0 nA cm^{-2} μM^{-1} (n = 6).

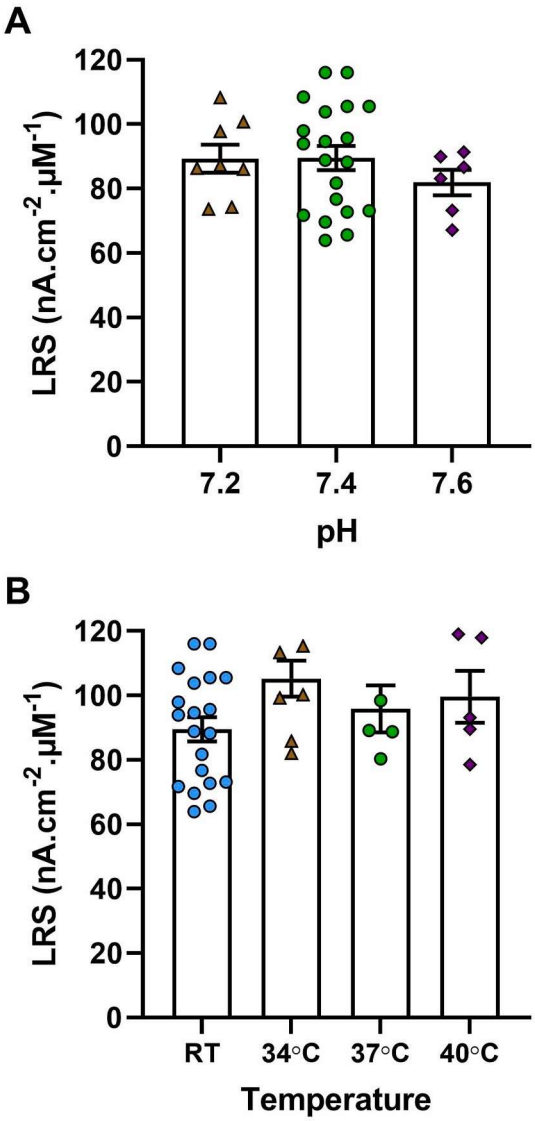

Fig. 4. The effect of changing pH (A) and temperature (B) on the sensitivity (Linear Region Slope) of the Pt_D(*Po*PD)(Sty)(GluOx/BSA:GA/PEI)$_{15}$ biosensor over physiologically relevant ranges; 7.2 to 7.6 and room temperature (RT, 21 °C) to 40 °C respectively. Average current-concentration responses are shown in Fig. 3S.

For temperature, variations between 35.5 °C and 38.8 °C, associated with behaviour and pharmacological interventions, have been reported in freely-moving animals [60]. Fig. 4B shows the effect of changing temperature over the range 21 °C–40 °C on the glutamate response. Similar sensitivities ($F_{(3,34)}$ = 1.855, p = 0.1559, one-way ANOVA) were observed at each of the temperatures tested indicating that the biosensor has the ability to accurately measure glutamate free from temperature induced bias: 21 °C, 89.5 ± 3.8 nA cm^{-2} μM^{-1} (n = 20); 34 °C, 105 ± 6 nA cm^{-2} μM^{-1} (n = 8); 37 °C, 95.9 ± 7.3 nA cm^{-2} μM^{-1} (n = 5); and 40 °C, 99.62 ± 8.06 nA cm^{-2} μM^{-1} (n = 5). Other groups have also reported temperature independence for chemically modified GluOx-based electrochemical sensors [61].

3.5. Limit of detection, response time and stability

A limit of detection (LOD) of 0.44 ± 0.05 μM (n = 4) was determined from three times the standard deviation of the baseline biosensor signal in background electrolyte divided by the LRS [36,38]. The response time, defined as the time taken for the biosensor signal at a fixed concentration to rise from 10% to 90% of the maximum amplitude ($t_{10-90\%}$) was less than the mixing time (*ca.* 5 s); the signal change (Fig. 5S) was instantaneous following injection with $t_{10-90\%}$ estimated at 1.67 ± 0.06 s (n = 4) for 10 μM glutamate.

Stability is the study of the longevity of a biosensor [17,28]. That is, whether the particular design gives accurate and reliable results over the required timeframe with respect to the intended application. Typically, a minimum of at least two weeks is needed for chronic *in vivo* neurochemical experiments. As the sensitivity of an implanted biosensor can be compromised immediately following biological implantation due to the presence of surface modifying agents (e.g. lipids) and electrode poisons (e.g. proteins) [62] we tested the biocompatibility of the Pt_D(PoPD)(Sty)(GluOx/BSA:GA/PEI)$_{15}$ sensor by calibrating a batch of sensors before and after storage for two weeks in moist brain tissue at 4 °C (Fig. 5A). A small decrease ($t_{(7)}$ = 1.17, p = 0.2804, n = 8) of *ca.* 10% was observed in the sensitivity measured on Day 14 (70.8 ± 8.4 nA cm^{-2} μM^{-1}) compared to Day 1 (78.9 ± 4.0 nA cm^{-2} μM^{-1}), and compares favourably with other reports where reduced sensitivities of between 20% and 50% have been reported following implantation [46]. We also investigated the stability of the biosensor by examining baseline *in vivo* data for recording periods out to 16 days following implantation (see *Section 3.6*).

Appraisal of shelf-life (Fig. 5B), i.e., the time under defined storage conditions during which the sensor remains viable, involved comparing the sensitivities of batches of biosensors which were stored dry at 4 °C until one-off calibration on Days 1, 14 and 28. Responses were similar ($F_{(2,28)}$ = 1.317, p = 0.2841, one-way ANOVA) for all three days: Day 1, 96.4 ± 3.4 nA cm^{-2} μM^{-1} (n = 15); Day 14, 105.8 ± 4.6 nA cm^{-2} μM^{-1} (n = 8); and Day 28, 97.5 ± 5.2 nA cm^{-2} μM^{-1} (n = 8). As repeated calibrations can sometimes have a negative effect on the sensitivity of polymer-enzyme composite biosensors [28,53] we additionally examined the effect of calibrating the same batch of biosensors over the same time interval (Fig. 5B). Again, no significant difference ($F_{(2,14)}$ = 1.412, p = 0.2764, one-way repeated measures ANOVA, n = 8) in sensitivity was observed: Day 1, 95.6 ± 4.9 nA cm^{-2} μM^{-1}; Day 14, 104.1 ± 2.9 nA cm^{-2} μM^{-1}; and Day 28, 104.4 ± 4.2 nA cm^{-2} μM^{-1}. Finally, the effect of sterilisation (Fig. 5C) on biosensor performance was investigated using freshly prepared biosensors which were calibrated (Day 1, 97.7 ± 5.9 nA cm^{-2} μM^{-1}) prior to being sent for commercial electron beam irradiation at 50 kGy min^{-1}. The post-sterilisation sensitivity (Day 8, 92.8 ± 8.9 nA cm^{-2} μM^{-1}) was not significantly different from the pre-calibration value ($t_{(7)}$ = 0.5883, p = 0.5748, n = 8).

Overall, these characteristics indicate good stability in terms of biocompatibility, storage and use, and compare favourably with other glutamate biosensors reported to retain their sensitivity following implantation [63], and for up to 5 [17,36] months of storage. The absence of enzyme inactivation from the electron beam sterilisation process opens the possibility of potentially extending applications to areas such as medical monitoring. The calculated LOD and response time are also similar to previously reported values for glutamate biosensors [53], and when considered with the stability data suggest that the Pt_D(PoPD)(Sty)(GluOx/BSA:GA/PEI)$_{15}$ biosensor is ideally suited to performing neurochemical

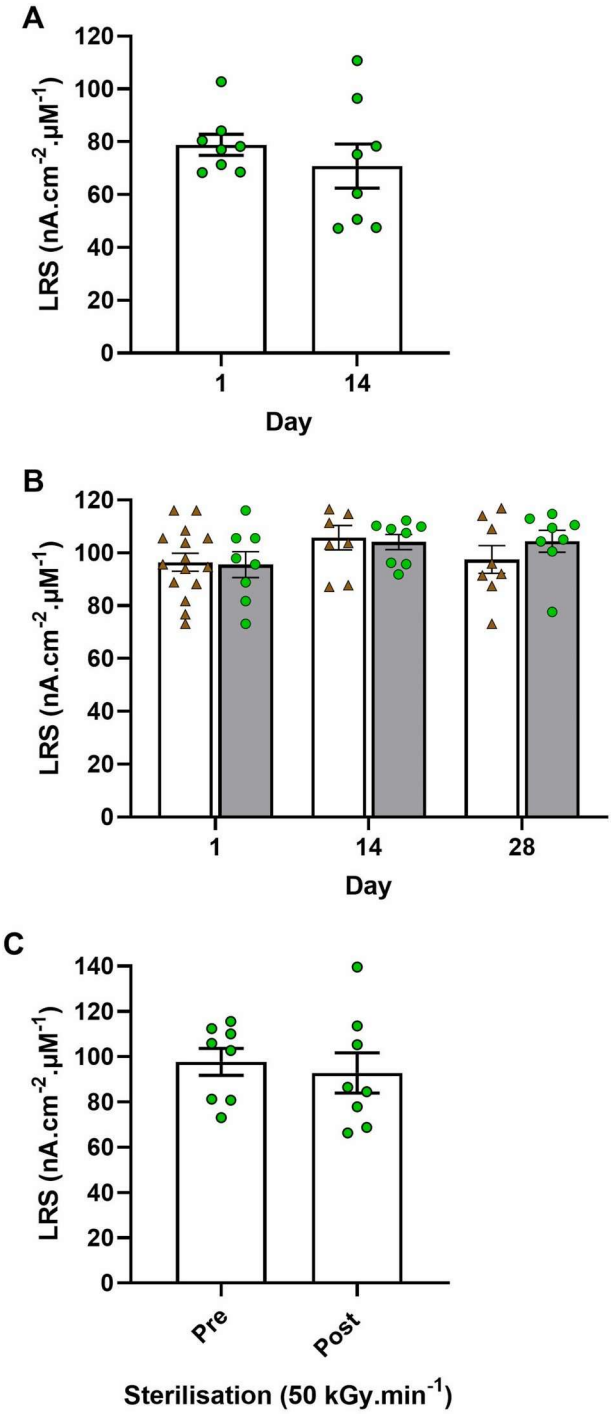

Fig. 5. (A) The effect of two weeks storage in *ex-vivo* rodent brain tissue at 4 °C on the Pt_D(PoPD)(Sty)(GluOx/BSA:GA/PEI)$_{15}$ biosensor sensitivity (Linear Region Slope; Mean ± SEM, n = 8). (B) Clear - comparison of sensitivities for biosensors stored dry at 4 °C until one-off calibration on Day 1 (n = 15), Day 14 (n = 8) and Day 28 (n = 8). Grey - comparison of sensitivities (n = 8) for a batch of biosensors measured following storage between initial calibration on Day 1, and repeated calibrations on Days 14 and 28. (C) The effect of electron beam irradiation at 50 kGy min^{-1}. Average current-concentration responses are shown in Fig. 4S.

measurements associated with behavioural and/or pharmacological manipulations. While BSA:GA mixtures have been used extensively in biosensor designs to increase sensitivity/stability, it is most likely that the extended characteristics observed here can be attributed to the incorporation of the polycation PEI, through its ability to facilitate charge counterbalance with the polyanionic GluOx [37].

3.6. In-vivo recording

Preliminary *in vivo* experiments were performed to examine biocompatibility/stability and to validate the ability of the Pt_D(P*o*PD)(Sty)(GluOx/BSA:GA/PEI)$_{15}$ biosensor to detect extracellular changes in glutamate. Baseline signals were analysed over the same time interval (08:00–09:00), for recording phases between Day 6 and Day 16, and no significant variation in current was observed (Fig. 6A; $F_{(8,61)} = 0.1741$, $p = 0.9936$, one-way ANOVA). A sample continuous 12 h trace (dark phase) with simultaneously recorded motor activity clearly highlights periods of activity which are coincident with increases in glutamate (Fig. 6B). Such naturally occurring changes are often associated with behavioural phenomena such as grooming, feeding and locomotor activity [39,40].

Similarly, physiological stimulation induced in response to stress (e.g. tail-pinch), has previously been shown to elicitate neuronal activation with concomittant increases in glutamate measured using both microdialysis [64] and biosensors [43,63]. As such, we examined the effect of mild stress in the form of a 5 min restraint (see *Experimental conditions in-vivo*); the signal, recorded from prefrontal cortex, increased during the procedure with a return to baseline that was dependent on the activity/behaviour of the animal post stimulus (Fig. 6C). Taken together, these preliminary results support the *in vitro* data indicating that the developed biosensor is capable of detecting brain extracellular glutamate, and is suitable for recording changes for at least three weeks following implantation. Future *in vivo* work will involve further behavioural experiments and targeted pharmacological studies to characterise and validate signal integrety.

4. Conclusions

This research work set out to complete the development and *in vitro* characterisation of a glutamate oxidase-based microelectrode biosensor capable of *in vivo* measurements. The optimal Pt_D(P*o*PD)(Sty)(GluOx/BSA:GA/PEI)$_{15}$ design achieved a sensitivity comparable to previously reported sensors, a shelf-life of several weeks, and displayed no loss of sensitivity with repeated calibrations, exposure to *ex-vivo* rodent brain tissue, or electron beam sterilisation. Potential interference signal contributions from physiologically relevant electroactive species were tested for both basal and neurotoxic levels of glutamate and found to be negligible. Oxygen interference studies suggest that the biosensor signal should not suffer significantly from oxygen fluctuations in brain ECF under all but extreme anaerobic conditions. In addition, physiologically relevant pH and temperature changes had minimal effect on the biosensor performance, which, when taken with a calculated low µM detection limit and rapid response time, suggests that this composite sensor should reliably detect L-glutamate when used for neurochemical monitoring. These results were supported by preliminary *in vivo* experiments performed in freely-moving animals where expected signal changes were observed for both natural and induced behavioural/ neuronal activation, from a baseline which was stable 16 days following implantation. Future *in vivo* studies will focus on consolidating this conclusion, and identifying the sources (e.g. neuronal and/or glial) contributing to the recorded glutamate signal.

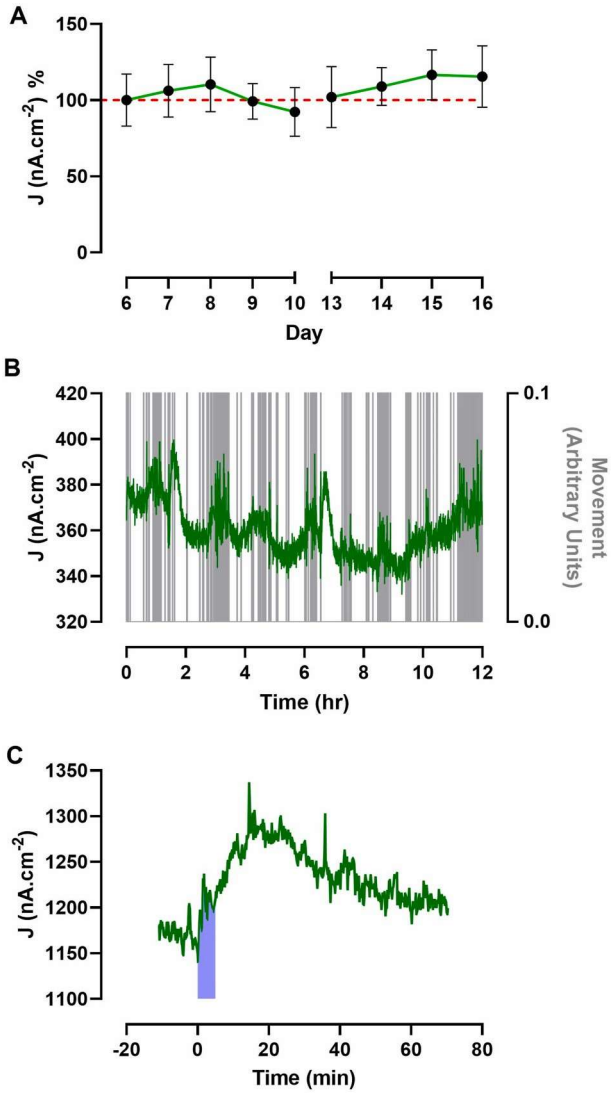

Fig. 6. (A) Average (±SEM, n = 5–11) baseline *in vivo* data (pooled from 8 freely-moving animals) for the Pt_D(P*o*PD)(Sty)(GluOx/BSA:GA/PEI)$_{15}$ biosensor recorded from striatum using CPA at +700 mV over an 11 day period. All data taken from the same daily 1-h (8–9 a.m.) period when the animals were mostly inactive and normalised to Day 6, (average = 106 ± 3). (B) A typical example of a continuous real-time *in vivo* recording from prefrontal cortex over a 12 h period (dark phase, 7 p.m. - 7 a.m.). Grey lines represent simultaneously monitored motor activity. (C) Typical signal change associated with a period of restraint stress (5-min, shaded area).

CRediT authorship contribution statement

Kobi P. Bermingham: Investigation, Formal analysis, Writing – original draft, Project administration. **Michelle M. Doran:** Investigation, Formal analysis, Writing – original draft, Supervision, Project administration. **Fiachra B. Bolger:** Investigation, Formal analysis. **John P. Lowry:** Conceptualization, Formal analysis, Visualization, Writing – original draft, Writing – review & editing, Project administration, Supervision, Funding acquisition.

Declaration of competing interest

The authors declare that they have no known competing financial interests or personal relationships that could have appeared to influence the work reported in this paper.

Data availability

Data will be made available on request.

Acknowledgements

This work has emanated from research conducted with the financial support of Enterprise Ireland/European Regional Development Fund (EI/ERDF, Grant Number TD/2008/107), and Science Foundation Ireland (SFI) under Grant Number 15/IA/3176.

Appendix A. Supplementary data

Supplementary data to this article can be found online at https://doi.org/10.1016/j.aca.2022.340205.

References

[1] J.V. Nadler, Plasticity of glutamate synaptic mechanisms, Epilepsia 51 (2010), 17–17.
[2] B.S. Meldrum, Glutamate as a neurotransmitter in the brain: review of physiology and pathology, J. Nutr. 130 (2000) 1007S–1015S.
[3] H. Furukawa, S.K. Singh, R. Mancusso, E. Gouaux, Subunit arrangement and function in NMDA receptors, Nature 438 (2005) 185–192.
[4] H.F. Bradford, Glutamate, GABA and epilepsy, prog. Neurobiol. 47 (1995) 477–511.
[5] J.T. Coyle, Glutamate, Schizophrenia: beyond the dopamine hypothesis, Cell. Mol. Neurobiol. 26 (2006) 363–382.
[6] R. Fern, C. Matute, Glutamate receptors and white matter stroke, Neurosci. Lett. 694 (2019) 86–92.
[7] A. Lau, M. Tymianski, Glutamate receptors, neurotoxicity and neurodegeneration, Pflueg. Arch. Eur. J. Physiol. 460 (2010) 525–542.
[8] D.W. Choi, Glutamate neurotoxicity and diseases of the nervous system, Neuron 1 (1988) 623–634.
[9] J.J. Burmeister, V.A. Davis, J.E. Quintero, F. Pomerleau, P. Huettl, G.A. Gerhardt, Glutaraldehyde cross-linked glutamate oxidase coated microelectrode arrays: selectivity and resting levels of glutamate in the CNS, ACS Chem. Neurosci. 4 (2013) 721–728.
[10] M. Miele, M. Berners, M.G. Boutelle, H. Kusakabe, M. Fillenz, The determination of the extracellular concentration of brain glutamate using quantitative microdialysis, Brain Res. 707 (1996) 131–133.
[11] M.R. Ryan, J.P. Lowry, R.D. O'Neill, Biosensor for neurotransmitter L-glutamic acid designed for efficient use of L-glutamate oxidase and effective rejection of interference, Analyst 122 (1997) 1419–1424.
[12] A. Galvan, Y. Smith, T. Wichmann, Continuous monitoring of intracerebral glutamate levels in awake monkeys using microdialysis and enzyme fluorometric detection, J. Neurosci. Methods 126 (2003) 175–185.
[13] L.A. Dawson, J.M. Stow, A.M. Palmer, Improved method for the measurement of glutamate and aspartate using capillary electrophoresis with laser induced fluorescence detection and its application to brain microdialysis, J. Chromatogr. B Biomed. Appl. 694 (1997) 455–460.
[14] N. Kiba, T. Miwa, M. Tachibana, K. Tani, H. Koizumi, Chemiluminometric sensor for simultaneous determination of L-glutamate and L-lysine with immobilized oxidases in a flow injection system, Anal. Chem. 74 (2002) 1269–1274.
[15] R.-a. Doong, H.-m. Shih, Glutamate optical biosensor based on the immobilization of glutamate dehydrogenase in titanium dioxide sol–gel matrix, Biosens. Bioelectron. 22 (2006) 185–191.
[16] C. Chatard, A. Meiller, S. Marinesco, Microelectrode biosensors for in vivo analysis of brain interstitial fluid, Electroanalysis 30 (2018) 977–998.
[17] F. Tian, A.V. Gourine, R.T.R. Huckstepp, N. Dale, A microelectrode biosensor for real time monitoring of l-glutamate release, Anal. Chim, Acta 645 (2009) 86–91. [18] S. Qin, M. Van der Zeyden, W.H. Oldenziel, T.I.F.H. Cremers, B.H.C. Westerink, Microsensors for in vivo measurement of glutamate in brain tissue, Sensors 8 (2008) 6860–6884.
[19] C. Tan, E.M. Robbins, B. Wu, X.T. Cui, Recent advances in in vivo neurochemical monitoring, Micromachines 12 (2021) 208.
[20] S.M. Kirwan, G. Rocchitta, C.P. McMahon, J.D. Craig, S.J. Killoran, K.B. O'Brien, P. A. Serra, J.P. Lowry, R.D. O'Neill, Modifications of poly(o-phenylenediamine) permselective layer on Pt-Ir for biosensor application in neurochemical monitoring, Sensors 7 (2007) 420–437.
[21] J.P. Lowry, R.D. O'Neill, Partial characterization in vitro of glucose oxidase- modified poly(phenylenediamine)-coated electrodes for neurochemical analysis in vivo, Electroanalysis 6 (1994) 369–379.
[22] D. Polcari, A. Kwan, M.R. Van Horn, L. Danis, L. Pollegioni, E.S. Ruthazer, J. Mauzeroll, Disk-shaped amperometric enzymatic biosensor for in vivo detection of d-serine, Anal. Chem. 86 (2014) 3501–3507.
[23] M. Singh, P.K. Kathuroju, N. Jampana, Polypyrrole based amperometric glucose biosensors, Sens. Actuators B: Chem 143 (2009) 430–443.
[24] A. Kausaite-Minkstimiene, V. Mazeiko, A. Ramanaviciene, A. Ramanavicius, Evaluation of amperometric glucose biosensors based on glucose oxidase encapsulated within enzymatically synthesized polyaniline and polypyrrole, Sens. Actuators B: Chem 158 (2011) 278–285.
[25] X. Liu, L. Shi, W. Niu, H. Li, G. Xu, Amperometric glucose biosensor based on single-walled carbon nanohorns, Biosens. Bioelectron. 23 (2008) 1887–1890.
[26] C.P. McMahon, R.D. O'Neill, Polymer– Enzyme composite biosensor with high glutamate sensitivity and low oxygen dependence, Anal. Chem. 77 (2005) 1196–1199.
[27] M.M. Doran, N.J. Finnerty, J.P. Lowry, In–Vitro development and characterisation of a superoxide dismutase-based biosensor, ChemistrySelect 2 (2017) 4157–4164.
[28] K.L. Baker, F.B. Bolger, M.M. Doran, J.P. Lowry, Characterisation of a Platinum- based electrochemical biosensor for real-time neurochemical analysis of choline, Electroanalysis 31 (2019) 129–136.
[29] K.L. Baker, F.B. Bolger, J.P. Lowry, Development of a microelectrochemical biosensor for the real-time detection of choline, Sens. Actuators B: Chem 243 (2017) 412–420.
[30] K.B. O'Brien, S.J. Killoran, R.D. O'Neill, J.P. Lowry, Development and characterization in vitro of a catalase-based biosensor for hydrogen peroxide monitoring, Biosens. Bioelectron. 22 (2007) 2994–3000.
[31] S.L. O'Riordan, J.P. Lowry, In vivo characterisation of a catalase-based biosensor for real-time electrochemical monitoring of brain hydrogen peroxide in freely- moving animals, Anal. Methods 9 (2017) 1253–1264.
[32] S.J. Killoran, R.D. O'Neill, Characterization of permselective coatings electrosynthesized on Pt–Ir from the three phenylenediamine isomers for biosensor applications, Electrochim. Acta 53 (2008) 7303–7312.
[33] F.O. Brown, J.P. Lowry, Microelectrochemical sensors for in vivo brain analysis: an investigation of procedures for modifying Pt electrodes using Nafion®, Analyst 128 (2003) 700–705.
[34] N.V. Kulagina, L. Shankar, A.C. Michael, Monitoring glutamate and ascorbate in the extracellular space of brain tissue with electrochemical microsensors, Anal. Chem. 71 (1999) 5093–5100.
[35] T.-C. Chou, Derivation and properties of Michaelis-Menten type and Hill type equations for reference ligands, J. Theor. Biol. 59 (1976) 253–276.
[36] R. Ford, S.J. Quinn, R.D. O'Neill, Characterization of biosensors based on recombinant glutamate oxidase: comparison of crosslinking agents in terms of enzyme loading and efficiency parameters, Sensors 16 (2016) 1565–1581.
[37] C.P. McMahon, G. Rocchitta, S.M. Kirwan, S.J. Killoran, P.A. Serra, J.P. Lowry, R. D. O'Neill, Oxygen tolerance of an implantable polymer/enzyme composite glutamate biosensor displaying polycation-enhanced substrate sensitivity, Biosens. Bioelectron. 22 (2007) 1466–1473.
[38] R.D. O'Neill, J.P. Lowry, G. Rocchitta, C.P. McMahon, P.A. Serra, Designing sensitive and selective polymer/enzyme composite biosensors for brain monitoring in vivo, TrAC, Trends Anal. Chem. 27 (2008) 78–88.
[39] K.L. Baker, F.B. Bolger, J.P. Lowry, A microelectrochemical biosensor for real-time in vivo monitoring of brain extracellular choline, Analyst 140 (2015) 3738–3745.
[40] N.J. Finnerty, F.B. Bolger, E. Palsson, J.P. Lowry, An investigation of hypofrontality in an animal model of schizophrenia using real-time microelectrochemical sensors for glucose, oxygen, and nitric oxide, ACS Chem. Neurosci. 4 (2013) 825–831.
[41] E. Carstens, G.P. Moberg, Recognizing pain and distress in laboratory animals, ILAR J. 41 (2000) 62–71.
[42] S. Govindarajan, C.J. McNeil, J.P. Lowry, C.P. McMahon, R.D. O'Neill, Highly selective and stable microdisc biosensors for L-glutamate monitoring, Sens. Actuators B: Chem 178 (2013) 606–614.
[43] J.P. Lowry, M.R. Ryan, R.D. O'Neill, Behaviourally induced changes in extracellular levels of brain glutamate monitored at 1 s resolution with an implanted biosensor, Anal. Commun. 35 (1998) 87–89.
[44] M.B. Dash, M. Bellesi, G. Tononi, C. Cirelli, Sleep/wake dependent changes in cortical glucose concentrations, J. Neurochem. 124 (2013) 79–89.
[45] Y. Hu, G.S. Wilson, A temporary local energy pool coupled to neuronal activity: fluctuations of extracellular lactate levels in rat brain monitored with rapid- response enzyme-based sensor, J. Neurochem. 69 (1997) 1484–1490.
[46] Y.B. Hu, K.M. Mitchell, F.N. Albahadily, E.K. Michaelis, G.S. Wilson, Direct measurement of glutamate release in the brain using a dual enzyme-based electrochemical sensor, Brain Res. 659 (1994) 117–125.
[47] J.P. Lowry, K. McAteer, S.S. El Atrash, A. Duff, R.D. O'Neill, Characterization of glucose oxidase-modified poly(phenylenediamine)-coated electrodes in vitro and in vivo: homogeneous interference by ascorbic acid in hydrogen peroxide detection, Anal. Chem. 66 (1994) 1754–1761.
[48] M. Miele, M. Fillenz, In vivo determination of extracellular brain ascorbate, J. Neurosci. Methods 70 (1996) 15–19.
[49] G.V. Rebec, R.C. Pierce, A vitamin as neuromodulator: ascorbate release into the extracellular fluid of the brain regulates dopaminergic and glutamatergic transmission, Prog. Neurobiol. 43 (1994) 537–565.
[50] J.P. Lowry, M. Miele, R.D. O'Neill, M.G. Boutelle, M. Fillenz, An amperometric glucose-oxidase/poly(o-phenylenediamine) biosensor for monitoring brain extracellular glucose: in vivo characterisation in the striatum of freely-moving rats, J. Neurosci. Methods 79 (1998) 65–74.
[51] S. Li´ebana, Guido A. Drago, Bioconjugation and stabilisation of biomolecules in biosensors, Essays Biochem. 60 (2016) 59–68.
[52] J.P. Lowry, R.D. O'Neill, Neuroanalytical chemistry in vivo using biosensors, in: C. A. Grimes, E.C. Dickey (Eds.), Encyclopedia of Sensors, American Scientific Publishers, CA, USA, 2006, pp. 501–524.

[53] M. Ganesana, E. Trikantzopoulos, Y. Maniar, S.T. Lee, B.J. Venton, Development of a novel micro biosensor for in vivo monitoring of glutamate release in the brain, Biosens. Bioelectron. 130 (2019) 103–109.
[54] E. Walker, J. Wang, N. Hamdi, H.G. Monbouquette, N.T. Maidment, Selective detection of extracellularglutamate in brain tissue using microelectrode arrays coated with over-oxidized polypyrrole, Analyst 132 (2007) 1107–1111.
[55] J.M. Breier, M.G. Bankson, B.K. Yamamoto, L-Tyrosine contributes to (+)-3,4-methylenedioxymethamphetamine-induced serotonin depletions, J. Neurosci. 26 (2006) 290–299.
[56] P.K. Nair, D.G. Buerk, J.H. Halsey Jr., Comparisons of oxygen metabolism and tissue PO_2 in cortex and hippocampus of gerbil brain, Stroke 18 (1987) 616–622.
[57] A. Vaarmann, S. Kovac, K.M. Holmstrom, S. Gandhi, A.Y. Abramov, Dopamine¨ protects neurons against glutamate-induced excitotoxicity, Cell Death Dis. 4 (2013) e455–e455.
[58] B.M. Dixon, J.P. Lowry, R.D. O'Neill, Characterization in vitro and in vivo of the oxygen dependence of an enzyme/polymer biosensor for monitoring brain glucose, J. Neurosci. Methods 119 (2002) 135–142.
[59] E. Llaudet, S. Hatz, M. Droniou, N. Dale, Microelectrode biosensor for real-time measurement of ATP in biological tissue, Anal. Chem. 77 (2005) 3267–3273.
[60] E.A. Kiyatkin, The hidden side of drug action: brain temperature changes induced by neuroactive drugs, Psychopharmacology 225 (2013) 765–780.
[61] O. Frey, T. Holtzman, R.M. McNamara, D.E.H. Theobald, P.D. van der Wal, N.F. de Rooij, J.W. Dalley, M. Koudelka-Hep, Enzyme-based choline and l-glutamate biosensor electrodes on silicon microprobe arrays, Biosens. Bioelectron. 26 (2010) 477–484.
[62] R.D. O'Neill, Sensor–tissue interactions in neurochemical analysis with carbon paste electrodes in vivo, Analyst 118 (1993) 433–438.
[63] T.T.-C. Tseng, C.-F. Chang, W.-C. Chan, Fabrication of implantable, enzyme- immobilized glutamate sensors for the monitoring of glutamate concentration changes in vitro and in vivo, Molecules 19 (2014) 7341–7355.
[64] D. Lupinsky, L. Moquin, A. Gratton, Interhemispheric regulation of the medial prefrontal cortical glutamate stress response in rats, J. Neurosci. 30 (2010) 7624.

Appendix 2: Characterisation of a microelectrochemical biosensor for real-time detection of brain extracellular D-serine

It has been proposed that D-serine released by glia exhibits a regulatory role as a necessary co-agonist for the glutamate activation of the N-methyl-D-aspartate (NMDA) receptor [1]. Thereby, requiring D-serine and L-glutamate in the activation of the NMDA receptor. D-Serine not only promotes neural signalling but synaptic plasticity as well [2]. Specialised glial cells known as astrocytes ensheath the NMDA receptors, and it is here that D-serine is stored [3]. Thusly, a widely agreed upon expanded model for glutamate synapses was established in which glutamate released from the presynaptic neuron interacts with both the postsynaptic neuron and more interestingly, on the ensheathing astrocyte [4]. This results in the metabotropic glutamate receptors being activated and a following degradation of phosphatidylinositol 4,5-bisphosphate (PIP_2) by phospholipase C (PLC). The NMDA receptor on the postsynaptic neuron can open through the dual binding of L-glutamate and D-serine. The compelling nature of this model comes from the potential activation mechanism of the D-serine synthesis required for NMDA neurotransmission [5] (see Figure 1).

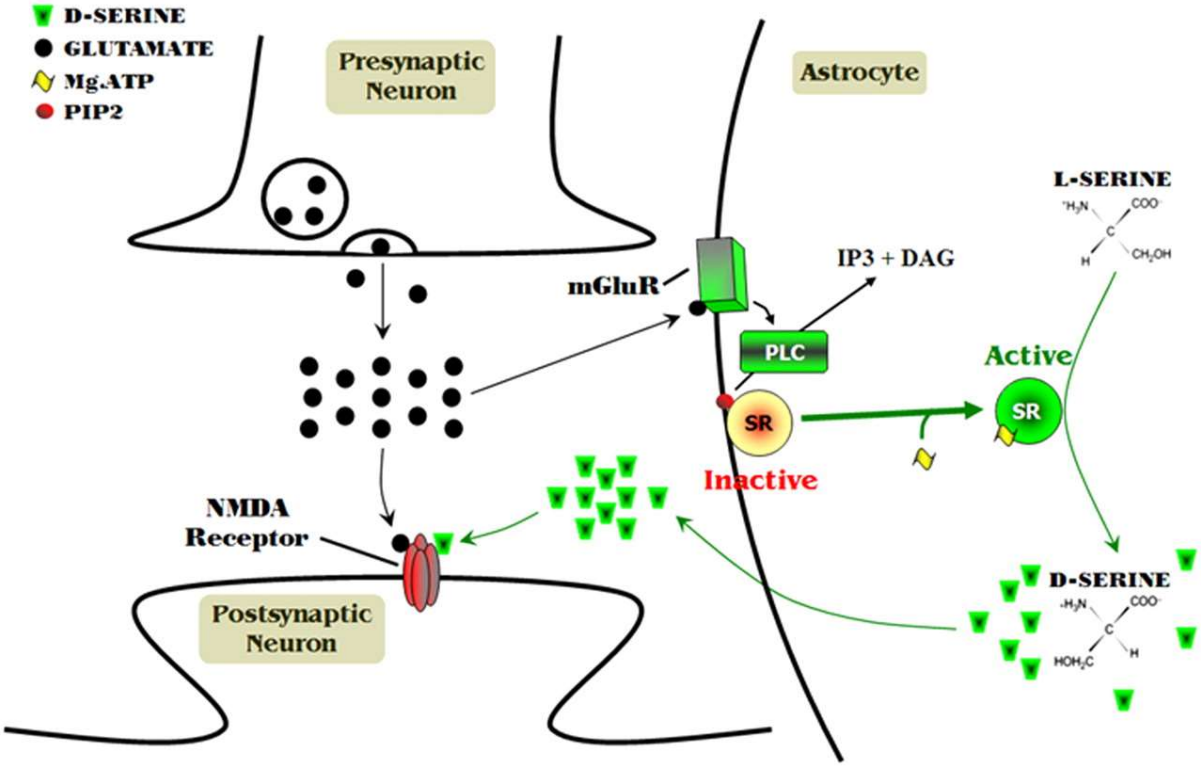

Figure 1: Glutamatergic regulation of serine racemase via reversal of PIP_2 inhibition [5].

Some research was undertaken regarding the development and characterisation of a D-serine biosensor due to the intrinsic related nature with L-glutamate. Dual monitoring of L-glutamate and D-serine *in vivo* could potentially elucidate the pathway and progress of the various diseases related to dysregulation of the NMDA receptor. Contributions were made to the pH and temperature studies (see Figure 2).

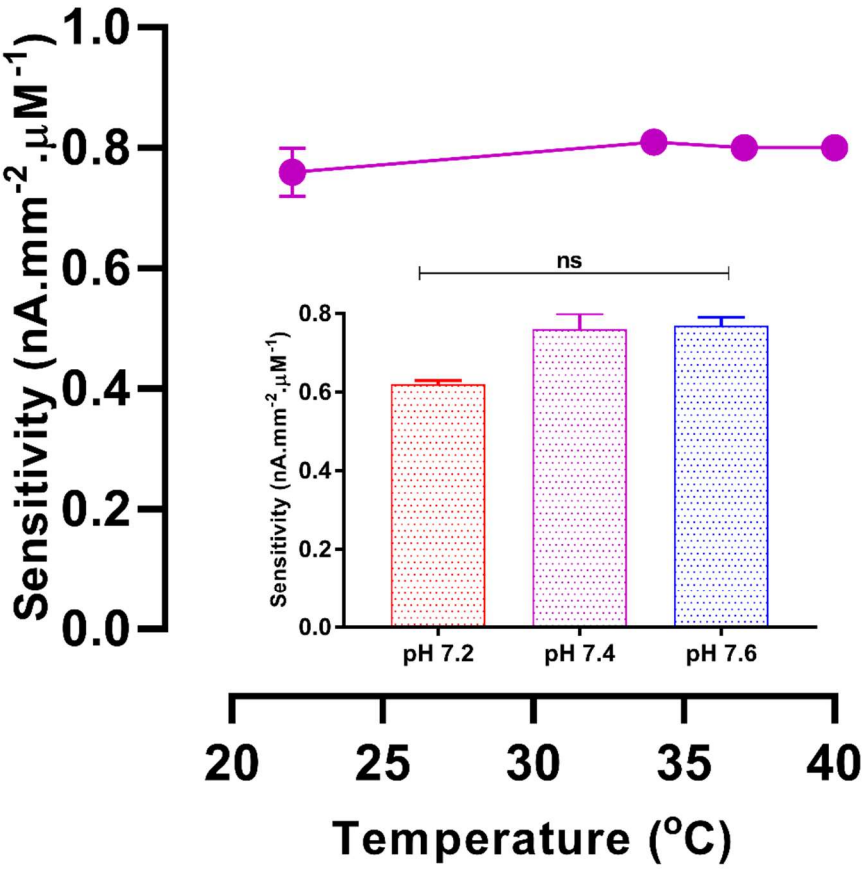

Figure 2: The effect of changing temperature and pH (***inset***) on the sensitivity (LRS) of the Pt_D-MMA-$((DAAO\text{-}4)_5\text{-}30)_3$-GA biosensor. No significant difference in sensitivity was observed for temperature (P = 0.5634, one-way ANOVA) or pH (P = 0.0753, one way ANOVA). D-Serine calibrations (0-10 mM) performed at +700 mV *vs*. SCE in PBS (pH 7.4).

The paper following is in preparation for submission to Analytical Chemistry, aiming to be submitted before the end of the year.

References

1. Barañano, D.E., C.D. Ferris, and S.H. Snyder, *Atypical neural messengers.* Trends in Neurosciences, 2001. **24**(2): p. 99-106.
2. Polcari, D., et al., *Disk-Shaped Amperometric Enzymatic Biosensor for in Vivo Detection of d-serine.* Analytical Chemistry, 2014. **86**(7): p. 3501-3507.
3. Martineau, M., G. Baux, and J.P. Mothet, *Gliotransmission at central glutamatergic synapses: D-serine on stage.* J Physiol Paris, 2006. **99**(2-3): p. 103-10.
4. Wolosker, H., S. Blackshaw, and S.H. Snyder, *Serine racemase: a glial enzyme synthesizing D-serine to regulate glutamate-N-methyl-D-aspartate neurotransmission.* Proc Natl Acad Sci U S A, 1999. **96**(23): p. 13409-14.
5. Mustafa, A.K., M.M. Gadalla, and S.H. Snyder, *Signaling by gasotransmitters.* Science signaling, 2009. **2**(68): p. re2-re2.

A submission to Analytical Chemistry

Characterisation of a microelectrochemical biosensor for real-time detection of brain extracellular D-serine

Michelle M. Doran*[1], Kobi P. Bermingham[1], Mark D. Tricklebank[2] and John P. Lowry*[1]

[1]Neurochemistry Laboratory, Maynooth University Department of Chemistry, Maynooth University, Maynooth, Co. Kildare, Ireland

[2]Department of Neuroimaging Sciences, Institute of Psychiatry, Psychology & Neuroscience, King's College London, UK

***Correspondence**

Michelle.Doran@mu.ie
John.Lowry@mu.ie

Abstract

A modified development protocol and concomitant characterisation of a first generation biosensor for the detection of brain extracellular D-serine is reported. Functional parameters important for neurochemical monitoring, including sensor sensitivity, O_2 interference, selectivity, shelf-life and biocompatibility were examined. Construction and development involved the enzyme D-amino acid oxidase (DAAO), utilising a dip-coating immobilisation method employing a new extended drying approach. The resultant Pt-based polymer enzyme composite sensor achieved high sensitivity to D-serine (0.76 ± 0.04 nA.mm^{-2}. μM^{-1}) and a low μM limit of detection (0.33 ± 0.02 μM). The *in-vitro* response time was within the solution stirring time, suggesting potential sub-second *in-vivo* response characteristics. Oxygen interference studies demonstrated a 1% reduction in current at 50 μM O_2 when compared to atmospheric O_2 levels (200 μM), indicating that the sensor can be used for reliable neurochemical monitoring of D-serine, free from changes in current associated with physiological O_2 fluctuations. Potential interference signals generated by the principal electroactive analytes present in the brain were minimised by using a permselective layer of poly(*o*-phenylenediamine), and although several D-amino acids are possible substrates for DAAO, their physiologically relevant signals were small relative to that for D-serine. Additionally, changing both temperature and pH over possible *in vivo* ranges (34 - 40 °C and 7.2 - 7.6 respectively) resulted in no significant effect on performance. Finally, the biosensor was implanted in the striatum of freely moving rats and used to monitor physiological changes in D-serine over a two-week period.

Keywords: D-Serine; D-Amino acid oxidase; Microbiosensor; Amperometry; *In-vivo* monitoring

1. Introduction

D-serine, the predominant D-amino acid found in the central nervous system [1, 2], is a gliotransmitter that modulates neurotransmission at glutamatergic synapses and has a low micromolar *in-vivo* concentration of *ca.* 2-6 μM [3-5]. It is an endogenous co-agonist of the glycine modulatory site of the glutamatergic N-methyl D-aspartate (NMDA) receptor [5, 6], modulating both neuronal transmission and synaptic plasticity [7-9]. The continuous measurement of D-serine is highly desirable in order to better understand its role in normal and pathophysiological processes. This is particularly so for psychiatric and neurodegenerative disorders: decreased D-serine levels have been observed in CSF samples from schizophrenic patients [10, 11]; administration of D-serine, in combination with neuroleptics or newer antipsychotic drugs, improves positive, negative and cognitive symptoms[11, 12]; while excessive levels of D-serine have been associated with neurodegenerative diseases [13-15] however, some research findings has hypothesised decreased D-serine levels in Alzheimer's disease [16, 17]. Furthermore, recent findings show the potential importance of plasma D-serine as a promising biomarker for the antidepressant response to ketamine [18].

To date, several analytical techniques have been employed for the neurochemical detection of D-serine including chromatography[19, 20], capillary electrophoresis [21], microdialysis [22] and electrochemical biosensors [2, 3, 23-26]. Microdialysis suffers from several drawbacks including low temporal resolution and slow response times, however, the use of enzyme-based biosensors offers an alternative option for the real-time neurochemical monitoring of this enantiomer. Several, D-serine biosensors incorporating the enzyme D-amino acid oxidase (DAAO) have been reported in the literature for use in various applications [27]. These biosensors rely on a two-step reaction scheme in order to detect D-serine. The first involves the DAAO converting D-serine into its corresponding α-ketoacid (hydroxypyruvate), yielding ammonia and the reduced enzymatic flavin adenine dinucleotide ($FADH_2$). Subsequently, an oxidative half-reaction with molecular oxygen occurs to regenerate FAD which produces equimolar amounts of H_2O_2:

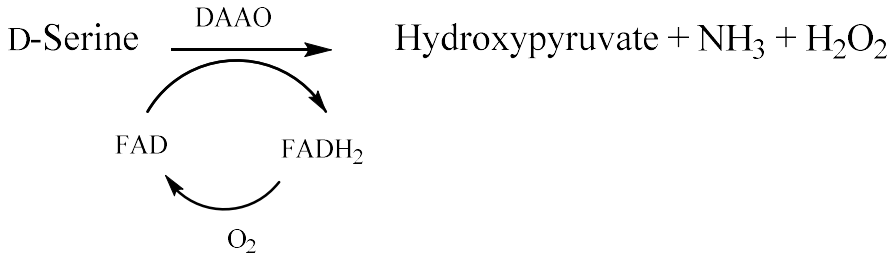

The H_2O_2 is then oxidised at the electrode surface and the resultant current corresponds to the D-serine concentration:

$$H_2O_2 \xrightarrow{\text{Pt (+700 mV)}} 2H^+ + O_2 + 2e^-$$

We have previously reported the development and characterisation of Pt-based microelectrochemical biosensors designed for neurochemical monitoring of analytes such as glucose, H_2O_2, choline and glutamate based on novel polymer enzyme composite designs[28-32] . Performance and operational characteristics including sensitivity, selectivity, response time, stability, and limit of detection were extensively studied for each biosensor and their target analyte. The newly developed D-serine sensor reported herein utilises past knowledge from previous manufacturing designs to facilitate immobilisation of DAAO onto a Pt surface, using poly(*o*-phenylenediamine) for interference rejection, and stabilising agents methyl methacrylate (MMA) and glutaraldehyde (GA) [3, 30, 33] to enhance the biosensor's overall performance. The resultant optimised composite design builds on previously published literature [3, 34], incorporating a novel extended drying time which significantly increases sensitivity. We also present a detailed characterisation study which suggests ideal suitability for *in-vivo* neurochemical monitoring of D-serine.

2. Experimental Section

2.1 Chemicals and Solutions

The *o*-phenylenediamine (*o*-PD, 1,2-diaminobenzene, ≥ 98 %), methyl methacrylate (MMA, 99 %), glutaraldehyde (GA, Grade 1, 25 %), bovine serum albumin (BSA, fraction V from bovine plasma), phosphate buffered saline (PBS) tablets, and D-serine (≥ 97 %) were obtained from Sigma-Aldrich Ireland Ltd (Dublin). Compounds used in the interference study were all purchased from Sigma-Aldrich Ireland Ltd: ascorbic acid (AA), dopamine (DA), 5-

hydroxytryptamine, 3,4-dihydroxyphenylacetic, homovanillic acid, L-tyrosine, L-cysteine, L-tryptophan, L-glutathione, uric acid (potassium salt), 5-hydroxyindoleacetic acid, D-aspartic acid, D-alanine, D-leucine and D-proline. The D-amino acid oxidase (DAAO; from porcine kidney, EC.1.4.3.3) was purchased from BBI Solutions, Crumlin, NP11 3EF, UK. A unit activity of 1200 U/mL (specific activity of 8,333 U/g protein) dissolved in PBS (pH 8.5) was used throughout.

In-vitro electrochemical experiments were performed in a 10 mM PBS solution, pH 7.4; 2.7 mM KCl and 137 mM NaOH prepared from commercial tablets. Fresh solutions of D-serine (100 mM), *o*-PD monomer (300 mM in N_2-saturated PBS), glutaraldehyde (1%), and BSA (1%) were prepared before use. Interferent solutions were prepared as required, and depending on stability used fresh (e.g. DA and AA) or stored frozen (-80 ^{o}C) between use.

2.2 Biosensor Preparation

Cylinder and disc electrodes were manufactured from Teflon-coated platinum/iridium (Pt/Ir 90%/10%) wire (127-µm bare diameter, 203-µm coated diameter, Science Products GmbH, Hofheimer Straße63, D-65719 Hofheim, Germany). The electrodes were *ca.* 6 cm in length with 3 mm of the Teflon® insulation removed from the wire. This was subsequently soldered into a gold clip (*In-vitro* - Fine Science Tools GmbH, 69115 Heidelberg, Germany; *In-vivo* - Plastics One, Roanoke, VA, USA) which provided both an electrical connection to the potentiostat and rigidity. Both cylinder and disc electrodes were used: the opposite end of the wire to the gold clip served as the active electrode surface and a fresh disc was cut at this end; cylinder electrodes were prepared by subsequently removing a 0.5 mm portion of the insulation. Poly(*o*-phenylenediamine) (PPD) was electrochemically deposited from *o*-PD to produce a thin self-sealing insulating polymer on the Pt surface [35], and the electrodes were then stored at room temperature for a minimum of 3 hours before modification.

A dip-adsorption method was used to coat each electrode with the various biosensor constituents applying a previously reported layering procedure [30, 33]. In brief, the electrodes (both cylinder ($Pt_{cyl)}$ or disc (Pt_D) geometries)were dipped for *ca.* 0.5 seconds into the immobiliser methyl methacrylate (MMA). They were then consecutively dipped 15 times into DAAO (1200 U/mL) and given a 4 min drying time between each dip sequence, and an extended drying time of 30 minutes after every 5 layers of enzyme (see Fig. 1). This process was repeated 3 times before addition of the final layer of glutaraldehyde (1%) (MMA-((DAAO-4)$_5$-30)$_3$-GA). The composite blank electrode was manufactured using the same dipping

process, except that the enzyme (DAAO) was substituted with the protein BSA (1%). All sensor modifications were allowed to dry overnight at 4 °C before being calibrated.

2.3 Biosensor Calibrations

The working electrodes (4 biosensors at a time) were calibrated in a standard three-electrode glass electrochemical cell containing 20 mL PBS (pH 7.4) at room temperature (21-23 °C), unless otherwise stated. A saturated calomel electrode (SCE) was used as the reference, and a Pt wire as the auxiliary electrode. A fixed potential of +700 mV (*vs.* SCE) was applied to the working electrodes which were given time to stabilise under the influence of the applied potential until the capacitance current had reached a steady baseline (*ca.* 3 hours). D-Serine calibrations (0-10 mM) were then performed by the addition of aliquots of analyte every 4 minutes. After each addition, followed a period of stirring/mixing (*ca.* 10 s), the current response for each concentration step was measured immediately before the addition of the next aliquot. Temperature controlled experiments were performed in a jacketed cell (ALS Ltd, IJ Cambria Scientific Ltd, Llanelli, UK) which was attached to a water bath (Julabo Corio CD-BC4, Fisher Scientific, Dublin, Ireland). The temperature was continuously recorded throughout the calibration using a T-type implantable thermocouple (ADInstruments Ltd., Oxford, UK) connected to a temperature pod (ADInstruments Ltd).

2.4 Oxygen Dependence

For this study, the PBS was de-aerated by vigorously purging the solution with N_2 for a minimum of 30 minutes before commencing recording. A N_2 atmosphere was then maintained over the solution while the biosensors settled. A 100 µM D-serine aliquot was introduced into the cell followed by 25 µM aliquots of O_2 (0-200 µM) every 3 minutes, with a brief stirring period (10 s) after each addition.

2.5 Stability and Biocompatibility

The storage stability (shelf-life) was investigated by calibrating the same batch of biosensors on day 1 and day 14 following dry storage at 4 °C. For biocompatibility testing, sensors were carefully placed in moist brain tissue and stored in the fridge at 4 °C between calibrations on days 1 and 14.

2.6 Instrumentation and Software

Constant potential amperometry (CPA) was performed in all electrochemical experiments using either a custom designed low noise potentistat (Biostat IV, ACM Instruments, Cumbria, UK), or eDAQ QuadStat (Green Leaf Scientific, Dublin, Ireland). Data acquisition was carried out with a notebook PC (*in-vitro*) or Mac® (*in-vivo*), a PowerLab® 8/30 (ADInstruments Ltd) or eDAQ e-corder (Green-Leaf Scientific) interface system, and LabChart® for Windows (Version 6, ADInstruments Ltd.) or eDAQ Chart (Version 5.5.23, eDAQ Pty Ltd., NSW 2112, Australia).

2.7 Data Analysis

The graphical presentation and analysis of data was performed using GraphPad Prism 7 (GraphPad Software, Inc., CA, USA). Michaelis-Menten non-linear regression analysis was used to calculate the enzyme kinetic parameters V_{MAXapp} and K_{Mapp} [29]. Sensitivity, here defined as the Linear Region Slope (LRS), was determined from linear regression analysis of the biosensor signal between 0-100 μM. All data is presented as mean current density (J, $nA.mm^{-2}$) ± SEM where n denotes the number of electrodes, unless otherwise stated. The calculated area for the Pt_D and Pt_C biosensors is $0.0127mm^2$ and $0.212mm^2$ respectively. All experimental signals were background subtracted. Statistical significance tests were performed using *t*-tests (two-tailed paired or unpaired where appropriate) or one-way ANOVA (with Bonferroni post-hoc analysis). Values of $P < 0.05$ were considered to indicate statistical significance.

2.8 Surgical Procedures

Male Wistar rats (3, 250-350 g; Charles River Laboratories International, Inc., UK) were anesthetised using the volatile agent Isoflurane (4% in air for induction, 1.5-3% for maintenance; Bioresource Unit (BRU), Maynooth University) using a Univentor 400 Anaesthetic Unit (AgnTho's AB, Sweden). Once surgical anaesthesia was established the animals were placed in a stereotaxic frame and the biosensors, along with their composite blank electrodes (*ca.* 1 mm apart), were implanted following a previously reported method [36], with the level of anaesthesia checked regularly (pedal withdrawal reflex). Coordinates for striatum

with the skull levelled between bregma and lambda were: AP + 1.0, M/L ± 2.5 and D/V -5. A reference electrode (8T Ag, 200-µm diameter; Advent Research Materials, Suffolk, UK) was implanted in the cortex while the auxiliary electrode (8T Ag wire) was wrapped around one of the 4 support screws (Fine Science Tools GmbH, 69115 Heidelberg, Germany) used to fix the sensors/electrodes to the skull along with dental acrylate (Dentalon Plus, AgnTho's AB). Immediately following surgery all animals were administered saline and analgesic (buprecare; BRU, Maynooth University), and given time (several hours) to recover in a thermostatically controlled cage (Thermacage MkII, Datesand Ltd, Manchester, UK). They were assessed for good health according to published guidelines [37, 38] immediately following recovery from anaesthesia and at the beginning of every day.

Acute non-recovery experiments were performed using a similar surgical protocol. The reference electrode was placed in the cortex and the auxiliary electrode (soldered to a support screw) was positioned to the rear of the cannula. The biosensor and the corresponding composite blank were glued to a guide cannula (BASi®, West Lafayette, IN, USA) pre-surgery, attached to a stereotaxic micromanipulator and lowered slowly into the striatum to the desired coordinates (as above). A small amount of dental acrylate was applied for support.

All animal work was carried out with approval from Maynooth University Research Ethics Committee (BSRESC-2017-019), and under license (HPRA AE19124/PO19) in accordance with Part 5 of the European Union (Protection of Animals Used for Scientific Purposes) Regulations 2012 (S.I. No. 543 of 2012).

2.9 Experimental Conditions in-vivo

Animals were given at least forty-eight hours to recover from surgery. Experimental periods involved 96 hours (4 days/nights) of continuous recording where the animals were singly housed in Raturn® sampling cage systems (BASi, West Lafayette, IN, USA) in a temperature controlled facility with a 12 hour light/dark cycle (lights on at 07:00) with access *ad libitum* to food and water. The animals were then disconnected from the instrumentation and housed (buddy-bowl) with at least one other familiar animal for a minimum of 76 hours (3 days/nights). The sensors were connected directly to the potentiostat via a six pin Teflon socket (MS363, Plastics One, Roanoke, VA, USA) using a flexible screened six core cable (363-363 6TCM, Plastics One). This arrangement allowed free movement during recording and had minimal

effect on behaviour as all animals were habituated to the system for at least one week before surgery. After application of the potential (+700 mV *vs.* SCE) each animal was given a further 24 hour before commencing experiments to ensure the background currents for the sensors had stabilised. A sampling rate of 4 Hz was used for all recordings with a low-pass digital filter (50 Hz cut-off) applied to eliminate mains AC noise.

In acute experiments signals were allowed to reach a stable baseline (~ 2 hour post-implantation) following application of the potential and before initiating the microinjections. The infusion probe (BASi®, West Lafayette, IN, USA) was connected by PTFE (or PEEK check + details, e.g. PlasticsOne?) tubing to a 50 µL pre-filled gas-tight syringe mounted in a programmable syringe drive (Legato 130, AgnTho's AB, Sweden), and the solution pushed through until it was visible at the end of the cannula. The latter was then inserted into the implanted guide and a 800 nL microinjection of 200 mM D-serine was performed. A low pass digital filter (50 Hz cut-off) was applied and a sampling rate of 200 Hz was used for all recordings.

3. Results and Discussion

3.1 Optimising Biosensor Design

Several first generation biosensors have been developed for D-serine detection. These have utilised various transducers, geometries and immobilisation methods in their fabrication. Some utilise the recombinant *rhodotorula gracilis* D-amino acid oxidase (RgDAAO) as their biological recognition element [2, 23-25, 39]. This is overexpressed in Escherichia coli which is purified to homogeneity. D-amino acid oxidase sourced from porcine kidney (pkDAAO) has also been used [2, 3, 26]. However, biosensors that incorporate the RgDAAO enzyme tend to record increased sensitivity when compared to those using pkDAAO. This is summarised in Table 1.

Table 1. Comparison of sensitivity data for D-serine biosensors incorporating the enzymes RgDAAO and pkDAAO

Source	Geometry (µm)[a]	Composition	Sensitivity ($\mu A.cm^{-2}.mM^{-1}$)
		RgDAAO	
Vasylieva *et al*. [39]	Cylindrical(25x 100)	Pt/PPD/DAAO-PEGDE	183 ± 48 (n = 19)
Pernot *et al*. [2]	Cylindrical(25x 150)	Pt/PPD/DAAO-BSA-Gly/GA/Naf	75 ± 28 (n = 25)
Polcari *et al.* [23]	Disc (25)	Pt/PPD/DAAO-BSA-Gly/GA	279 ± 21 (n = 3)
Campos-Beltrán et al. [25]	Rectangular (333 × 15)	Pt/PPD/BSA/GA/DAAO	86.1 ± 8.3 (n = 12)
		pkDAAO	
Zain *et al.* [3]	Cylindrical (125x 1000)	Pt/PPD/Naf/GA/DAAO	48 ± 4 (n = 4)
Zain *et al.* [3]	Disc (125)	Pt/PPD/Naf/GA/DAAO	61 ± 7 (n = 4)
Design 3[b]	Cylindrical(127x 500)	Pt-MMA-$((DAAO\text{-}4)_5\text{-}30)_3$-GA	60 ± 2 (n = 47)
Design 4[b]	Disc (127)	Pt-MMA-$((DAAO\text{-}4)_5\text{-}30)_3$-GA	76 ± 4 (n = 41)

[a]Diametre x Height [b]This study - See Experimental (Biosensor Preparation)

The biosensor reported herein incorporates the pkDAAO enzyme and builds on previously published work [3, 34]. However, several advancements were implemented in this newly developed design protocol, the inclusion of an initial immobilisation layer of MMA to facilitate the entrapment of the enzyme layers with the number absorbed significantly increased and decreasing the GA concentration utilised to 1% incorporated only as a final layer to crosslink the previous enzyme layers. These advancements and the inclusion of an extended 30 minute drying time results in improved LRS sensitivity and the optimisation of the kinetic parameters compared to previously published work [3, 34].

The design Pt-MMA-$((DAAO\text{-}4)_5\text{-}30)_3$-GA was first tried on a 0.5 mm cylinder (Design 1) but was also tested on a disc electrode (Design 2), whose geometry can be more favourable for accessing smaller brain regions (see Fig. 2A). The kinetic parameters for the disc geometry($V_{MAXapp,}$ 730.6 ± 15 $nA.mm^{-2}$; K_{Mapp}, 632 ± 47 µM, n = 41) significantly improved compared to the 0.5 mm cylinder ($V_{MAXapp,}$ 473 ± 9 $nA.mm^{-2}$, $P < 0.0001$; K_{Mapp}, 453 ± 35 µM, $P < 0.0001$, n = 47) in line with previous observations [3]. Sensitivity was also improved ($P = 0.0004$): disc, 0.76 ± 0.04 $nA.mm^{-2}.\mu M^{-1}$ (n = 41); cylinder, 0.6 ± 0.02 $nA.mm^{-2}.\mu M^{-1}$ (n = 47). It is clear from these results that enzymatic sensitivities towards D-serine reflected in the increased V_{MAXapp} and K_{Mapp} values are dependent on the immobilisation protocol and electrode

geometry with the Pt_D exhibiting increased V_{MAXapp} and K_{Mapp} values compared to the Pt_C. This disc design with optimised drying time also shows enhanced response characteristics when compared with other D-serine biosensors utilising the pkDAAO enzyme (see Table 1), but has still, on average, lower sensitivity than that observed for biosensors incorporating purified RgDAAO. However, increased sensitivity is not necessarily a positive when designing oxidase-based biosensors for neurochemical monitoring as oxygen dependence can become a limiting factor [40]. As such, we further characterised the Pt-MMA-((DAAO-4)$_5$-30)$_3$-GA design in terms of its operational characteristics under *in-vitro* conditions mimicking the physiological environment in order to determine its potential suitability for monitoring in the living brain.

Table 2. Comparison of V_{MAXapp}, K_{Mapp} and sensitivity (Linear Region Slope, LRS) for the D-serine biosensor designs incorporating an extended drying period.

	Design	n	V_{MAXapp} (nA.mm^{-2})	K_{Mapp} (µM)	LRS (nA.mm^{-2}.µM^{-1})
1	Pt_C-MMA-((DAAO-4)$_5$-30)$_3$-GA	47	473 ± 9	453 ± 35	0.60 ± 0.02
2	Pt_D-MMA-((DAAO-4)$_5$-30)$_3$-GA	41	731 ± 15	632 ± 47	0.76 ± 0.04

3.2 Oxygen Dependence

The enzyme DAAO requires O_2 to complete its catalytic cycle regenerating FAD (see *1. Introduction*). This gives rise to a potential interference problem associated with first generation biosensors designed to be applied in biological tissues; the possibility that changes in local O_2 may interfere with the substrate response [28]. As such, it is important to characterise O_2 dependence. This was achieved using a fixed concentration of D-serine (100 µM) well in excess of basal levels so as to cover the range of potential changes that might be observed *in-vivo*. The concentration of O_2 was incrementally varied between 0 (N_2 saturation) and 200 µM (air saturation, see Fig. 3A). Addition of 25 µM resulted in an increase in D-serine current from 0 to 78.3 ± 5.6 % (n = 6) of the maximum current ($J_{MAX,}$ 100 µM) response for

air-saturated PBS, with 98.3 ± 6.1 % achieved at 50 μM. As brain O_2 levels have been reported between 40-80 μM [41-43], and given that low substrate concentrations tend to display lower biosensor dependence [28], these results indicate that the Pt_D-MMA-$((DAAO\text{-}4)_5\text{-}30)_3$-GA biosensor has minimal interference from O_2 over physiological concentrations with a $K_M[O_2]$ value of 7.7 ± 1.98 μM, suggesting its suitability for use *in-vivo*. Other groups have reported similar results, with D-serine detection at physiological levels not dependent on O_2 except potentially during pathological states such as ischemia [2].

3.3 Interference Studies

The brain is an anatomically complex environment containing several electroactive interferents which could potentially undermine the specificity of the biosensor. One such interferent is ascorbic acid (AA) [44]. With estimated basal concentrations reported at *ca.* 400 μM [45] this interferent alone could potentially mask the low micromolar D-serine signal. The electropolymerisation of a poly(*o*-phenylenediamine) layer has previously been utilised in glucose[29, 46], H_2O_2 [31] and glutamate [32, 47, 48] biosensors for its ability to effectively eliminate the AA signal through a saturation and self-blocking process [29, 49], while still facilitating high permeability to surface generated H_2O_2 [50-52]. Inclusion of a PPD layer in the manufacturing process resulted in only small current responses being detected at the Pt_D-MMA-$((DAAO\text{-}4)_5\text{-}30)_3$-GA biosensor for AA; Fig. 3B (inset) shows sensitivity as a function of AA concentration highlighting the significant interference rejection.

Other potential interferents tested included the neurotransmitters dopamine (DA) and 5-hydroxytryptamine (5-HT), their metabolites 3,4-dihydroxyphenylacetic acid (DOPAC), homovanillic acid (HVA) and 5-hydroxyindoleacetic acid (5-HIAA), the amino acids L-tyrosine, L-cysteine, L-tryptophan, the antioxidant L-glutathione, the purine metabolite uric acid (UA) Table 3 shows the average current recorded after administration of physiologically relevant concentrations of each analyte. Small negative currents attributed to baseline drift were recorded for some interferents. With the exception of L-cysteine, all signals recorded were small (≤ 5 %) compared to the current (6.36 ± 0.6 $nA.mm^{-2}$, n = 41) for basal D-serine levels (5 μM). However, the extracellular concentration of cysteine in the brain is reported to be in the nanomolar to low micromolar range [53] , so therefore its contribution may be negligible *in-vivo*. Also, such signals would be further reduced *in-vivo* through co-implantation of a composite blank sensor (Pt_D-MMA-$((BSA)_5\text{-}30)_3$-GA) and differential signal analysis, improving the selectivity of the biosensor.

The enzyme pkDAAO catalyses the stereospecific deamination of D-amino acids into their corresponding α-imino acids which are then hydrolysed spontaneously to α-oxo-acids and ammonia [54]. While D-serine is the predominant D-amino acid found in the CNS with a low micromolar concentration (*ca.* 5 μM), others are also present [55]. D-alanine has a good affinity for DAAO but its concentration is less than 3% of that of D-serine. D-aspartate on the other hand is a poor substrate for DAAO while present at approximately 10% of the D-serine level. Both were tested for potential interference along with the other most abundant D-amino acids, D-leucine and D-proline [55]. All exhibited small pA changes for physiologically relevant concentrations (see Fig. 3B) which were non-significant compared to that for D-serine ($P < 0.0001$). As expected, D-alanine produced the largest response but was still < 5% of the D-serine signal at physiological concentrations. As expected when we tested the Pt_D-MMA-$((DAAO\text{-}4)_5\text{-}30)_3$-GA biosensor at an equimolar concentration (5 μM) the D-amino acids recorded signal responses of 5.53 ± 0.79 nA.mm^{-2} (n = 8, D-alanine), 3.79 ± 0.47 nA.mm^{-2} (n = 7, D-proline), 4.03 ± 0.47 nA.mm^{-2} (n = 8, D-leucine) and 0.59 ± 0.28 nA.mm^{-2} (n = 7, D-aspartate) with these results emphasising the fact that the enzyme D-amino acid oxidase is not selective to D-serine but can be utilised for the detection of many D-amino acids, however, for neurochemical monitoring this developed biosensor is selective to D-serine due to the significantly higher ECF concentration of this specific D-amino acid.

Overall, this data compares favourably with other published D-serine biosensors developed utilising pkDAAO [3], and suggests that the Pt_D-MMA-$((DAAO\text{-}4)_5\text{-}30)_3$-GA biosensor should be selective for D-serine when used for neurochemical monitoring. As many biosensors designed for neurochemical monitoring incorporate a sentinel or blank electrode [2, 25, 56, 57] to increase interference rejection, we propose the co-implantation of a composite blank sensor (Pt_D-MMA-$((BSA\text{-}4)_5\text{-}30)_3$-GA; see section 2.8 surgical procedures) and differential signal analysis to improve permselectivity and mitigate any potential interference from species such as L-cysteine and DOPAC. The role of this sentinel blank will be further characterised and investigated in a future *in-vivo* study.

Table 3. Current response of the Pt_D-MMA-((DAAO-4)$_5$-30)$_3$-GA biosensor to potential interferent molecules found *in-vivo*.

	n	[Interferent] (µM)	Current[e] (nA.mm^{-2})	% Change (*vs.* 5 µM D-Serine)
D-Aspartate	7	≈0.5[a]	0.06 ± 0.03	0.9%
D-Alanine	8	≈0.15[a]	0.17 ± 0.03	2.7%
D-Proline	6	≈0.05[a]	0.04 ± 0.005	0.6%
D-Leucine	6	≈0.05[a]	0.05 ± 0.003	0.8%
AA	20	500	0.24 ± 0.94	3.8%
Dopamine	13	0.05[b]	-	0%
DOPAC	9	20[b]	0.23 ± 0.62	3.6%
HVA	13	10[b]	-	0%
5-HT	13	0.01[b]	-	0%
5-HIAA	10	50[b]	-	0%
Uric Acid	13	50[b]	-	0%
L-Glutathione	13	50[d]	-	0%
L-Cysteine	16	4[c]	0.40 ± 0.45	6.3%
L-Tryptophan	10	20[d]	-	0%
L-Tyrosine	9	20[d]	-	0%
Glycine	8	10[a]	-	0%
L-Serine	8	10[a]	-	0%

[a] [55], [b][58], [c] [59], [d] High µM values chosen as ECF concentrations not known [e] Small negative currents attributable to baseline drift were recorded for some neurochemicals.

3.4 Temperature and pH

All calibrations reported so far were performed at room temperature (21-23 °C) and at pH 7.4. However, changes in temperature could potentially modify the catalytic activity of the immobilised enzyme and thus alter biosensor performance [60]. For this reason, the effect of changing temperature on the kinetic parameters of the biosensor was investigated, especially

as brain temperature fluctuations have been observed during behaviour, and after pharmacological manipulations in freely-moving animals [61-63]. Generally, under normal conditions the temperature range *in-vivo* is typically between 35.5 and 38.8 °C. However, during certain circumstances this range can be altered, such as during pentobarbital anaesthesia (33 °C) and after psychomotor stimulant administration (40 °C) [64]. Fig. 4 shows the effect on D-serine sensitivity of temperature changes over the range 34 – 40 °C. Almost identical sensitivities (P = 0.5634, one-way ANOVA) were recorded at each of the temperatures: RT, 0.76 ± 0.04 nA.mm^{-2}.µM^{-1} (n = 11); 34 °C, 0.81 ± 0.01 nA.mm^{-2}.µM^{-1} (n = 7); 37 °C, 0.80 ± 0.02 nA.mm^{-2}.µM^{-1} (n = 9); and 40 °C, 0.80 ± 0.01 nA.mm^{-2}.µM^{-1} (n = 8). These results highlight the ability to detect changes in D-serine *in-vivo* without influence from temperature variations, similar to previously published biosensors [65, 66].

Biosensors developed for *in-vivo* use are also typically calibrated over a range of physiologically relevant pH values (typically 6.8 to 8) to ensure that performance is not compromised by potential pH changes [42, 67]. As pH is tightly regulated *in-vivo*, a range between 7.2 and 7.6 was tested (see Fig. 4, inset). No significant difference was observed (P = 0.0752, one-way ANOVA) in sensitivity: pH 7.2, 0.62 ± 0.01 nA.mm^{-2}.µM^{-1} (n = 4); pH 7.4, 0.76 ± 0.04 nA.mm^{-2}.µM^{-1} (n = 11); and pH 7.6, 0.77 ± 0.02 nA.mm^{-2}.µM^{-1} (n = 5).

3.5 Response time and Limit of Detection

Other performance parameters considered were response time and limit of detection (LOD). The former is defined as the time taken for the response to increase from 10 to 90 % ($t_{10\text{-}90\%}$) of the maximum current for a fixed concentration. While it is difficult to separate this parameter from the mixing time in a classical electrochemical cell, the calculated value of 9.86 ± 0.46 s (n = 7) is within the stirring time (*ca.* 10 s). Similar *in-vitro* response times have been reported for other Pt-based biosensors [31, 33, 65, 67, 68] , and typically, such devices tend to display faster response times (e.g. 1 s or less) *in-vivo* [42, 57, 66, 69, 70]. The LOD, or lowest concentration reliably detected by the biosensor, was calculated using the widely accepted criterion of three times the standard deviation of the baseline [59, 71-73]. The calculated value of 0.33 ± 0.02 µM (n = 18) suggests that the Pt_D-MMA-((DAAO-4)$_5$-30)$_3$-GA biosensor should be capable of monitoring physiological changes in D-serine from its estimated basal concentration of *ca.* 5 µM.

3.6 Biofouling and Stability

It is also important to consider and characterise any potential changes that could result from long-term application in the target medium which might compromise the functional characteristics of the device [74]. As the objective here is real-time neurochemical monitoring, we tested the biosensor under conditions mimicking those found in the brain, which consists of surfactants, electrode poisons, and a tissue matrix that can hinder mass transport [58, 75]. Biofouling studies where thus performed by storing a batch of biosensors in moist brain tissue at 4 °C for 14 days following calibration on day 1. A 4 % decrease in sensitivity was recorded on day 14 (0.52 ± 0.005 $nA.mm^{-2}.\mu M^{-1}$, n = 6) compared to day 1 (0.54 ± 0.03 $nA.mm^{-2}.\mu M^{-1}$, n = 6, P = 0.72), indicating excellent biocompatibility characteristics. Usually following implantation a decrease in sensitivity of between 20 and 50 % is observed [76, 77], after which signals tend to stabilise for up to 14 days [69, 70]. The results presented here suggest that this D-serine biosensor may function beyond this period.

Finally, it is important to consider the shelf-life which can also provide a good indication of stability [65]. This characteristic was tested by calibrating a batch of biosensors on day 1, and then recalibrating following 14 days dry storage at 4 °C. No intervening days were tested as previous research has highlighted the potential detrimental effect of repeated calibrations on biosensor sensitivity [65]. Both day 1 (0.52 ± 0.02 $nA.mm^{-2}.\mu M^{-1}$, n = 5) and day 14 (0.51 ± 0.013 $nA.mm^{-2}.\mu M^{-1}$, n = 5, P = 0.88) were found to have similar average sensitivities supporting the biocompatibility data.

3.7 In-vivo Recording

We performed preliminary application experiments investigating the *in-vivo* biocompatibility/stability properties of the Pt_D-MMA-$((DAAO\text{-}4)_5\text{-}30)_3$-GA biosensor by implanting in the striatum of freely moving animals and examining changes in the baseline current over several days (see Fig. 5A). Animals were given at least 48 hours recovery from surgery (Day 0) before connection, and then following the application of the applied potential sensors were given a minimum of 12 hours to stabilise in order to eliminate non-faradaic contributions. Each baseline value was calculated at the same time period (08:00-09:00), prior to any experimental procedures. No significant variation (P = 0.9312, one-way ANOVA) in baseline current was observed over a 13 day period for the implanted biosensors (n = 7

biosensors/3 animals). These results confirm that the developed biosensor is suitable for recording D-serine changes for at least two weeks following implantation. This newly developed biosensor (Pt_D-MMA-((DAAO-4)$_5$-30)$_3$-GA) shows a marked improvement in operational stability as our previous pkDAAO-based biosensor showed a decrease in sensitivity following 3 days of continuous use [3]. Figure 5A (inset) shows a typical example of the effects of a 800 nL microinjection of 200 µM D-serine on the Pt_D-MMA-((DAAO-4)$_5$-30)$_3$-GA biosensor and Pt_D-MMA-((BSA-4)$_5$-30)$_3$-GA composite blank implanted in the striatum. The Pt_D-MMA-((DAAO-4)$_5$-30)$_3$-GA shows a 100% increase in current after the local administration of 200 µM D-serine, while no change was observed at the blank (Pt_D-MMA-((BSA-4)$_5$-30)$_3$-GA), confirming this change in current is as a result of changes in D-serine concentration.

Fig. 5B shows typical *in-vivo* traces for both the biosensor (Pt_D-MMA-((DAAO-4)$_5$-30)$_3$-GA) and a composite blank electrode (Pt_D-MMA-((BSA-4)$_5$-30)$_3$-GA) recorded over a 6 hour period during the light phase between 10:00-16:00. It also shows the differential D-serine signal (purple trace, Fig. 5B), which using *in vitro* calibrations, would suggest an approximate basal ECF concentration of 10 µM. This is in good agreement with values estimated by other groups using biosensors (2.3 µM-frontal cortex and 2.8 µM- hippocampus [5]) and microdialysis (5.8 µM-mPFC and 7.3 µM-striatum [4]). Generally, during a 24 hour period *in-vivo* signals recorded from freely moving animals exhibit changes from baseline levels varying from rapid short changes, to more prolonged ones lasting one or more hours [78]. These changes are often associated with physiological phenomena including activity (e.g. feeding, and grooming) and sleep [78],[79]. Such changes are clearly visible in the D-serine signal (D-serine - Blank) over the 6 hour period highlighted. Future work will involve further *in-vivo* characterisation experiments to investigate sensitivity, selectivity and the dynamic relationship between substrate and blank signals. The latter have been predominantly monitored in anaesthetised animals where general CNS depression results in clean signals devoid of the physiological changes observed in the awake animal. Additionally, such recordings tend to be performed over relatively short time periods (e.g. minutes), typically during a pharmacological manipulation involving pressure ejections, see e.g.[57, 77, 80] .

4. Conclusions

A sensitive, selective and stable biosensor for neurochemical monitoring of D-serine was successfully developed and characterised *in-vitro*. The incorporation of MMA as the immobiliser facilitated the entrapment of the DAAO enzyme onto the active surface of the electrode using a dip-coating approach, while inclusion of the cross-linker GA enabled optimisation of the V_{MAXapp}, $K_{M,app}$ and sensitivity. The introduction of an extended drying period and disc geometry improved these parameters further compared to previous designs [3, 34]. The biosensor performed well following storage at 4 °C for 14 days (dry) or in *ex-vivo* brain tissue, with no significant decrease observed in sensitivity. The inclusion of a poly(*o*-phenylenediamine) layer, and the proposed co-implantation of a composite blank electrode *in-vivo*, successfully rejects a range of potential electroactive interferents, with the biosensor also displaying oxygen independence over physiologically relevant concentrations, and negligible signal contributions from other endogenous DAAO substrates. Furthermore, temperature and pH changes had minimal effect on sensitivity. When considered with the calculated low µM detection limit and rapid response time, these characteristics suggest that the developed composite biosensor is suitable for detecting neurochemical levels of D-serine. Preliminary *in-vivo* experiments performed over a two-week period support this conclusion

Acknowledgement

This publication has emanated from research supported by Science Foundation Ireland (SFI) under grant number 15/IA/3176. We thank Dr. Keeley L. Baker for helpful discussions on enzyme concentration.

Declaration of Competing Interest

All authors declare no conflict of interest.

References

[1] A. Hashimoto, T. Nishikawa, T. Hayashi, N. Fujii, K. Harada, T. Oka, K. Takahashi, The presence of free D-serine in rat brain, FEBS Letters, 296 (1992) 33-36.
[2] P. Pernot, J.-P. Mothet, O. Schuvailo, A. Soldatkin, L. Pollegioni, M. Pilone, M.-T. Adeline, R. Cespuglio, S. Marinesco, Characterization of a Yeast d-Amino Acid Oxidase Microbiosensor for d-Serine Detection in the Central Nervous System, Analytical Chemistry, 80 (2008) 1589-1597.
[3] Z.M. Zain, R.D. O'Neill, J.P. Lowry, K.W. Pierce, M. Tricklebank, A. Dewa, S.A. Ghani, Development of an implantable d-serine biosensor for in vivo monitoring using mammalian d-amino acid oxidase on a poly (o-phenylenediamine) and Nafion-modified platinum–iridium disk electrode, Biosensors and Bioelectronics, 25 (2010) 1454-1459.
[4] A. Hashimoto, T. Oka, T. Nishikawa, Extracellular concentration of endogenous free d-serine in the rat brain as revealed by in vivo microdialysis, Neuroscience, 66 (1995) 635-643.
[5] P. Pernot, C. Maucler, Y. Tholance, N. Vasylieva, G. Debilly, L. Pollegioni, R. Cespuglio, S. Marinesco, d-Serine diffusion through the blood–brain barrier: Effect on d-serine compartmentalization and storage, Neurochemistry International, 60 (2012) 837-845.
[6] T. Papouin, P.G. Haydon, D-serine Measurements in Brain Slices or Other Tissue Explants, Bio Protoc, 8 (2018) e2698.
[7] M. Van Horn, M. Sild, E. Ruthazer, D-serine as a gliotransmitter and its roles in brain development and disease, Frontiers in Cellular Neuroscience, 7 (2013).
[8] H. Wolosker, E. Dumin, L. Balan, V.N. Foltyn, d-Amino acids in the brain: d-serine in neurotransmission and neurodegeneration, The FEBS Journal, 275 (2008) 3514-3526.
[9] S.K. Bardaweel, M. Alzweiri, A.A. Ishaqat, D-Serine in Neurobiology: CNS Neurotransmission and Neuromodulation, Canadian Journal of Neurological Sciences / Journal Canadien des Sciences Neurologiques, 41 (2014) 164-176.
[10] K. Hashimoto, G. Engberg, E. Shimizu, C. Nordin, L.H. Lindström, M. Iyo, Reduced d-serine to total serine ratio in the cerebrospinal fluid of drug naive schizophrenic patients, Progress in Neuro-Psychopharmacology and Biological Psychiatry, 29 (2005) 767-769.
[11] M.-A.B. MacKay, M. Kravtsenyuk, R. Thomas, N.D. Mitchell, S.M. Dursun, G.B. Baker, D-Serine: Potential Therapeutic Agent and/or Biomarker in Schizophrenia and Depression?, Frontiers in Psychiatry, 10 (2019).
[12] S.-E. Cho, K.-S. Na, S.-J. Cho, S.G. Kang, Low d-serine levels in schizophrenia: A systematic review and meta-analysis, Neuroscience Letters, 634 (2016) 42-51.
[13] C. Madeira, M.V. Lourenco, C. Vargas-Lopes, C.K. Suemoto, C.O. Brandão, T. Reis, R.E. Leite, J. Laks, W. Jacob-Filho, C.A. Pasqualucci, d-serine levels in Alzheimer's disease: implications for novel biomarker development, Translational psychiatry, 5 (2015) e561-e561.
[14] J. Sasabe, Y. Miyoshi, M. Suzuki, M. Mita, R. Konno, M. Matsuoka, K. Hamase, S. Aiso, d-Amino acid oxidase controls motoneuron degeneration through d-serine, Proceedings of the National Academy of Sciences, 109 (2012) 627.
[15] A. El Arfani, G. Albertini, E. Bentea, T. Demuyser, A. Van Eeckhaut, I. Smolders, A. Massie, Alterations in the motor cortical and striatal glutamatergic system and d-serine levels in the bilateral 6-hydroxydopamine rat model for Parkinson's disease, Neurochemistry International, 88 (2015) 88-96.
[16] J. Le Douce, M. Maugard, J. Veran, M. Matos, P. Jégo, P.-A. Vigneron, E. Faivre, X. Toussay, M. Vandenberghe, Y. Balbastre, Impairment of glycolysis-derived L-serine production in astrocytes contributes to cognitive deficits in Alzheimer's disease, Cell metabolism, 31 (2020) 503-517. e508.

[17] Y. Xing, X. Li, X. Guo, Y. Cui, Simultaneous determination of 18 D-amino acids in rat plasma by an ultrahigh-performance liquid chromatography-tandem mass spectrometry method: application to explore the potential relationship between Alzheimer's disease and D-amino acid level alterations, Analytical and bioanalytical chemistry, 408 (2016) 141-150.
[18] R. Moaddel, D.A. Luckenbaugh, Y. Xie, A. Villaseñor, N.E. Brutsche, R. Machado-Vieira, A. Ramamoorthy, M.P. Lorenzo, A. Garcia, M. Bernier, M.C. Torjman, C. Barbas, C.A. Zarate, I.W. Wainer, D-serine plasma concentration is a potential biomarker of (R,S)-ketamine antidepressant response in subjects with treatment-resistant depression, Psychopharmacology, 232 (2015) 399-409.
[19] M.J. Berna, B.L. Ackermann, Quantification of serine enantiomers in rat brain microdialysate using Marfey's reagent and LC/MS/MS, Journal of Chromatography B, 846 (2007) 359-363.
[20] S.L. Grant, Y. Shulman, P. Tibbo, D.R. Hampson, G.B. Baker, Determination of d-serine and related neuroactive amino acids in human plasma by high-performance liquid chromatography with fluorimetric detection, Journal of Chromatography B, 844 (2006) 278-282.
[21] N.S. Singh, R.K. Paul, M. Sichler, R. Moaddel, M. Bernier, I.W. Wainer, Capillary electrophoresis–laser-induced fluorescence (CE-LIF) assay for measurement of intracellular d-serine and serine racemase activity, Analytical Biochemistry, 421 (2012) 460-466.
[22] A. Hashimoto, M. Yoshikawa, Effect of aminooxyacetic acid on extracellular level of d-serine in rat striatum: An in vivo microdialysis study, European Journal of Pharmacology, 525 (2005) 91-93.
[23] D. Polcari, A. Kwan, M.R. Van Horn, L. Danis, L. Pollegioni, E.S. Ruthazer, J. Mauzeroll, Disk-Shaped Amperometric Enzymatic Biosensor for in Vivo Detection of d-serine, Analytical Chemistry, 86 (2014) 3501-3507.
[24] D. Polcari, S.C. Perry, L. Pollegioni, M. Geissler, J. Mauzeroll, Localized Detection of d-Serine by using an Enzymatic Amperometric Biosensor and Scanning Electrochemical Microscopy, ChemElectroChem, 4 (2017) 920-926.
[25] D. Campos-Beltrán, Å. Konradsson-Geuken, J.E. Quintero, L. Marshall, Amperometric Self-Referencing Ceramic Based Microelectrode Arrays for D-Serine Detection, Biosensors, 8 (2018) 20.
[26] Z. Mohd Zain, S. Ab Ghani, R.D. O'Neill, Amperometric microbiosensor as an alternative tool for investigation of d-serine in brain, Amino Acids, 43 (2012) 1887-1894.
[27] E. Rosini, P. D'Antona, L. Pollegioni, Biosensors for D-Amino Acids: Detection Methods and Applications, International Journal of Molecular Sciences, 21 (2020) 4574.
[28] B.M. Dixon, J.P. Lowry, R.D. O'Neill, Characterization in vitro and in vivo of the oxygen dependence of an enzyme/polymer biosensor for monitoring brain glucose, Journal of Neuroscience Methods, 119 (2002) 135-142.
[29] J.P. Lowry, R.D. O'Neill, Partial characterization in vitro of glucose oxidase-modified poly(phenylenediamine)-coated electrodes for neurochemical analysis in vivo, Electroanalysis, 6 (1994) 369-379.
[30] K.L. Baker, F.B. Bolger, J.P. Lowry, Development of a microelectrochemical biosensor for the real-time detection of choline, Sensors and Actuators B: Chemical, 243 (2017) 412-420.
[31] S.L. O'Riordan, K. Mc Laughlin, J.P. Lowry, In vitro physiological performance factors of a catalase-based biosensor for real-time electrochemical detection of brain hydrogen peroxide in freely-moving animals, Analytical Methods, 8 (2016) 7614-7622.
[32] C.P. McMahon, G. Rocchitta, S.M. Kirwan, S.J. Killoran, P.A. Serra, J.P. Lowry, R.D. O'Neill, Oxygen tolerance of an implantable polymer/enzyme composite glutamate biosensor

displaying polycation-enhanced substrate sensitivity, Biosensors and Bioelectronics, 22 (2007) 1466-1473.
[33] M.M. Doran, N.J. Finnerty, J.P. Lowry, In–Vitro Development and Characterisation of a Superoxide Dismutase-Based Biosensor, ChemistrySelect, 2 (2017) 4157-4164.
[34] K.W. Pierce, The Design,Development and Charaterisation of a New Biosensor for In-Vivo Neurochemical Monitoring of D-serine, National University of Ireland Maynooth, 2012.
[35] S.J. Killoran, R.D. O'Neill, Characterization of permselective coatings electrosynthesized on Pt–Ir from the three phenylenediamine isomers for biosensor applications, Electrochimica Acta, 53 (2008) 7303-7312.
[36] J. Kealy, R. Bennett, J.P. Lowry, Simultaneous recording of hippocampal oxygen and glucose in real time using constant potential amperometry in the freely-moving rat, Journal of Neuroscience Methods, 215 (2013) 110-120.
[37] D.B. Morton, P.H. Griffiths, Guidelines on the recognition of pain, distress and discomfort in experimental animals and an hypothesis for assessment, The Veterinary record, 116 (1985) 431-436.
[38] E. Carstens, G.P. Moberg, Recognizing Pain and Distress in Laboratory Animals, ILAR Journal, 41 (2000) 62-71.
[39] N. Vasylieva, B. Barnych, A. Meiller, C. Maucler, L. Pollegioni, J.-S. Lin, D. Barbier, S. Marinesco, Covalent enzyme immobilization by poly(ethylene glycol) diglycidyl ether (PEGDE) for microelectrode biosensor preparation, Biosensors and Bioelectronics, 26 (2011) 3993-4000.
[40] Y. Zhang, G. Wilson, In vitro and in vivo evaluation of oxygen effects on a glucose oxidase based implantable glucose sensor, Analytica Chimica Acta, 281 (1993) 513-520.
[41] F.B. Bolger, J.P. Lowry, Brain Tissue Oxygen: In Vivo Monitoring with Carbon Paste Electrodes, Sensors, 5 (2005) 473-487.
[42] F.B. Bolger, S.B. McHugh, R. Bennett, J. Li, K. Ishiwari, J. Francois, M.W. Conway, G. Gilmour, D.M. Bannerman, M. Fillenz, M. Tricklebank, J.P. Lowry, Characterisation of carbon paste electrodes for real-time amperometric monitoring of brain tissue oxygen, Journal of Neuroscience Methods, 195 (2011) 135-142.
[43] R. Murr, S. Berger, L. Schürer, K. Peter, A. Baethmann, A novel, remote-controlled suspension device for brain tissue PO2 measurements with multiwire surface electrodes, Pflügers Archiv, 426 (1994) 348-350.
[44] F.O. Brown, J.P. Lowry, Microelectrochemical sensors for in vivo brain analysis: an investigation of procedures for modifying Pt electrodes using Nafion®, Analyst, 128 (2003) 700-705.
[45] M. Miele, M. Fillenz, In vivo determination of extracellular brain ascorbate, Journal of Neuroscience Methods, 70 (1996) 15-19.
[46] R. Garjonyte, A. Malinauskas, Amperometric glucose biosensor based on glucose oxidase immobilized in poly(o-phenylenediamine) layer, Sensors and Actuators B: Chemical, 56 (1999) 85-92.
[47] R. Ford, S.J. Quinn, R.D. O'Neill, Characterization of Biosensors Based on Recombinant Glutamate Oxidase: Comparison of Crosslinking Agents in Terms of Enzyme Loading and Efficiency Parameters, Sensors (Basel), 16 (2016) 1565.
[48] M. Ganesana, E. Trikantzopoulos, Y. Maniar, S.T. Lee, B.J. Venton, Development of a novel micro biosensor for in vivo monitoring of glutamate release in the brain, Biosensors and Bioelectronics, 130 (2019) 103-109.
[49] J.D. Craig, R.D. O'Neill, Electrosynthesis and permselective characterisation of phenol-based polymers for biosensor applications, Analytica Chimica Acta, 495 (2003) 33-43.
[50] S.A. Rothwell, R.D. O'Neill, Effects of applied potential on the mass of non-conducting poly(ortho-phenylenediamine) electro-deposited on EQCM electrodes: comparison with

biosensor selectivity parameters, Physical Chemistry Chemical Physics, 13 (2011) 5413-5421.
[51] L.J. Murphy, Reduction of Interference Response at a Hydrogen Peroxide Detecting Electrode Using Electropolymerized Films of Substituted Naphthalenes, Analytical Chemistry, 70 (1998) 2928-2935.
[52] Y.-Q. Dai, D.-M. Zhou, K.-K. Shiu, Permeability and permselectivity of polyphenylenediamine films synthesized at a palladium disk electrode, Electrochimica Acta, 52 (2006) 297-303.
[53] H. Landolt, T.W. Lutz, H. Langemann, D. Stäuble, A. Mendelowitsch, O. Gratzl, C.G. Honegger, Extracellular Antioxidants and Amino Acids in the Cortex of the Rat: Monitoring by Microdialysis of Early Ischemic Changes, Journal of Cerebral Blood Flow & Metabolism, 12 (1992) 96-102.
[54] M. Gabler, M. Hensel, L. Fischer, Detection and substrate selectivity of new microbial D-amino acid oxidases, Enzyme and Microbial Technology, 27 (2000) 605-611.
[55] K. Hamase, R. Konno, A. Morikawa, K. Zaitsu, Sensitive Determination of <small>D</small>-Amino Acids in Mammals and the Effect of <small>D</small>-Amino-Acid Oxidase Activity on Their Amounts, Biological and Pharmaceutical Bulletin, 28 (2005) 1578-1584.
[56] J.J. Burmeister, M. Palmer, G.A. Gerhardt, l-lactate measures in brain tissue with ceramic-based multisite microelectrodes, Biosensors and Bioelectronics, 20 (2005) 1772-1779.
[57] J.J. Burmeister, G.A. Gerhardt, Self-Referencing Ceramic-Based Multisite Microelectrodes for the Detection and Elimination of Interferences from the Measurement of l-Glutamate and Other Analytes, Analytical Chemistry, 73 (2001) 1037-1042.
[58] J. Lowry, R. O'Neill, Neuroanalytical chemistry in vivo using electrochemical sensors in Encyclopedia of Sensors, Grimes, CA, Dickey, EC & Pishko, MV ed (s), American Scientific Publishers, California, USA, California USA, 2006, pp. 1-23.
[59] N.V. Kulagina, L. Shankar, A.C. Michael, Monitoring Glutamate and Ascorbate in the Extracellular Space of Brain Tissue with Electrochemical Microsensors, Analytical Chemistry, 71 (1999) 5093-5100.
[60] G. Rocchitta, A. Spanu, S. Babudieri, G. Latte, G. Madeddu, G. Galleri, S. Nuvoli, P. Bagella, M. Demartis, V. Fiore, Enzyme biosensors for biomedical applications: Strategies for safeguarding analytical performances in biological fluids, Sensors, 16 (2016) 780.
[61] M. Shoup-Knox, A. Gallup, G. Gallup, E. McNay, Yawning and Stretching Predict Brain Temperature Changes in Rats: Support for the Thermoregulatory Hypothesis, Frontiers in Evolutionary Neuroscience, 2 (2010).
[62] E.A. Kiyatkin, Brain temperature fluctuations during physiological and pathological conditions, European Journal of Applied Physiology, 101 (2007) 3-17.
[63] H. Wang, B. Wang, K.P. Normoyle, K. Jackson, K. Spitler, M.F. Sharrock, C.M. Miller, C. Best, D. Llano, R. Du, Brain temperature and its fundamental properties: a review for clinical neuroscientists, Front Neurosci, 8 (2014) 307-307.
[64] E.A. Kiyatkin, K.T. Wakabayashi, M. Lenoir, Physiological Fluctuations in Brain Temperature as a Factor Affecting Electrochemical Evaluations of Extracellular Glutamate and Glucose in Behavioral Experiments, ACS Chemical Neuroscience, 4 (2013) 652-665.
[65] K.L. Baker, F.B. Bolger, M.M. Doran, J.P. Lowry, Characterisation of a Platinum-based Electrochemical Biosensor for Real-time Neurochemical Analysis of Choline, Electroanalysis, 31 (2019) 129-136.
[66] J.P. Lowry, M. Miele, R.D. O'Neill, M.G. Boutelle, M. Fillenz, An amperometric glucose-oxidase/poly(o-phenylenediamine) biosensor for monitoring brain extracellular

glucose: in vivo characterisation in the striatum of freely-moving rats, Journal of Neuroscience Methods, 79 (1998) 65-74.
[67] F. Tian, A.V. Gourine, R.T.R. Huckstepp, N. Dale, A microelectrode biosensor for real time monitoring of l-glutamate release, Analytica Chimica Acta, 645 (2009) 86-91.
[68] Y. Hu, G.S. Wilson, Rapid Changes in Local Extracellular Rat Brain Glucose Observed with an In Vivo Glucose Sensor, Journal of Neurochemistry, 68 (1997) 1745-1752.
[69] K.L. Baker, F.B. Bolger, J.P. Lowry, A microelectrochemical biosensor for real-time in vivo monitoring of brain extracellular choline, Analyst, 140 (2015) 3738-3745.
[70] S.L. O'Riordan, J.P. Lowry, In vivo characterisation of a catalase-based biosensor for real-time electrochemical monitoring of brain hydrogen peroxide in freely-moving animals, Analytical Methods, 9 (2017) 1253-1264.
[71] T.T. Nguyen-Boisse, J. Saulnier, N. Jaffrezic-Renault, F. Lagarde, Highly sensitive conductometric biosensors for total lactate, d- and l-lactate determination in dairy products, Sensors and Actuators B: Chemical, 179 (2013) 232-239.
[72] R.D. O'Neill, G. Rocchitta, C.P. McMahon, P.A. Serra, J.P. Lowry, Designing sensitive and selective polymer/enzyme composite biosensors for brain monitoring in vivo, TrAC Trends in Analytical Chemistry, 27 (2008) 78-88.
[73] J.M. Hinzman, J.L. Gibson, R.D. Tackla, M.S. Costello, J.J. Burmeister, J.E. Quintero, G.A. Gerhardt, J.A. Hartings, Real-time monitoring of extracellular adenosine using enzyme-linked microelectrode arrays, Biosensors and Bioelectronics, 74 (2015) 512-517.
[74] P.E.M. Phillips, R.M. Wightman, Critical guidelines for validation of the selectivity of in-vivo chemical microsensors, TrAC Trends in Analytical Chemistry, 22 (2003) 509-514.
[75] R.D. O'Neill, Sensor–tissue interactions in neurochemical analysis with carbon paste electrodes in vivo, Analyst, 118 (1993) 433-438.
[76] Y. Hu, K.M. Mitchell, F.N. Albahadily, E.K. Michaelis, G.S. Wilson, Direct measurement of glutamate release in the brain using a dual enzyme-based electrochemical sensor, Brain Research, 659 (1994) 117-125.
[77] M.G. Garguilo, A.C. Michael, Quantitation of Choline in the Extracellular Fluid of Brain Tissue with Amperometric Microsensors, Analytical Chemistry, 66 (1994) 2621-2629.
[78] N.J. Finnerty, F.B. Bolger, E. Pålsson, J.P. Lowry, An Investigation of Hypofrontality in an Animal Model of Schizophrenia Using Real-Time Microelectrochemical Sensors for Glucose, Oxygen, and Nitric Oxide, ACS Chemical Neuroscience, 4 (2013) 825-831.
[79] S.B. McHugh, M. Fillenz, J.P. Lowry, J.N.P. Rawlins, D.M. Bannerman, Brain tissue oxygen amperometry in behaving rats demonstrates functional dissociation of dorsal and ventral hippocampus during spatial processing and anxiety, European Journal of Neuroscience, 33 (2011) 322-337.
[80] J.P. Bruno, C. Gash, B. Martin, A. Zmarowski, F. Pomerleau, J. Burmeister, P. Huettl, G.A. Gerhardt, Second-by-second measurement of acetylcholine release in prefrontal cortex, European Journal of Neuroscience, 24 (2006) 2749-2757.

Figures

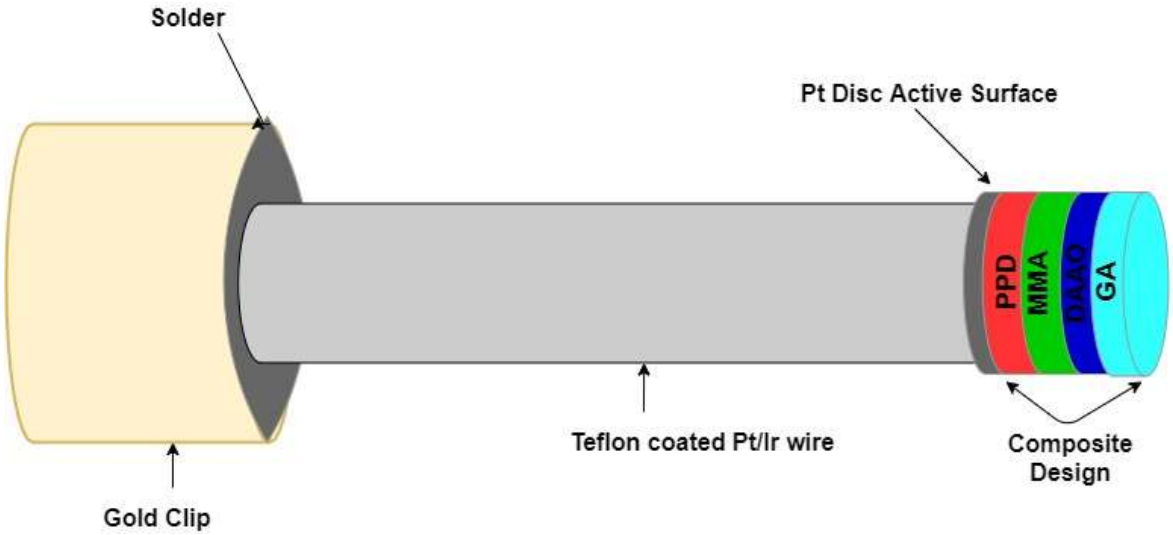

Fig. 1: Schematic of the electrode (disc geometry) and dip-coat layering involved in the manufacture and development of the D-serine biosensor: Layer 1 - Poly(*o*-phenylenediamine) (PPD, 300 mM); Layer 2 - Methyl methacrylate (MMA); Layer 3 - D-amino acid oxidase (DAAO, 1200 U/mL); and Layer 4 - Glutaraldehyde (GA, 1%).

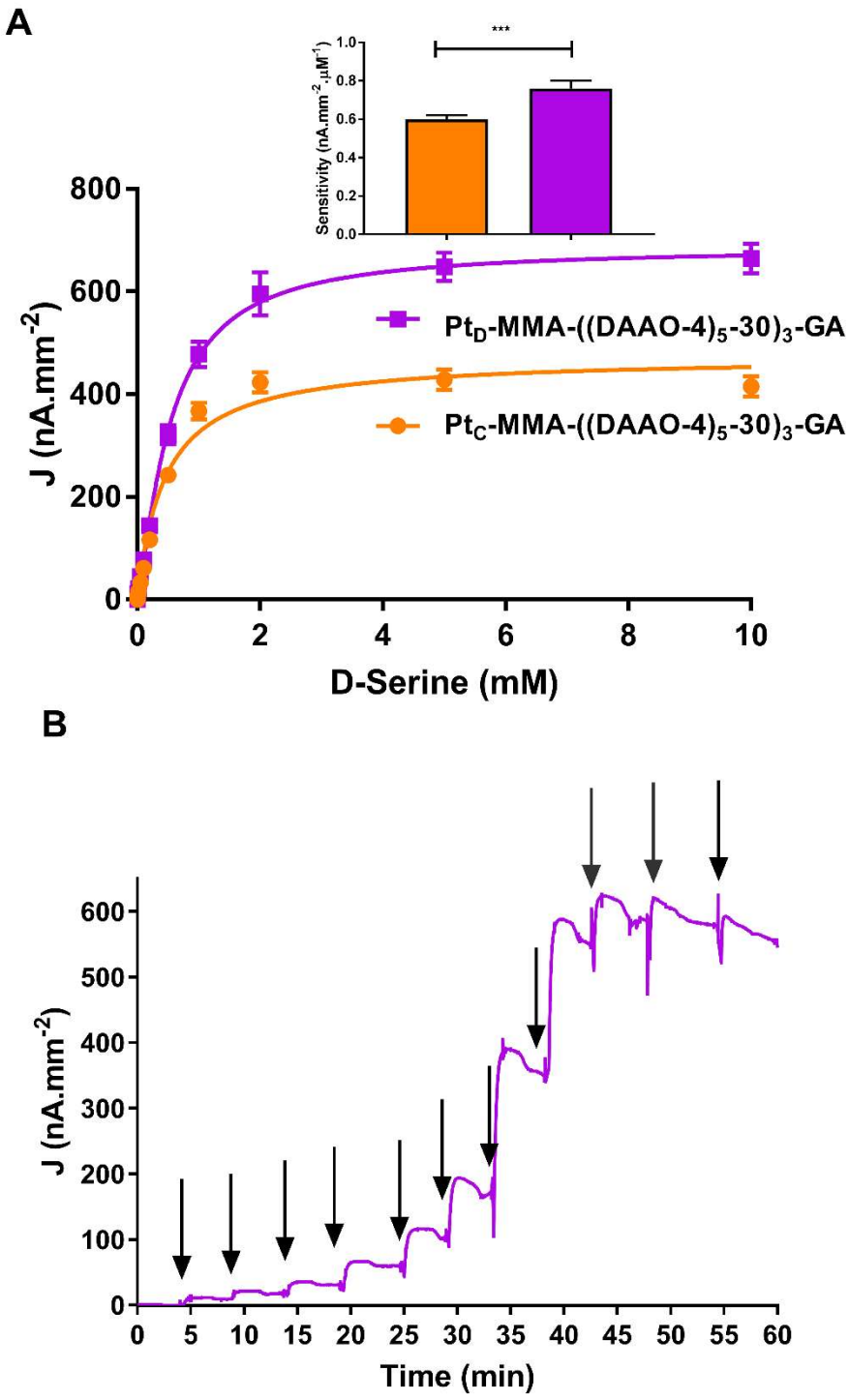

Fig. 2: **(A)** Current-concentration profiles for D-serine calibrations (0-10 mM) performed using biosensor Designs 1 (orange, cylinder, n = 47) and 2 (purple, disc, n = 41), in PBS (pH 7.4) at room temperature using CPA at +700 mV *vs.* SCE. ***Inset:*** Comparison of cylinder *vs.* disc sensitivities, **** $P = 0.0004$. **(B)** Typical raw data trace for design 2. Arrows indicate point of injection yielding concentrations of 5, 10, 20, 50, 100, 200, 500, 1000, 2000, 5000, 10000 µM of D-serine.

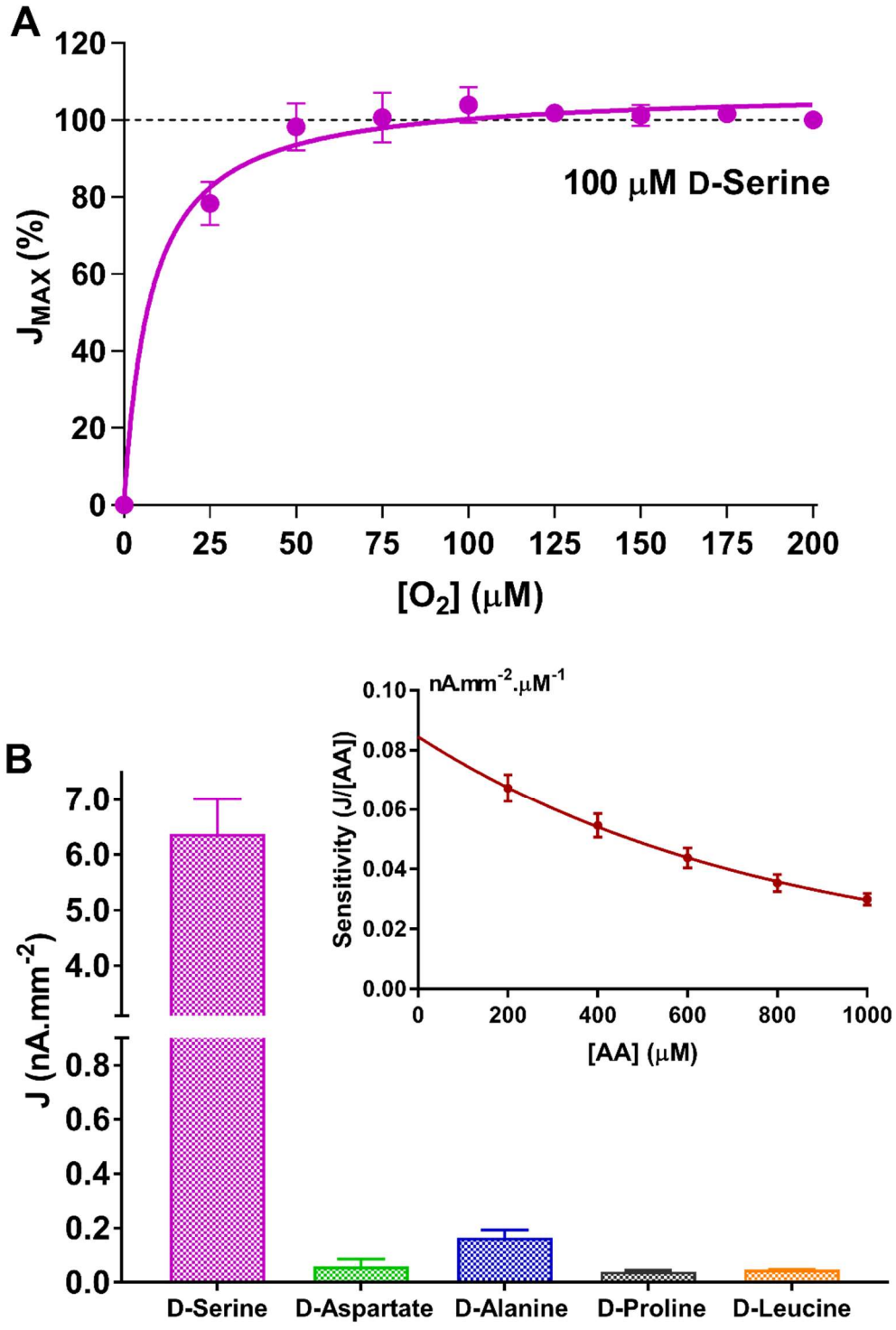

Fig. 3: Pt_D-MMA-((DAAO-4)$_5$-30)$_3$-GA biosensor Design 4 - **(A)** Normalised J_{MAX} D-serine (100 µM) response *vs.* oxygen concentration. **(B)** Comparison of sensitivity to D-serine (5 µM) with that for *in-vivo* concentrations of the most abundant amino acids found in the brain ($P <$ 0.0001); D-aspartate (0.5 µM , n = 7), D-alanine (0.15 µM, n = 8), D-proline (0.05 µM, n = 6) and D-leucine (0.05 µM, n = 6). ***Inset:*** Sensitivity as a function of concentration for ascorbic acid (AA) showing interference rejection and saturation characteristics at physiological levels.

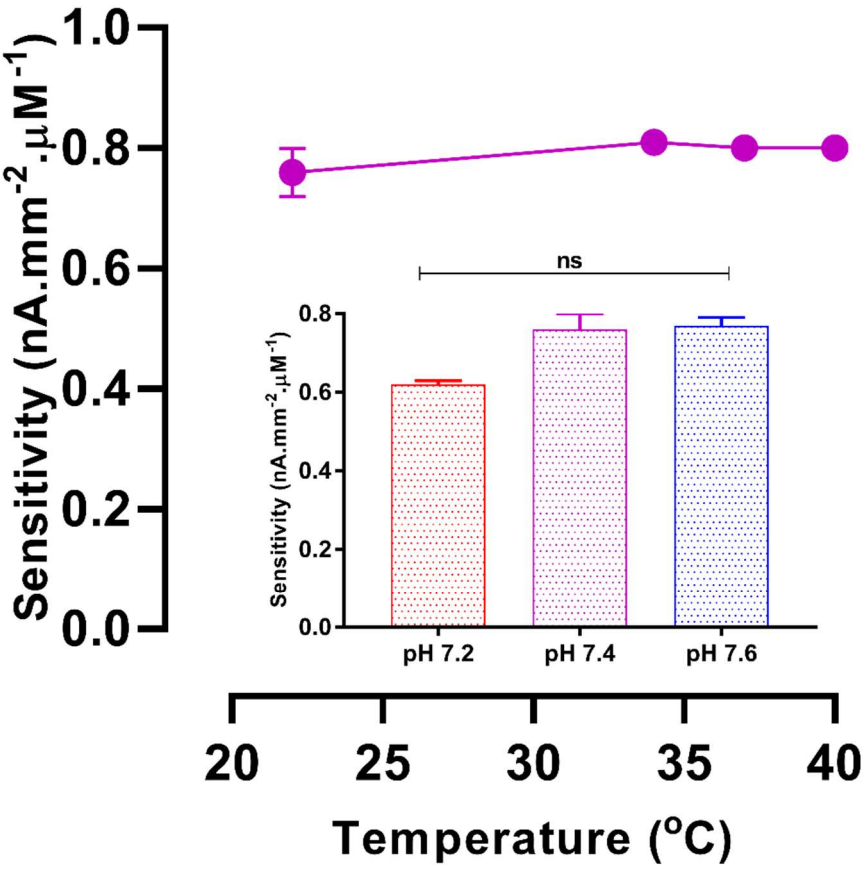

Fig. 4: The effect of changing temperature and pH (***inset***) on the sensitivity (LRS) of the Pt_D-MMA-$((DAAO\text{-}4)_5\text{-}30)_3$-GA biosensor. No significant difference in sensitivity was observed for temperature ($P = 0.5634$, one-way ANOVA) or pH ($P = 0.0753$, one way ANOVA)D-Serine calibrations (0-10 mM) performed at +700 mV *vs*. SCE in PBS (pH 7.4).

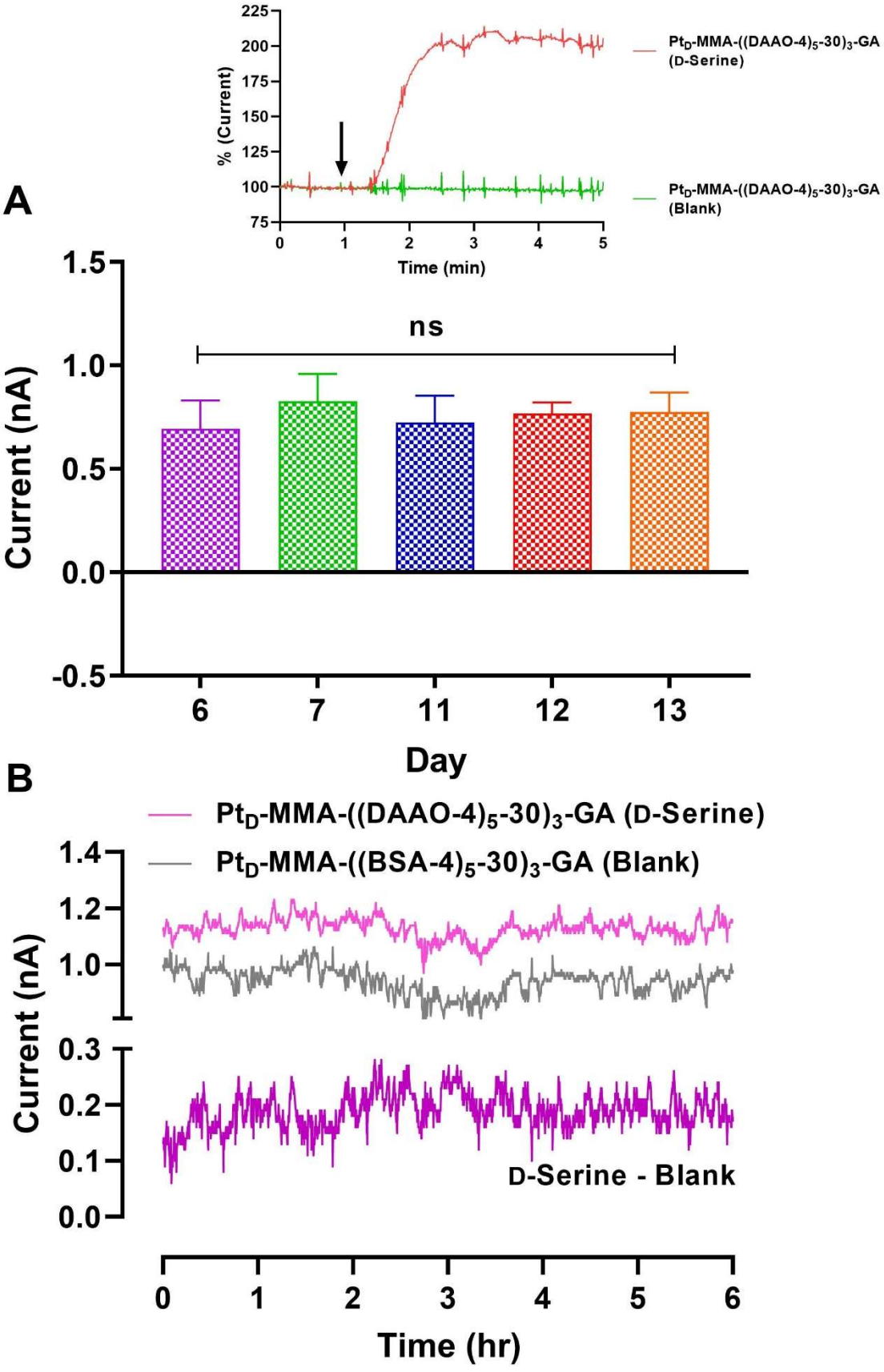
A
% (Current)
Time (min)
Pt$_D$-MMA-((DAAO-4)$_5$-30)$_3$-GA (D-Serine)
Pt$_D$-MMA-((DAAO-4)$_5$-30)$_3$-GA (Blank)
ns
Current (nA)
Day
B
Pt$_D$-MMA-((DAAO-4)$_5$-30)$_3$-GA (D-Serine)
Pt$_D$-MMA-((BSA-4)$_5$-30)$_3$-GA (Blank)
Current (nA)
D-Serine - Blank
Time (hr)

Fig. 5: (A) Average (± SEM, n = 7) baseline *in-vivo* data for the Pt_D-MMA-$((DAAO\text{-}4)_5\text{-}30)_3$-GA biosensor recorded in rat striatum (3 animals) using CPA at +700 mV over 13 days. All data taken daily between 08:00-09:00. Inset: Typical example of the effects of a 800 nL microinjection of 200 µM D-serine on the Pt_D-MMA-$((DAAO\text{-}4)_5\text{-}30)_3$-GA biosensor (red trace). Arrow represents the point of delivery of microinjection with current normalised with baseline set to 100%. (**B)** Typical 6 hour *in-vivo* trace (10:00-16:00) for both the biosensor (pink trace) and its composite blank Pt_D-MMA-$((BSA)_5\text{-}30)_3$-GA electrode (grey trace). The lower purple trace shows the differential signal (D-Serine – Blank).

Appendix 3: Conferences and Postgraduate Modules

Training Courses:

• LAST Ireland Training course (Category A, B, C, D) on the use of animals in scientific procedures in accordance with best international and national practices – General Module (Day 1) and Species Specific Module (Day 2) – 14th/15th February 2019.

• Attended Institute of Animal Technology (IAT, Ireland Branch) Symposium 2019 (22nd May), Trinity College Dublin

Conferences:

RSC 6th Analytical Biosciences Early Career Researcher Meeting, University of Cambridge, UK, 28th-29th March 2019:

• K.P. Bermingham, M.M. Doran, F.B. Bolger, J.P. Lowry. Characterisation of a biosensor for the real-time eurochemical Monitoring of L-Glutamate. Poster Presentation.

XXV International Symposium on Bioelectrochemistry and Bioenergetics, University of Limerick, 26th-30th May 2019:

• K.P. Bermingham, M.M. Doran, F.B. Bolger, J.P. Lowry. Characterisation of a biosensor for the real-time neurochemical monitoring of L-Glutamate. Poster Presentation.

• M.M. Doran, K.P. Bermingham, K.W. Pierce, M.D. Tricklebank, J.P. Lowry. The In-vivo validation of a D-Serine biosensor. Poster Presentation.

MU Structured PhD/MSc Programme – Modules Completed:

- Module CH801 – Core Skills and Research Techniques in Chemistry
- Module CH803 – Teaching Skills in Chemistry
- Module BI673T – LAST Ireland Animal Handling Course, Rodent Module
- Module GST2 – Finding Information for your Research
- Module GST10 – Innovation and Research Commercialisation
- Module GST1 – Professional Development and Employability